UCLA
UCLA Electronic Theses and Dissertations

Title
Design and Development of Dual Polarized, Stacked Patch Antenna Element for S-Band Dual-Pol Weather Radar Array

Permalink
https://escholarship.org/uc/item/8bt7c9b2

Author
Bhardwaj, Shubhendu

Publication Date
2012

Peer reviewed|Thesis/dissertation

eScholarship.org Powered by the California Digital Library
University of California

University of California

Los Angeles

Design and Development of Dual Polarized, Stacked Patch Antenna Element for S-Band Dual-Pol Weather Radar Array

A thesis submitted in partial satisfaction

of the requirements for the degree

Master of Science in Electrical Engineering

by

Shubhendu Bhardwaj

2012

© Copyright by
Shubhendu Bhardwaj
2012

Abstract of the Thesis

Design and Development of Dual Polarized, Stacked Patch Antenna Element for S-Band Dual-Pol Weather Radar Array

by

Shubhendu Bhardwaj

Master of Science in Electrical Engineering

University of California, Los Angeles, 2012

Professor Yahya Rahmat-Samii, Chair

Recently, dual-polarized weather radars are gaining popularity due to their promise of more accurate and faster weather prediction. This work presents design of a dual-polarized, patch antenna element operating in the band 2.7 GHz – 3.0 GHz, with 30 dB isolation between the ports, which can be utilized for a dual-polarized weather radar array. In order to characterize the applicability of the current design in weather forecast radar system, recently published parameters-called W-parameters, have been evaluated and studied for the demonstrated antenna element design. Further analytical study has also been conducted on these W-parameters to understand their behaviour with changing radiation pattern. In the process of reaching a low cross-pol, dual-polarized element design, basic mechanism of cross-polar radiation in a rectangular patch antenna has also been analyzed using a novel strategy of near-field analysis. Next, this near-field model has been used to study cross-polar radiation in differential feeding configuration (for single patch element) and rotating feeding configuration (for array) to understand the mechanism of cross-pol reduction in these designs. This work also includes a comprehensive comparative study of a class of popular slotted antennas in terms of their RF mechanism and radiation mechanism, which again utilizes the near-field model developed earlier. The new strategy of understanding the radiation properties based on the near-field provides a distinctive, visualization based understanding of the radiation mechanism in small antennas.

The thesis of Shubhendu Bhardwaj is approved.

Tatsuo Itoh

Yuanxun(Ethan) Wang

Yahya Rahmat-Samii, Committee Chair

University of California, Los Angeles

2012

This thesis is dedicated to my Mamma and Papa,
whose inspiration and motivation keeps me going.

Table of Contents

List of Figures

List of Tables

Acknowledgments

Foremost, I wish my sincere thanks and appreciation to Prof. Yahya Rahmat-Samii for his attention, guidance, insight and support during the course of this work.

I would like to thank all my fellow lab-mates at Antenna Research Analysis and Measurement Lab at UCLA. Special thanks to Dr. Harish Rajgopalan for his helpful comments during the preparation of this thesis. I am thankful to Joshua Kovitz for his help, with pre-shipping testing and diagnostics of the developed hardware. I am also thankful to Timothy Brockett for his time and patience for teaching me fabrication using photo-lithography and antenna pattern measurements. Also, special thanks to Minji Kim at Center for High Frequency Center, UCLA, for his help and support during hardware fabrication and measurements.

Finally, I am thankful to School of Meteorology, University of Oklahoma, for providing partial financial support for this work. I also thank Prof. Guifu Zhang, from University of Oklahoma, for his continued technical support which helped in finishing the work smoothly and in time.

CHAPTER 1

Introduction

1.1 Radars in Weather Detection

Weather radar is the most effective tool for detection and measurement of precipitation. Radars (abbreviation of Radio Detection and Ranging) have been widely used for precipitation measurement (specially thunderstorms) since 1940s. In simple terms, their operation can be explained as following. A directive antenna sends out bursts of electromagnetic waves (or pulses), which are reflected back from the particles in atmosphere. The energy reflected back can be used to understand the nature of the particles and identify them. The size of particle can be inferred from the energy level of reflected wave and the speed and direction of movement can be calculated using doppler effect in the returned signal. Conventionally, single polariazation doppler radars have been popular for weather detection. However, weather radar technology has been improving with new milestones in the applied electromagnetics research. More specifically, dual-polarization radars and phased array weather radars have been subject of latest research in this field. As a background work in this thesis, a brief discussion on the dual-polarized radars and phased array radars has been presented in following sub-sections.

1.1.1 Dual-polarized Radar

In general, a single polarized radar (conventional horizontal doppler radar) can estimate the horizontal dimension of the cloud and precipitation (rain, hail and snow particles). This, along with movement information of the particles, can be used in weather forecasts. Recently, a lot of interest has grown into the use of the dual-pol radars. Figure 1.1 shows some snippets of news articles recently published on internet, showing interest in dual-pol radars for the weather

Figure 1.1: Due to their advantages over conventional Doppler radar, Dual-pol radars are gaining popularity recently: Online news articles showing the recent growing interest in Dual-pol radars.

prediction. Use of dual-pol radars significantly improve the process of identifying the type of precipitation, since it adds information available in vertical orthogonal plane. This can prove crucial in faster and accurate prediction of hazardous weather.

In contrast to a conventional doppler radar, a dual-pol radar sends out pulses in vertical and horizontal planes [1] (consider zero degree elevation). Figure 1.2a shows the operation of a dual-pol radar for precipitation detection. The power reflected by the precipitation is measured by

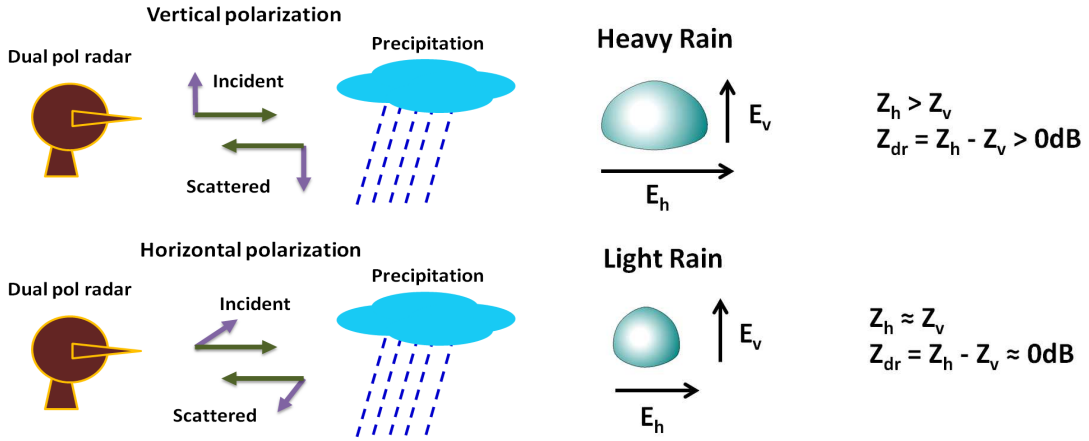

(a) Dual-pol operation **(b)** Differential reflectivity in rain

Figure 1.2: The operation of dual-pol radar for detection of precipitation.

the radar and is then used to calculate the *vertical reflectivity* and *horizontal reflectivity*, denoted by Z_v and Z_h respectively. In general, reflectivity is calculated by using the power observed by the radar all over the space for that particular component of reflected signal. As described in [2], these parameters can be defined as following,

$$Z_v = \langle S_{vv}^2 \rangle \tag{1.1}$$

$$Z_h = \langle S_{hh}^2 \rangle \tag{1.2}$$

Here, S_{vv} and S_{hh} are the backscattering coefficients of the scatterer. The parameter *Differential reflectivity (Z_{dr})* is calculated as ratio of observed horizontal reflectivity to the vertical reflectivity [3].

$$Z_{dr} = \frac{Z_h}{Z_v} \tag{1.3}$$

The obtained parameter Z_{dr} can be used to detect and identify the type of precipitation. The size of water droplet in a precipitation increases with intensity of precipitation. While falling through atmosphere, these drops attain an equilibrium shape of oblate spherical (like the

shape of a bun) [4]. This shape is flatter for bigger drops as compared to smaller drops, as illustrated in Figure 1.2b. Dual-pol radar exploits this nature of precipitation to measure the rain intensity. Since a flatter rain drop will have higher horizontal reflectivity as compared to vertical reflectivity [5], the differential reflectivity in dB will be positive for a heavy rain. For a light rain differential reflectivity will be close to zero. Similarly, conclusion can be drawn for other forms of precipitation like hail, snow and other weather conditions like storms.

1.1.2 Phased Array Radar

Phased array technology is also becoming popular in radar applications. It has been shown that pulse to pulse beam steering capability allows accurate measurements in shorter dwell time than mechanically rotating dish [6], resulting in faster data updates. In this work, the design and development of antenna element for a similar dual-pol phased array radar has been presented.

1.2 Patch Antenna Development for S-Band Weather Radar

The objective of this work is to develop a dual-polarized S-band antenna element to be used in dual-pol phased array radar. Since projected design of the radar is conformal, the patch antenna is chosen to be the element antenna type. The most important requirement of the design is achieving high bandwidth, while maintaining a dual-polarized operation with low cross-pol and high isolation between the ports. A brief discussion on the dual-pol operation followed by a summary of objectives is presented in following subsections.

1.2.1 Dual-pol requirement: Isolation and Cross-pol

Since the weather radar is dual-polarized, the required patch element should be also be dual polarized- linearly polarized in two orthogonal planes. For any dual-polarized antenna, the independence of the two polarizations is very important aspect. In this design, there is need of high degree of independence of two ports, since any error in measurement would create error in reflectivity calculations, leading to erroneous weather prediction.

The independence between the ports can be broken-up into two different requirements. First requirement is the low mutual coupling between the ports exciting the two orthogonal polarizations. This requirement can also be stated as high isolation between the ports. A high isolation between the ports ensures that any energy injected into port-one does not directly go into port-two, avoiding any interference with the received signal at the port-two. Second requirement is low cross-pol radiation from the antenna, when either of the ports is excited. A design with high cross-polar radiation would mean that a portion of energy meant to excite one polarization (e.g. vertical) is actually being radiated as other (e.g. horizontal) polarization. When this energy reflects back from the scatterer, it would be detected by horizontal port. This means that the horizontal port receives part of energy it never sent out to start with. This will cause deviation in the values of reflectivity as defined in Equations 1.1 and 1.2, lading to error in precipitation measurement.

It is important to note that these two aspects of antennas are not entirely different from each other. The isolation between the antennas can also be related to mutual impedance between the ports. The real part of mutual impedance between the ports is related to the space integral of the far-field patterns from the two ports [7]. This integral is evaluated for each of the E_θ and E_ϕ components separately, hence a high cross-polar radiation would contribute to increase in this integral, which equivalently means high mutual coupling and low isolation. However, this relation does not always mean that a low cross-polar radiation implies high isolation. Therefore, these two aspects of any design should be optimized and characterized separately.

1.2.2 The W-parameters

The differential reflectivity (as described in Section 1.1.1) can be influenced by a number of factors. Such a variation in differential reflectivity from external or internal factors is referred to as bias in differential reflectivity, and can be formulated as following [8]

$$\delta Z_{dr} = 10 \log_{10} \left(\frac{P_h}{P_v} \right) - Z_{dr} \tag{1.4}$$

where Z_{dr}, the intrinsic differential reflectivity is given by

$$Z_{dr} = 10 \log_{10} \left(\frac{(S_{hh})^2}{(S_{vv})^2} \right) \tag{1.5}$$

Here P_h and P_v are the actual power levels of the returned signal intercepted by the radar, assuming equal power was launched on both the ports. S_{hh} and S_{vv} are the backscattering coefficients of the scatterer and represent the power returning to the antenna in ideal case. There may be various factors which can contribute to bias in the differential reflectivity [9, 10]. Some of these are cross-polarizing scatterers [11], depolarizing media [12] and cross-pol radiation from the antenna [8,13,14]. These factors can convert some of the power from one polarization to another creating bias in measurement. However, it has also been shown that a non-depolarization media can create a phase shift in the propagating signal and hence influence the differential reflectivity [12]. Here focus is on the bias in the differential reflectivity due to cross-polar radiation from the antenna, since that will decide the performance of the developed antenna element. In [13], the influence cross-polar radiation has been analysed using far-field patterns. This work is further simplified in [8]. According to [8], the requirement to improve the bias in differential reflectivity can be simplified to decreasing certain parameters calculated from the antenna far-field. For example, for the horizontally polarized component, the bias in differential reflectivity can be reduced by reducing these numbers

$$W_{hv}{}^{*} = \frac{\int_\Omega F_{hh}^2(\theta,\phi) F_{hh}^*(\theta,\phi) F_{hv}^*(\theta,\phi) d\Omega}{\int_\Omega |F_{hh}(\theta,\phi)|^4 d\Omega} \tag{1.6}$$

$$W_4 = \frac{\int_\Omega |F_{hh}(\theta,\phi)|^2 |F_{hv}(\theta,\phi)|^2 d\Omega}{\int_\Omega |F_{hh}(\theta,\phi)|^4 d\Omega} \tag{1.7}$$

Here, F_{hh} represents the radiation pattern for co-pol radiation (horizontally-polarized) and F_{hv} is cross-polar pattern due to excitation of horizontal port. Similarly, the parameters can also be likewise defined for vertical polarized component of the signal. These parameters, referred to

*The original formulation for W_{hv} presented in the paper [8] is $W_{hv} = \frac{\int_\Omega F_{hh}^3(\theta,\phi)|F_{hv}(\theta,\phi)|d\Omega}{\int_\Omega F_{hh}^4(\theta,\phi)d\Omega}$. But, this formulation assumes that co-polar radiation will have uniform phase at all the points on the far-field sphere of observation. This assumption is not true for practical antennas, hence as per communication with the authors of [8], Dr. Guifu Zhang, the definition was altered as per Equation 1.6 for practical calculations. Similar changes were made for the definition of W_4, based on communication with Prof. Guifu.

as W-parameters in this work, are the key parameters in deciding the performance of a radar for weather radar application. In the current work, these parameters have been evaluated from simulated as well as measured far-field patterns for different patch antennas designed.

1.2.3 Summary of Objectives

Table 1.1 tabulates summary of specifications required for the design of the antenna element. The projected array design has element spacing of around 7 cm. Therefore the current design objective is to design a element within an planar area of 7 cm $\times$ 7 cm.

Table 1.1: Specification for the design of the element

Parameter	Specification
Operation Frequency	2.7 GHz - 3.0 GHz
Return loss level	-10 dB
Allowable element size	7 cm $\times$ 7 cm
Dual-polarization	yes
Port isolation	-30 dB

In general, a rectangular patch antenna can be used to obtain a bandwidth of around 5%. The bandwidth requirement here is almost double of what is achievable using a simple rectangular patch. Also, the cost effectiveness is very important for this design, since finally a large number of antenna elements would be fabricated for the array. It would be best if the objective of high bandwidth can be achieved using commercially available substrates, rather than having to obtain substrates with customized thickness values, which can lead to higher fabrication cost.

1.3 Organization of the Work

The complete work presented in this thesis can be divided into two broad categories: (1) Analysis and (2) Design and fabrication. Analysis part of the work, covered in Chapters 2 and 3, contains a study of basic aspects of a rectangular patch antenna. In Chapter 2, a study on the cross-

polar radiation generation in a simple square patch antenna is conducted , since reduction of cross-polarization is one of the objectives in the current antenna design. A detailed comparative study on slotted antennas has been conducted in Chapter 3 to understand various aspects of these antennas and to compare their performances for same frequency bandwidth.

Chapters 4 and 5 contain the design, fabrication and measurement part of the work. Chapter 4 mainly focuses on preliminary work which was done to explore various options for attaining the required bandwidth for the design. In the study, stacked patch antennas were found suitable for the given application. Chapter 5 summarizes a design of dual-polarized, stacked patch antenna with differential feeding, with low cross-pol and high isolation between the ports.

W-parameters, as discussed in Section 1.2.2, are important parameters for the weather radars. While working with these parameters for the designed antennas, some interesting properties of these parameters were revealed. A short discussion of these properties has been discussed in Chapter 6.

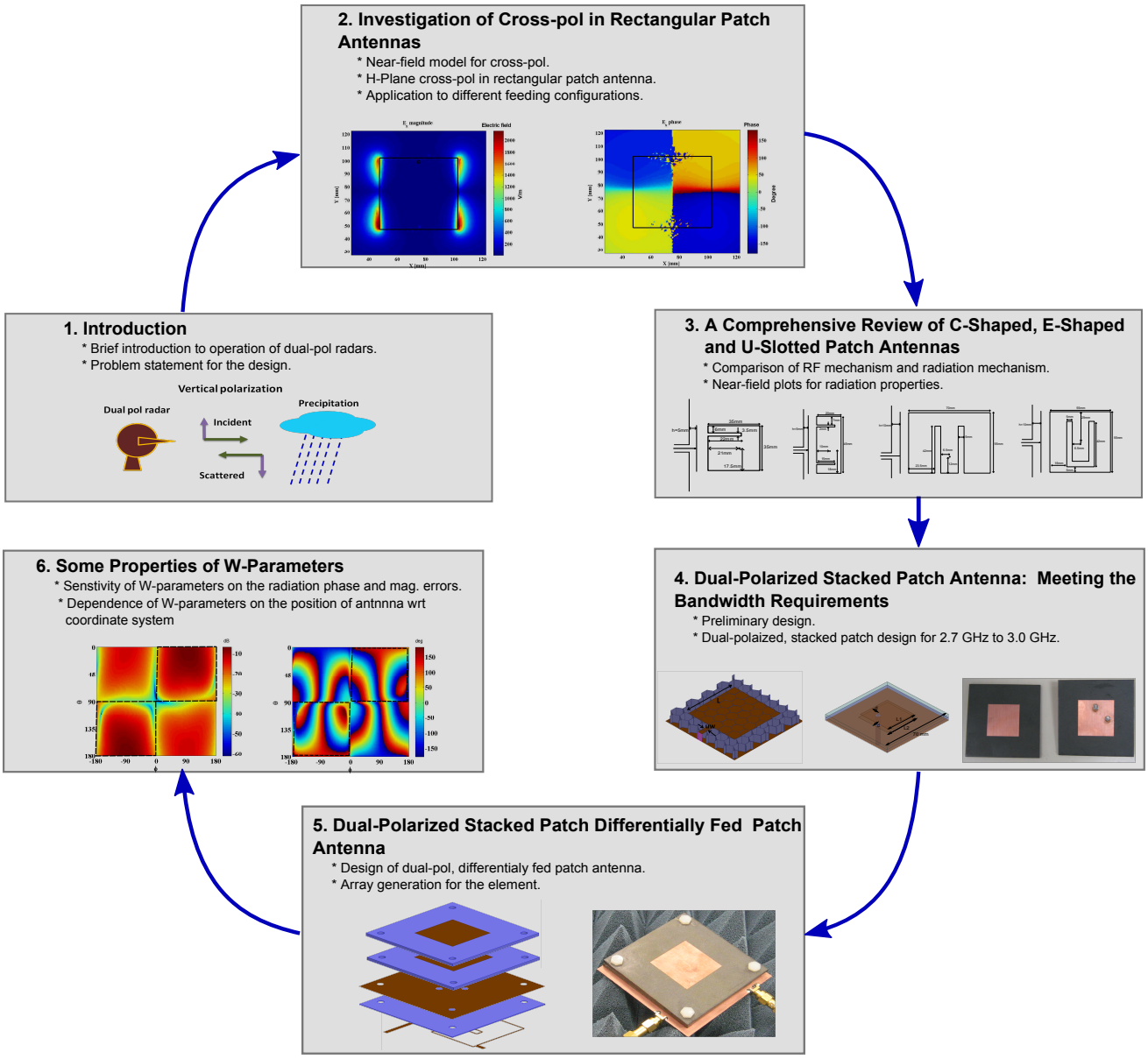

Figure 1.3: The flow of the chapters showing organization of the work in this thesis.

CHAPTER 2

Investigation of H-Plane Cross-pol in Rectangular Patch Antennas

In a dual-polarized antenna design, reduction of the cross-polar radiation carries special importance, since cross-polar radiation of one of the ports interferes with the co-polar component of the other port. This creates an error in the measurement of the reflected co-pol signal from the scatterer and leads to faulty precipitation measurement. Also, as emphasized before in section 1.2.1, in case of dual-pol antennas, high cross-pol would also increase the correlation between the two ports which is related to mutual coupling (or isolation) between the ports. Decreasing isolation is also an objective of the final design. Therefore, reduction of cross-pol is important for high performance dual-pol radar. In order to fundamentally understand the origin of the cross-pol in the patch antennas, cross-pol in rectangular patch antennas is studied in detailed manner using a new approach.

Basic simulations on the rectangular patch antennas reveal that, in general the H-plane cross-pol in these antennas is much higher than the E-plane cross-pol. This is the basic question, which has been answered in the chapter. The objective here is to understand the nature and behaviour of the H-plane cross-pol in a rectangular patch antenna in an intuitive manner, providing insight into how asymmetry in the patch antenna structure can manifest itself into high H-plane cross-pol in the far-field [15]. This has been accomplished using a novel approach to look at the near-fields of the antenna and then pin-pointing certain specific features in the near-field which are responsible for high cross-pol in the H-plane of the far-field.

2.1 Cross-pol in Patch Antennas

2.1.1 Background

Before going into the technique developed, some of the previous studies conducted by various authors have been summarized here. Many authors have presented models for characterizing cross-pol from a patch antenna. A model for calculating the radiation from a patch antenna using equivalence theorem has been presented in [16]. This model uses the dominant modes of resonance in rectangular cavity to obtain near-field in the vicinity of the edges of the patch antenna, which can be transformed to obtain the far-field using NF-FF transformation. Another approach by modelling the patch antenna as transmission line is presented in [17]. Authors in [18] and [19] expand radiation from a rectangular patch antenna in terms of summation of a basis functions. The basis function contains carefully chosen product terms of radiation from the probe and dominant cavity modes in a rectangular patch cavity. All of these approaches have been successful in predicting the cross-pol to a good degree of accuracy, as confirmed by various measurement studies [20, 21]. However, an intuitive understanding of the generation of the cross-pol has not been emphasized enough. Here aim is to develop physical understanding of the reason for cross-pol radiation from patch antenna in the H-plane in simple terms by looking at the near-field.

Conventionally, surface current on the antennas has been used to get physical insight into the generation of cross-pol in patch antennas. But this approach is not suitable for analyzing the radiation properties in patch antenna, since current on the surface of the patch antenna radiates in presence of ground plane. Such a radiation behaviour will be difficult to understand simply by looking at the surface currents on the patch. In order to understand the H-plane cross-pol generation from rectangular patch antenna, a new near field model is formulated and presented.

2.1.2 Mechanism of Cross-pol in Rectangular Patch Antenna

The radiation from the patch antenna can be explained using rectangular cavity model [22]. A rectangular patch can be approximated as cavity with magnetic walls as shown in Figure

2.1a. The fields within the cavity fringe out from the open boundaries of the patch and cause the radiation. Alternatively, the electric field can be seen as equivalent magnetic current which being parallel to the ground plane will produce a far-field radiation (Figure 2.1b).

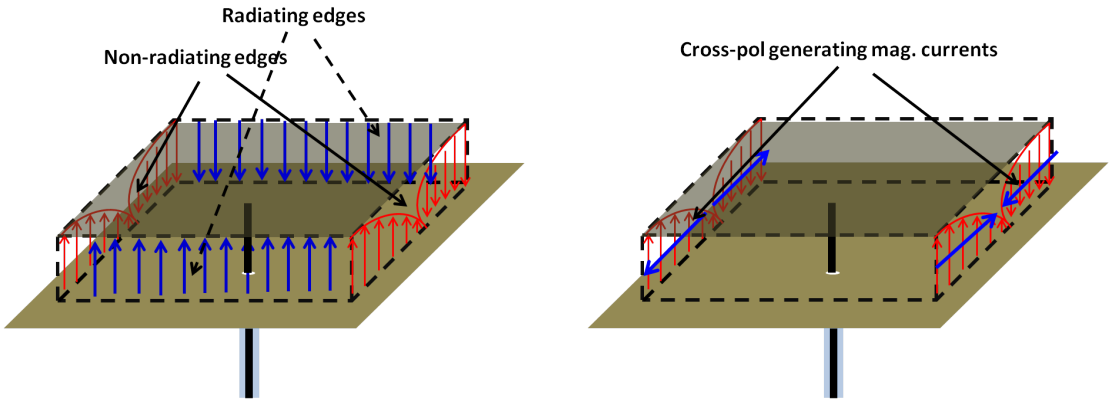

(a) Fringing electric field at the edges of the patch

(b) Equivalent magnetic currents generating cross-pol

Figure 2.1: Electric field and equivalent magnetic currents contributing to radiation from a rectangular patch antenna.

In theory, the dominant mode of the cavity resonance produces a cosine like distribution along the non-radiating edges and uniform distribution along the radiating edges of the patch (Figure 2.1a). The far-field co-pol radiation will be produced as a result of constructive interference of field distribution over the radiating edge of the patch, whereas the fields over the non-radiating edges create the far-field cross-polar radiation. It is easy to see that equivalent magnetic current distribution over the non-radiating edges is such that, the radiation from these edges would cancel out due to opposite polarity over the edges (Figure 2.1b), though this destructive interference will be occurring only in the principal planes (i.e. E- and H-planes). Therefore, even theoretically, cross-polar radiation is expected for non-principal planes points in space.

2.2 New Approach for Cross-polar analysis

To investigate the cross-polar radiation from a rectangular patch antenna, a new approach of looking at the near-fields of the antenna has been adopted. The motivation for analyzing the

near fields comes from the fact that far-field of the antenna is obtained by NF-FF transformation of the near field. Hence, various characteristics of far-field, such as cross-pol, can be associated to certain characteristics of the near field. The near field on the antenna is very much dependent on the geometry of the antenna, and its dimensional parameters. Hence, by using this approach cross-pol can be directly related to certain dimensional parameters of the patch antenna.

2.2.1 Problem Statement

To set up the problem, it is important to iterate the definitions of the E and H-planes for a rectangular patch antenna. Figure 2.2a shows orientation of E and H-planes for a rectangular patch antenna. It should be noted that the patch structure is symmetric with respect to the E-plane, but has an asymmetry with respect to the H-plane due to offset of probe feeding position. In fact, the probe offset decides the direction of the linear polarization of the antenna, hence defining the E and H-planes.

In previous section, it was pointed out that if only the dominant mode of resonance within the cavity (also called simple cavity model) is considered, the cross-polar radiation should be zero in principal planes. Although, the cross-pol would have a non-zero value in non-principal plane regions in space. But in practice, a high value of cross-polar radiation is observed in H-plane. In theoretical terms this, can be explained by existence of higher order modes excited within the patch cavity. But, intention here is to understand this ambiguity physically - in terms of the deviation of near-fields from as predicted by simple cavity model (or theoretical model). Figure 2.2b shows the 3-D far-field cross-polar radiation pattern as predicted by simple cavity model. In this model the far-field is calculated using the near-fields as generated by TM_{010} resonance in the cavity. Figure 2.2b shows a typical practical 3-D far-field cross-polar pattern for a rectangular patch antenna.

The figures clearly show the difference between the theoretically predicted cross-polar pattern and the practical cross-polar pattern. The theoretical pattern has deep nulls in the principal planes but in the practical case, the null in H-plane is filled up and a high cross-polar radiation can be seen there. E-plane null is still maintained in practical case. Hence, there is a difference

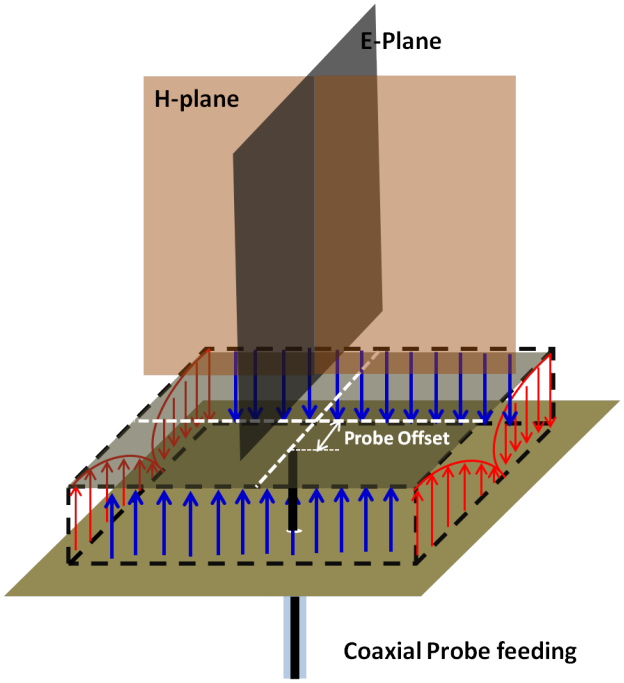

(a) E and H planes of a rectangular patch antenna

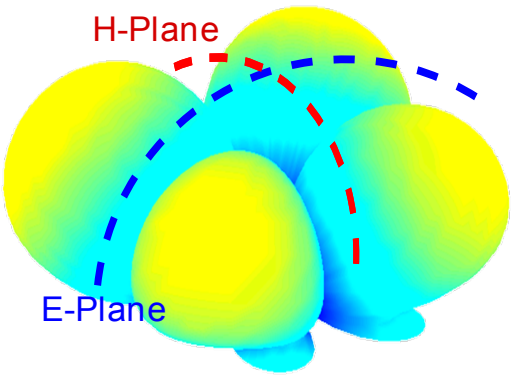

(b) Theoretical 3D far-field cross-pol pattern

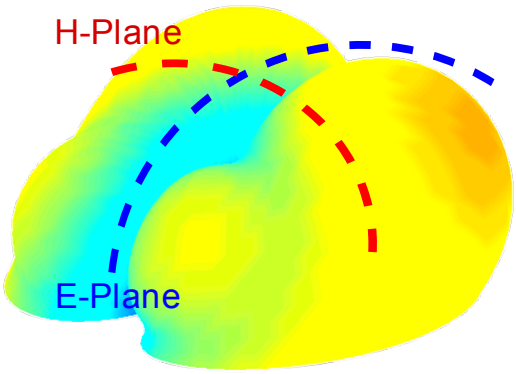

(c) A typical simulated/measured far-field cross-pol pattern

Figure 2.2: 3D patterns showing comparison of theoretically predicted and observed far-field cross-polar patterns. It can be seen that observed radiation pattern has high value of cross-pol in H-plane.

between the theoretically predicted far-field cross-polar pattern and the practically obtained one, specifically the H-plane cross-pol. The objective of this chapter is to explain this difference and

hence characterize the H-plane cross-pol in a rectangular patch antenna.

2.2.2 Near-field Approach: Introduction and Theory

To understand the theory of this approach, square patch antenna has been considered as shown in the Figure 2.3a. The Figure also shows the coordinate system being used in the analysis. In order to proceed with the analysis, it should be identified that (1) which region in the near-field should be considered for the analysis and (2) which component of the near field should be considered for explaining the H-plane cross-pol in the far-field. These questions have been addressed in following subsections.

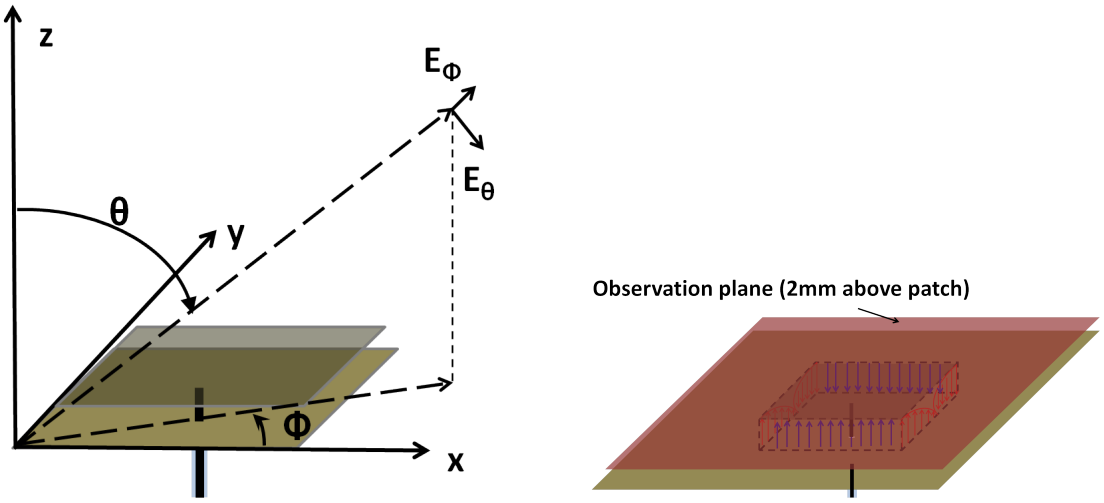

(a) Coordinate system being used for the analysis.

(b) Choice of observation plane 2 mm away from patch surface with each sides 3 times the dimension of the patch.

Figure 2.3: Coordinate system and choice of observation plane for the analysis.

2.2.2.1 *Which region?*

The region to be considered for the analysis should be simple enough to intuitively understand the nature of the near-field, yet should be able to account for all the far-field cross-pol generated in the H-plane from the antenna. A plane right above the surface of the patch antenna is chosen

for observing the near-field of the antenna (Figure 2.3b). The observation surface is chosen to be 2 mm away from the surface of the patch antenna, but this distance can vary as per convenience. Going higher away from patch means that the fields will be more spread out and it will be difficult to associate them with the physical dimensions of the patch, therefore it is better if the plane chosen is very near to the antenna surface. In Section 2.2.2.2, it has also been shown that chosen observation plane has enough information to account for the cross-pol in H-plane.

2.2.2.2 *Which component of near field?*

Another question to be asked here is which component of the near-field is needed to be analysed, since one component of the near-field will contribute to the co-pol in the far-field and other will cause cross-pol radiation (considering L-2 definition). Figure 2.3a shows that the antenna is y-polarized which means x-polarized near-field will create the cross-polar radiation in the far-field. However, this conclusion is strictly true for all points in far-field space, only if Ludwig's 2nd definition of cross-pol (L-2 definition) is considered [23]. If we consider L-3 definition, both x and y-components of the near fields will contribute to the cross-pol in the far-field. It should also be noted that, objective is to look at the H-plane cross-polar radiation from the rectangular patch and since all the cross-pol definitions are same for the principal planes of an antenna [23], it is not a concern that which definition of cross-pol is being used here. Even so, unless specified, the L-2 definition will be used everywhere in this work.

An alternate approach to identify the near field component responsible for H-plane cross-pol in the far-field would be to use vector potential method [24]. Using equivalence principal, the electrical field on the surface of the observation plane can be replaced with equivalent magnetic current radiating in free space as shown in Equation 2.1

$$\vec{M} = -2\vec{n} \times \vec{E} \tag{2.1}$$

Consider the far-field H-plane, which is x-z plane as shown in Figure 2.3a. The cross-pol component in this plane is E_θ component. Using vector potential approach, the E_θ component can be associated to the vector potential function L_ϕ by the relation:

$$E_\theta = \frac{-j\beta e^{j\beta r}}{4\pi r} L_\phi \tag{2.2}$$

There is no electric current potential term (N_θ) in this equation, since only magnetic current exists on the observation surface. The potential function L_ϕ can be written as in Equation 2.3. For H-plane case, the substitution $\phi = 0$ can be made to further reduce the equation.

$$\begin{aligned} L_\phi &= \iint_S [-M_x sin(\phi) + M_y cos(\phi)] e^{j\beta \vec{r'}.\hat{r}} ds' \\ &= \iint_S M_y e^{j\beta \vec{r'}.\hat{r}} ds' \end{aligned} \tag{2.3}$$

Here, $\hat{r}$ is the direction of observation, which can also be represented by (θ, ϕ), β is propagation constant in free space, and $\vec{r'}$ is the vector representing position of any point on the observation surface with respect to the origin. S is the total area of the observation plane as shown in Figure 2.3b. Finally, using $M_y = -2E_x$ following relation can be drawn for H-plane.

$$E_{cross-pol} = E_\theta = \frac{j\beta e^{j\beta R}}{4\pi R} \int_S 2E_x e^{j\beta \vec{r'}.\hat{r}} ds' \tag{2.4}$$

R is the distance of the observation point from origin. Here, Equation 2.4 confirms that H-plane cross-pol in the far-field depends on the near-field E_x component. This conclusion is same as what was concluded by first approach.

2.2.3 Confirmation of the Concept

The technique of looking at the aperture fields on a surface right above the patch antenna is very similar to the one applied for large reflector antennas or reflect arrays for obtaining the far-field. It is a concern that this approach will not be suitable for small antennas, where the radiation is not just limited to the broad-side direction. In general, in order to obtain far-field from near-field for small antennas, equivalence principal is applied on a closed surface around the antenna. This surface can be a radiation box, commonly used in commercial full-wave simulation

software (such as Ansoft-HFSS) or spherical surface used in measurements in spherical near-field chambers. Here in this section, the approach is confirmed for accuracy by comparing the results from a full wave simulation and by NF-FF transform of the fields taken from just one plane above the patch antenna as specified in previous section.

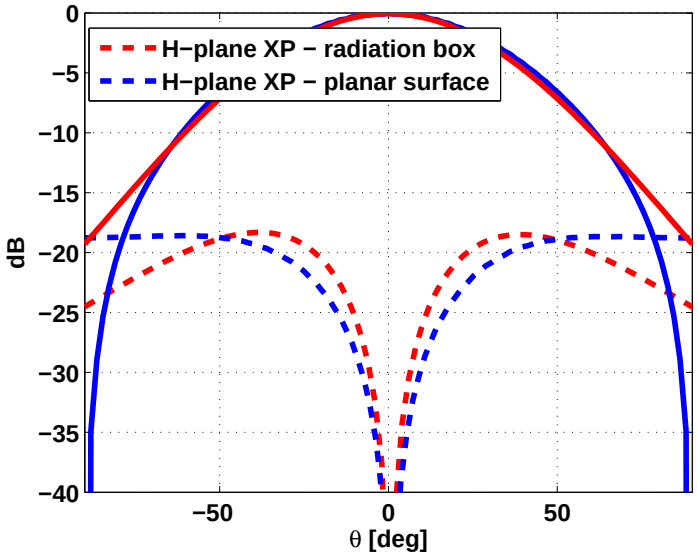

Figure 2.4: Comparison of the H-plane cross-pol obtained by two methods- full-wave simulation with radiation box and NF-FF transform of the fields in the observation plane as specified in Figure 2.3b.

Figure 2.4 shows the comparison of the cross-pol in H-plane as obtained by NF-FF transform of the fields chosen 2 mm above the surface of the patch antenna with the results of a full-wave simulation. It can be observed that the cross-pol results of the two cases match very well in the broad-side direction. There is around 1 to 2 dB difference in the results in the broadside direction, but the aim is to develop an intuitive approach rather than quantitative one, hence small difference in results can be ignored.

2.3 Application of the concept

So far, the basic theory for the near-field approach has been presented and it has also been shown that chosen plane above the patch antenna has the required information to comment about the

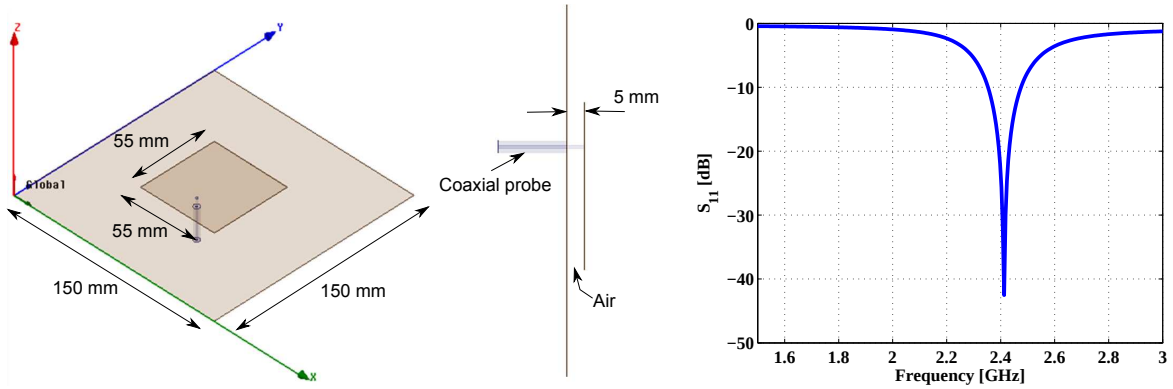

(a) The dimensions and structure of the patch antenna

(b) S_{11} response of the patch

Figure 2.5: Dimensions and return loss response of the antenna under study.

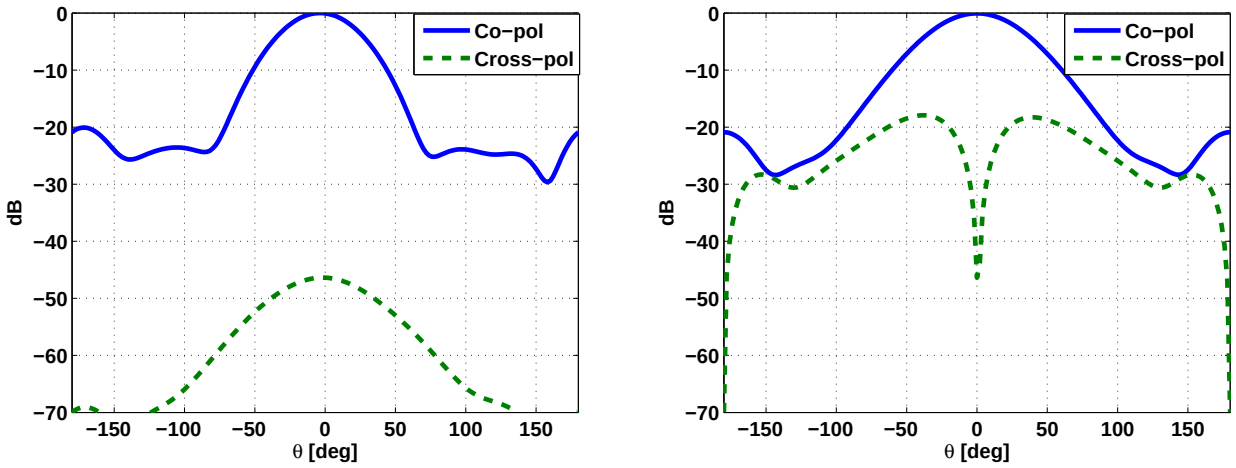

(a) E-plane radiation pattern

(b) H-plane radiation pattern

Figure 2.6: Simulated radiation patterns of the patch antenna at 2.4 GHz.

H-plane cross-pol properties of the patch. Now this concept is being applied to a case of square patch antenna. The antenna structure chosen for the study and its dimensions have been shown in Figure 2.5a. The antenna is optimized for 2.4 GHz and its simulated S_{11} response is shown in Figure 2.5b. The simulated far-field patterns of the antenna at the resonance frequency are shown in Figure 2.6. It can be observed that E-plane cross-pol is much lower (-40 dB) as compared to H-plane cross-pol (-18dB). This observation conflicts with the cavity model for patch antenna,

which predicts low cross-pol in both the principal planes

2.3.1 Near-field plots

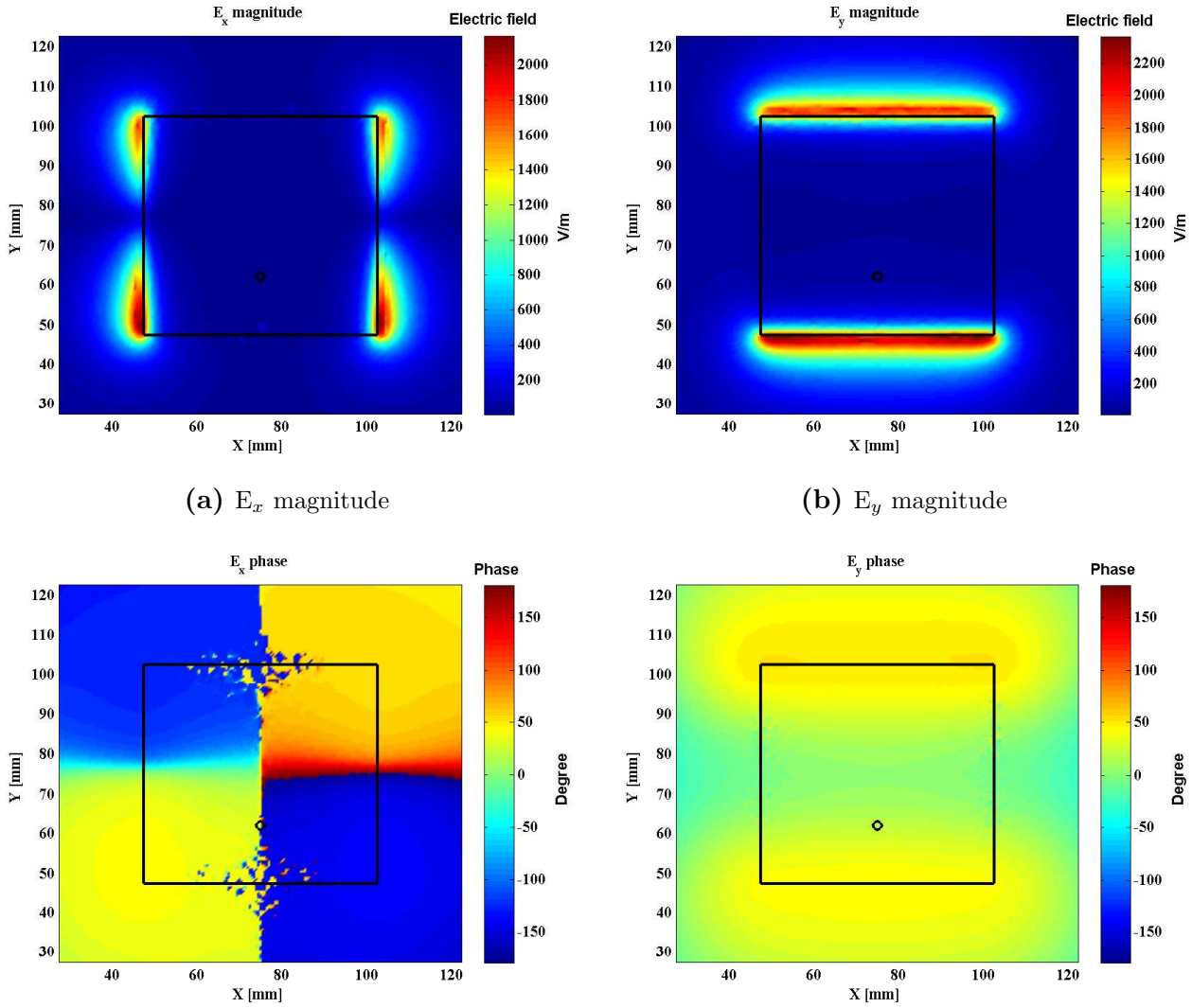

(a) E_x magnitude

(b) E_y magnitude

(c) E_x phase

(d) E_y phase

Figure 2.7: 2-D plots showing E_x and E_y components of electric field observed on the plane 2 mm above the patch antenna. The patch surface boundary and feeding point has been shown in black in each plot.

Figure 2.7 shows the electric field as observed at the chosen plane (2 mm above the patch surface). Plots shown in the figure provide the basic understanding of radiation from a patch

antenna. It can be seen that y-component of the electric field is dominant over the radiating edges of the patch and the phase of this component of the field is uniform over the two radiating edges (Figures 2.7b and 2.7d). These fields contribute to co-polar radiation in the far-field, since they will interfere constructively in the broadside direction because of uniform phase on the aperture. The E_x component of the field is dominant over the non-radiating edges of the patch. Because of the cosine distribution of the field within the cavity, the E_x component of the field can be seen as four lobes of Figure 2.7a, fringing out of the non-radiating edges. Each of these four lobes are 180° out of phase with respect to neighbouring lobe (Figure 2.7c). This means that when these fields radiate, they are going to cancel each other out in principal planes in the far-field. But, radiation will be non-zero in the non-principal plane regions of the space. These fields from the non-radiating edges of the patch constitute the cross-polar radiation pattern of the patch antenna.

2.3.1.1 Error in near-field plot

It has been established in previous sections that the far-field cross-pol in H-plane will depend on the near-field x-component of the electric field. Therefore, in order to understand the H-plane cross-pol, here E_x component of the field is being considered. According to the cavity model, there would be cosine distribution of electric field within the cavity along y-direction, which means that four lobes seen in the E_x magnitude plot in Figure 2.7a should all be equal in magnitude and should be symmetrically distributed on the plane. This is the prime criteria for achieving zero cross-polar radiation in principal planes of the rectangular patch antenna, since the symmetrically distributed field with anti-symmetric phase would cancel out in principal planes.

A cursory glance at the E_x magnitude distribution plot Figure 2.7a reveals that field distribution is not symmetric with respect to x-z plane (H-plane). It can be observed that the field distribution in the lower half of the plane is stronger as compared to the upper half of the planar region. The field distribution is, however, symmetrical with respect to the y-z plane (left to right symmetry in figure). Clearly, this is an effect caused by the unsymmetrical position of

probe feeding the antenna. For the purpose of impedance matching and excitation of dominant radiating mode in the patch cavity, the probe has to be at an offset position, making the patch structure asymmetrical with respect to H-plane. This asymmetry with respect to the H-plane creates a deviation from the ideal theoretically predicted near-field, which would be referred to as near-field errors from now on. Also, since the asymmetry is only along one of the principal planes, the other plane (E-plane) has low cross-polar radiation as expected from theoretical cavity model.

2.3.1.2 Quantization of the near-field error

The near-field distribution of the E_x component of the electric field deviates from what is expected ideally. In order to understand and characterize this anomaly, it should be quantitatively evaluated and represented in terms of numbers. Figure 2.8 shows the values of the near-field E_x component (phase and magnitude) obtained from simulation, when the antenna is excited with 1 W power. In order to simplify the numbers, the field magnitude values have been averaged over each lobe*, whereas phase is considered as obtained at the point right at the corner of the patch. It should be noted that ideally the magnitude of the E_x field should be same in all four lobes along non-radiating edges. The phase in each lobe should be 180° out of phase with respect to their vertical or horizontal neighbour lobe. But Figure 2.8 shows that the probe asymmetry creates difference in the field strength along y-axis. The phase difference between two lobes along y-direction is around 169° (for left hand edge) and 191° (for right hand edge), each of them are deviated from expected 180° by 11°. Along x-axis, the magnitude for the two lobes is same and the phase difference is exactly 180°, as expected from the theory.

The observed anomaly in the near-field can be modelled using two numbers representing the phase and magnitude errors in the near-field. The amplitude and phase observed at the diagonally opposite corners of the patch should be same for an ideal case, assuming there are no phase or magnitude errors. Hence, near-field errors can be conveniently defined by comparing the fields over the diagonally opposite corners. To estimate the error in amplitude from one diagonal

*Distribution of field around each peak is referred to as lobe

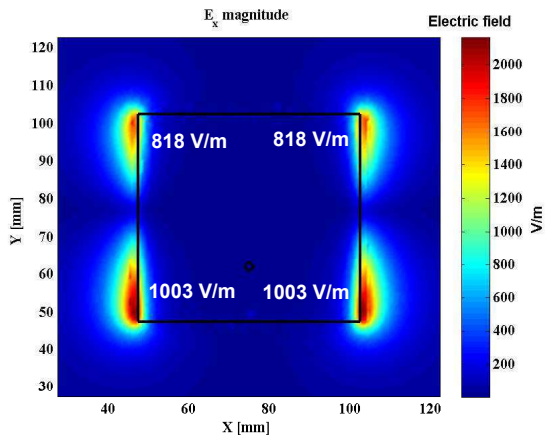

(a) Near-field amplitude error (1 Watt port excitation)

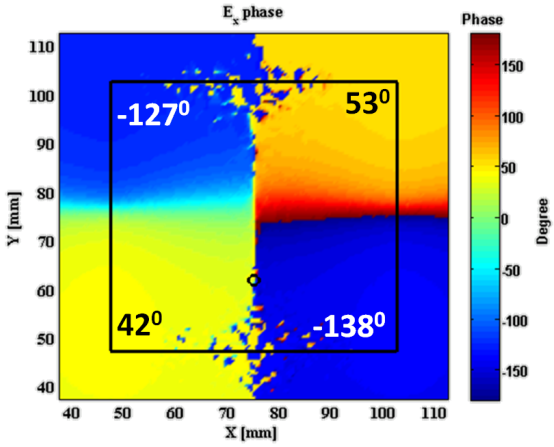

(b) Near-field errors in phase (1 Watt port excitation)

Figure 2.8: The asymmetry in the near-field E_x component modelled in terms of phase and amplitude variations.

point to the other, average value of the magnitude of electric field in a rectangular region just above the corner of the patch antenna is calculated. The chosen region for such calculation has been shown as boxed region in Figure 2.9a. To estimate the phase error, a difference between the phase values of the fields right above the corner of the patch can be calculated. The amplitude and phase errors can be defined as following:

$$e_{amp} = 20 \log \frac{E_1}{E_2} \tag{2.5}$$

$$e_{phase} = \phi_1 - \phi_2 \tag{2.6}$$

Table 2.1: Near-field data for the design shown in Figure 2.5a

Parameters	E_1	E_2	e_{amp}	ϕ_1	ϕ_2	e_{phase}	XP†
Values	1003 V/m	818 V/m	2 dB	42°	53°	-11°	-17.7 dB

†XP means far-field cross-pol

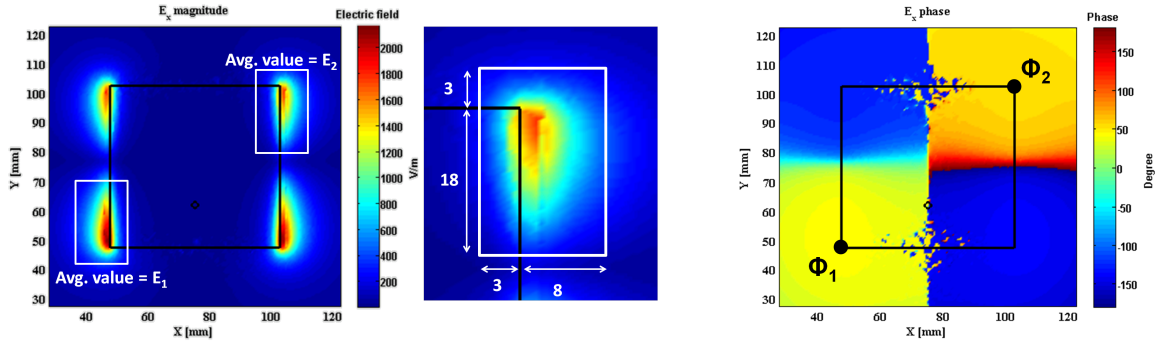

(a) Choice of region for averaging the fields near the corner of patch. Magnified view to show the dimensions (in mm) of the chosen box.

(b) Phase values are chosen right above the corner points of the patch antenna.

Figure 2.9: Near field phase and amplitude error quantization.

Here E_1 and E_2 are the average values of the fields calculated in the boxed regions as shown in Figure 2.9a and ϕ_1 and ϕ_2 are the phase values of E_x component of the field at the diagonally opposite corners, as shown in Figure 2.9b. It should be noted that cross-pol level (denoted by XP) for any cutis defined as the maximum cross-pol level found for all values of θ, normalized with the maxima co-pol component. e.i:

$$XP = \max_{-\frac{\pi}{2} \leq \theta \leq \frac{\pi}{2}} \left[E_{XP}^{dB}(\theta, \phi) \right] - \max_{-\frac{\pi}{2} \leq \theta \leq \frac{\pi}{2}} \left[E_{CO}^{dB}(\theta, \phi) \right] \tag{2.7}$$

For the patch antenna shown in Figure 2.5a, the near-field phase and amplitude values and corresponding errors have been tabulated in Table 2.1. Note that this data is obtained at the frequency of resonance of the antenna, i.e. 2.4 GHz. It can be observed that there is considerable deviation of in the magnitude and phase of electric field E_x component giving rise to high H-plane cross-pol in far-field.

2.3.2 Frequency dependence of near-field errors

The near-field of the patch antenna is generated from the distribution of the cavity mode fields within the patch. Therefore, the error in the near field means that there is similar error in the cosine distribution of the field within in the patch cavity. Hence, it can be said that, due to

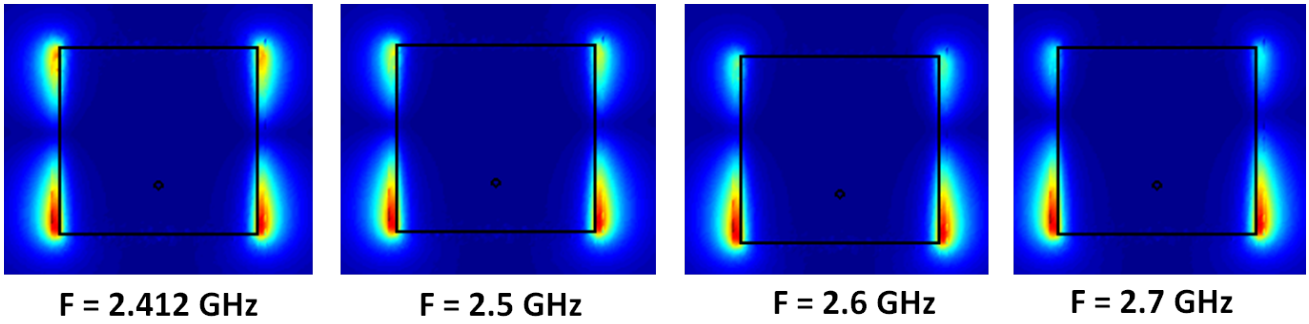

Figure 2.10: Variation of near-field E_x field magnitude with changing frequency.

presence of asymmetrical excitation, the fields within the cavity re-distribute themselves such that lobes across H-plane are of different phase and magnitude values. But, the re-distribution is still a result of resonance within the structure and would certainly change if the frequency of excitation is changed. It would an interesting exercise to understand the nature of behaviour of these near-fields with changing frequency of operation. Figure 2.10 shows the variation magnitude of E_x field with increasing frequency. This figure shows how the distribution of field can be a function of frequency and can be adjusted by changing the frequency. To see the variation trend of the phase and amplitude error of E_x component, they have been plotted with respect to changing frequency in Figure 2.11. Note that these results are obtained from simulation of the patch antenna shown in Figure 2.5a. The plot presents the variation of absolute value of error, since both negative as well as positive errors will contribute to higher cross-pol. Figure 2.11a shows that the amplitude and phase error increase with increasing frequency above frequency of resonance (2.4 GHz). At 2.3 GHz, both frequency and phase errors are minimum. Below 2.3 GHz, again the amplitude errors increase. The minimum phase error is observed at 2.2 GHz.

The far-field cross-pol of the antenna, with varying frequency, is plotted in Figure 2.11b. The cross-pol level is defined as in equation 2.7. Note that this cross-pol data is directly obtained from far-field results from full wave simulation. The trend in the far-field cross-pol is in agreement with the near-field phase and amplitude errors. The minimum cross-pol is found to be at around 2.3 GHz, which is also the frequency with minimum near-field errors.

The presented results show that deviation of the near-field from ideal cavity model is very much dependent on the frequency of operation. This variation of near-field distribution gives

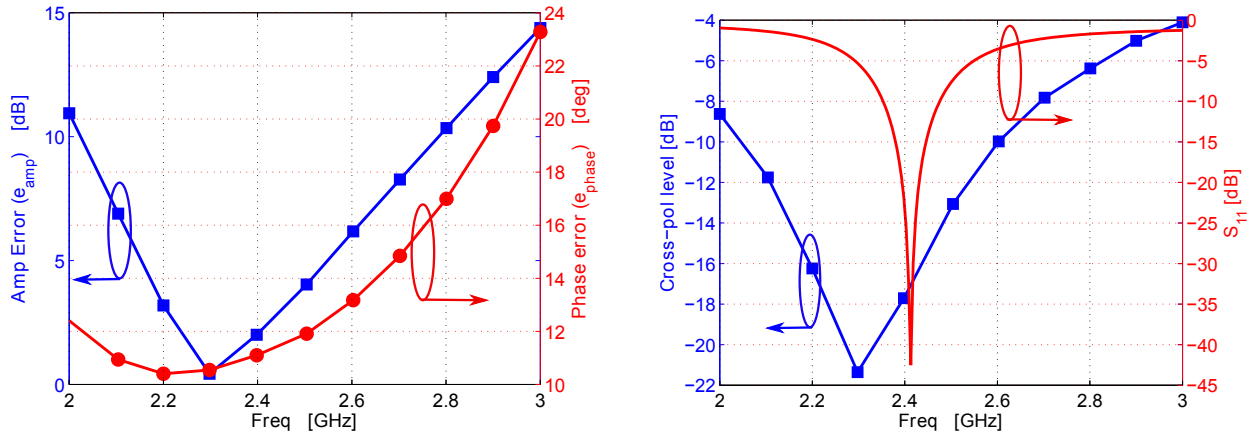

(a) Amplitude and phase errors with changing frequency

(b) H-plane cross-pol level with changing frequency

Figure 2.11: Variation of near-field errors and corresponding variation in far-field cross-pol level.

rise to fluctuating changes in the far-field cross-pol. This phenomenon can be potentially used to minimize the cross-pol in the patch antenna. For the given case of patch antenna, near-field amplitude errors can be reduced to almost zero, while the phase errors can be reduced to 10°, by selecting appropriate frequency of operation. Of course, such an optimized frequency of operation may be out of the frequency band of -10 dB S_{11} response, as shown in Figure 2.11b. It is belief that, it is possible to design a structure which can have resonance at the frequency where the cross-pol is minimum, however such a study is left as future scope of this work.

2.3.3 Parametric study

Since the field distribution within the structure is dependent on various dimensional parameters of the structure, the near-field errors will change with changing parameters. A study was conducted to understand the change in the near-field distribution with changing dimensional parameters. Three parameters have been chosen for this parametric study - port position, width of the patch and the thickness of the patch.

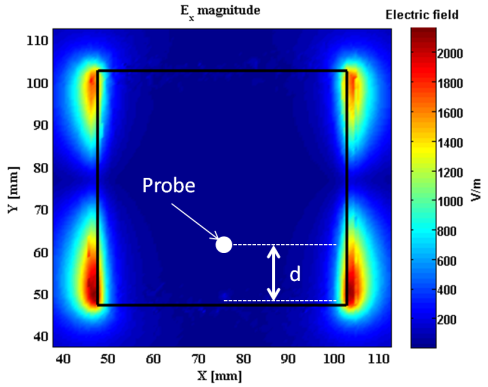

(a) The parameter variation under study

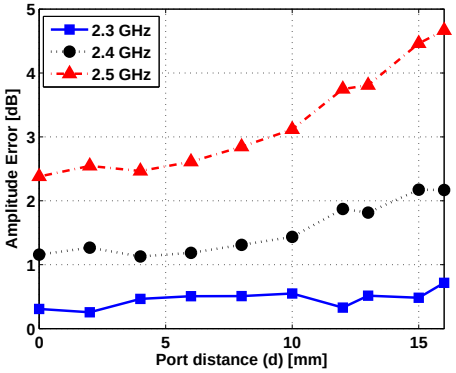

(b) Variation of amplitude errors with changing position of probe at different frequencies

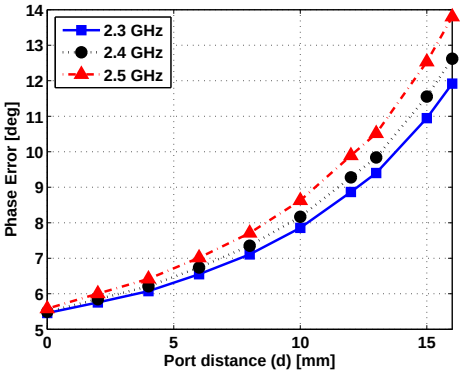

(c) Variation of phase errors with changing position of probe at different frequencies

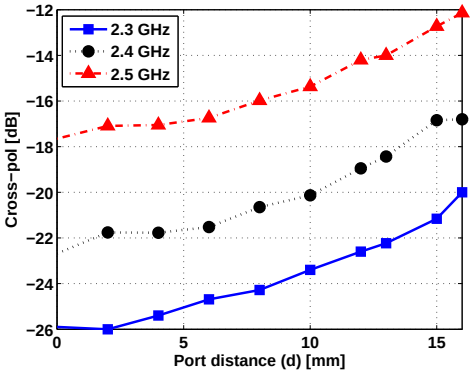

(d) Far-field cross-pol variation with changing probe position at different frequencies

Figure 2.12: Variation of near-field errors and corresponding variation in far-field cross-pol level with changing port distance from edge.

2.3.3.1 Port position

So far, it has been shown that the errors in the near-field are due to the asymmetrical patch structure with respect to the H-plane. This asymmetry is because of the asymmetry in the feeding position and therefore the near-field error is expected to be a function of position of the feeding probe. Figure 2.12 shows the variation in the near-field phase and amplitude errors with changing port position from the edge of the patch, for three frequencies.

As the position of feeding probe moves away from the edge, the phase and magnitude errors increase leading to higher cross-pol, as shown in Figure 2.12b - 2.12d. Similar results have been previously shown in [25] for inset fed patch antenna. It has been argued in [25] that in case of inset feeding, the notch causes disturbance in the original rectangular patch shape. This disturbance is more when the feeding position is far from edge. Such a deviation from original rectangular shape causes disturbance in the currents causing higher cross-pol. Such a disturbance in currents increases with increasing notch depth.

It is interesting to see that the cross-pol increases when the feeding probe is moved away from the edge, even in probe fed case. However, the reasoning of disturbance of rectangular shape cannot be applied here, since probe feeding does not disturb the rectangular shape of the patch. For probe fed case, near-field errors explain the change of cross-pol level depending on the changing probe position. The changing position of excitation changes the field distribution within the cavity creating variations in near-field error. This decreases the cross-pol in the far-field. However, the reason for decrease in the near-field errors with decreasing distance from the edge is not clear so far.

2.3.3.2 Width of the patch

The relation between the width of the patch and H-plane cross-pol level has been studied previously in [21, 26]. For probe fed case [21], it was found that the lowest H-plane cross-pol is found for a width to length ratio of 1.5. In [26], similar study is conducted for both inset fed and coaxially fed patch antenna and it was reported that for edge fed patch, width to length ratio of 1.5 is optimum for minimum cross-pol, whereas for the probe fed case, the cross-pol monotonically

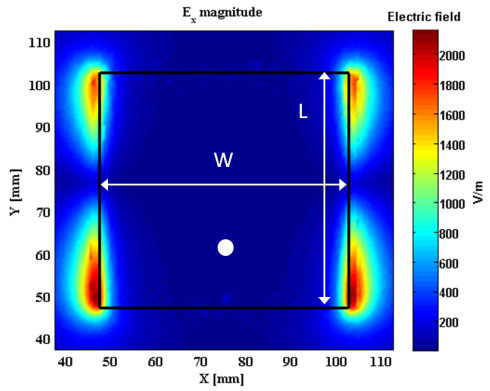

(a) The parameter variation under study

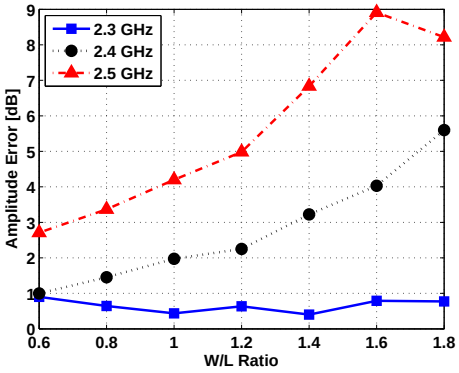

(b) Variation of amplitude errors with changing width

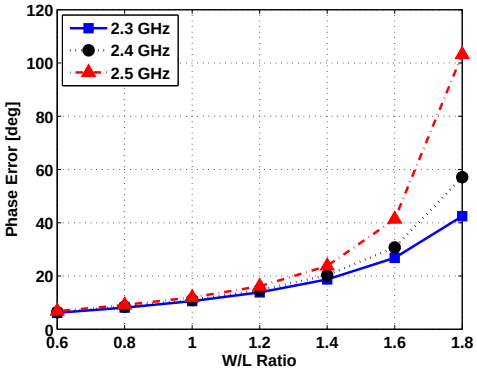

(c) Variation of phase errors with changing width

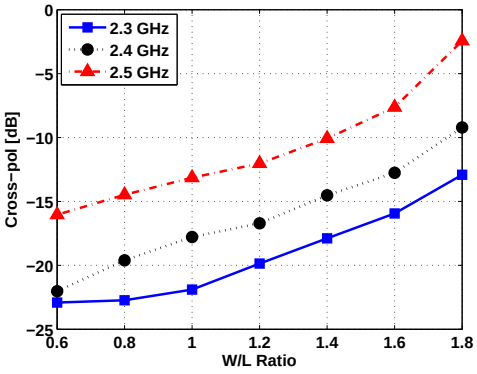

(d) Far-field cross-pol variation with changing width

Figure 2.13: Variation of near-field errors and corresponding variation in far-field cross-pol level with changing width of the patch.

increases after unity ratio. For the probe fed case, the probe location chosen in [21] and [26] is different which explains the difference in obtained results in these two papers.

The results of parametric study conducted in this work is presented in Figure 2.13. Te general trend is increase in near-field phase and magnitude errors, with increasing width, leading to increasing cross-pol. This is in agreement with [26], where authors have shown by measurement that for coaxially fed case, the cross-pol monotonically increases with W/L ratio till it reaches 2.

Apart from general trends, some other key features are noteworthy in the plots in Figure 2.13. At frequency 2.3 GHz, the amplitude errors increase very slightly on changing the width and similar trend is observed for phase errors. However in the region W/L = 1.6 to 1.8, the phase errors increase rapidly. Similar observations are made by authors in [26] in the region after W/L = 1.8. In general, frequency 2.3 GHz, shows more resistance to cross-pol degradation, which has been observed in previous sections too.

2.3.3.3 Thickness of the patch

It has been shown in [20] that cross-pol of patch antenna increases with increasing thickness of the substrate for low values of substrate permittivity and decreases with increasing thickness for higher values of substrate permittivity. In this study, it was found that amplitude errors in the patch antenna first decrease and then increase, when the thickness of the patch is increased (Figure 2.14b). However, the low-point for amplitude error can change depending on the frequency of observation. The phase errors show increasing behaviour with changing thickness as presented in Figure 2.14c. As a result of these variations, cross-pol level in H-plane shows first decreasing and then increasing behaviour with changing thickness of the patch antenna. The cross-pol behaviour is very similar to amplitude errors, since difference in phase errors is very small among frequencies under consideration. Therefore, cross-pol behaviour over various thickness values is dominated by amplitude error behaviour.

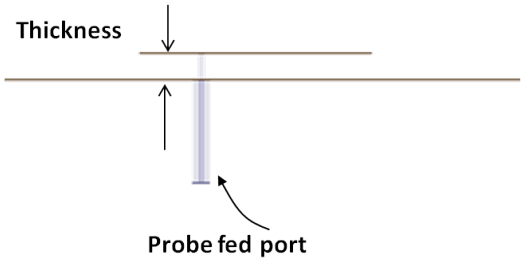

(a) The parameter variation under study

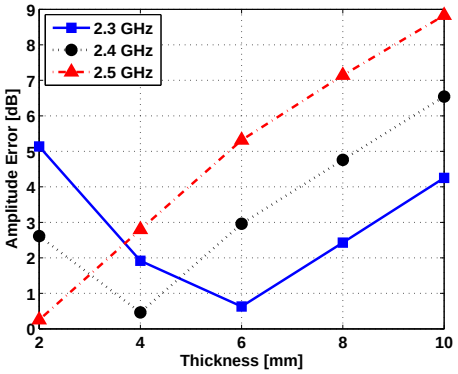

(b) Variation of amplitude errors with changing thickness of the patch

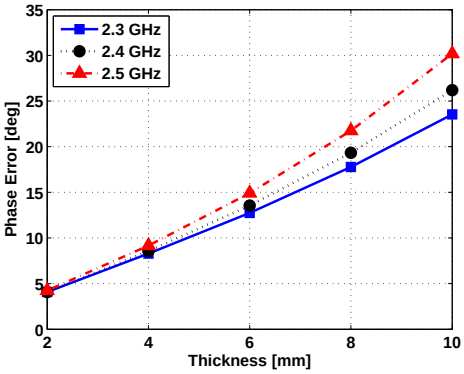

(c) Variation of phase errors with changing thickness

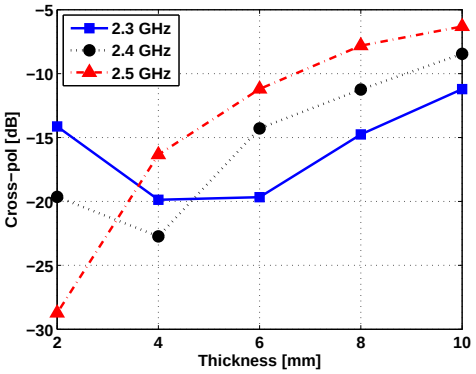

(d) Far-field cross-pol variation with changing thickness

Figure 2.14: Variation of near-field errors and corresponding variation in far-field cross-pol level with changing thickness of the patch.

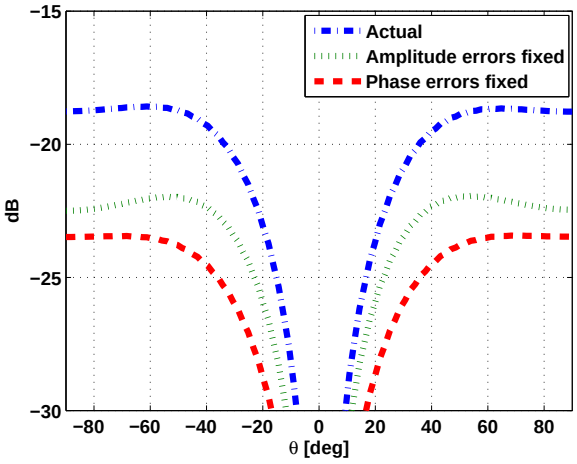

Figure 2.15: Comparison of H-plane cross-pol of the patch antenna for three cases showing the cross-pol reduction by only correcting amplitude error and only phase error.

2.4 Application of the Concept to Low Cross-pol Configurations

In order to have a reduced cross-pol in the far-field of a patch antenna, it is necessary that the near-field errors should be reduced. It can be shown that reduction of phase as well as amplitude errors is required to fully decrease the H-plane cross-pol of the antenna. Figure 2.15 shows the cross-pol from patch antenna in three different cases. The 'actual case' in the figure is the cross-pol as obtained from full-wave simulation of the patch antenna structure shown before. Other two cases in the figure correspond to the hypothetical cases, in which the actual near-fields in the observation plane have been modified and then far-field cross-pol in H-plane is calculated.

The 'amplitude errors fixed' case is the case, when only the amplitude errors in the observation plane are corrected making all four lobes in the Figure 2.8a equal and symmetrical. Similarly, the 'phase errors fixed' case corresponds to the case when phase is made exactly anti symmetrical making $\phi_1 = \phi_2$ in Figure 2.8b. This plot comparing the three cases is useful in understanding the breakup of the H-plane cross-pol generated by amplitude and phase errors. For the given case, it is clear that the phase errors create more cross-pol as compared to amplitude errors in the near-field. However, in order to have a good cross-pol response from the patch antenna, both phase and amplitude errors should be corrected in the near-field.

One of the most popular and simple technique of reducing the cross-pol in patch antennas is use of differential feeding [27]. In case of arrays, same concept can be extended to so called "rotating feed", which helps in the reduction of cross-pol [28]. In both techniques the antenna is fed from symmetrically opposite points with 180° phase difference. Such an arrangement constructively adds the power from the two feeding points for co-pol radiation. However, according to [27], the introduction of differential probe in the patch antenna generates additional leakage radiation from the second probe, which is out of phase from the original leakage radiation of the first probe. This causes cancellation of the spurious field resulting in low cross-pol in H-plane. In [28], the technique has been extended without any further explanation on its operation. Here, these techniques are studied in greater detail under the light of the developed tool for understanding cross-pol radiation from rectangular patch antennas.

2.4.1 Differential feeding

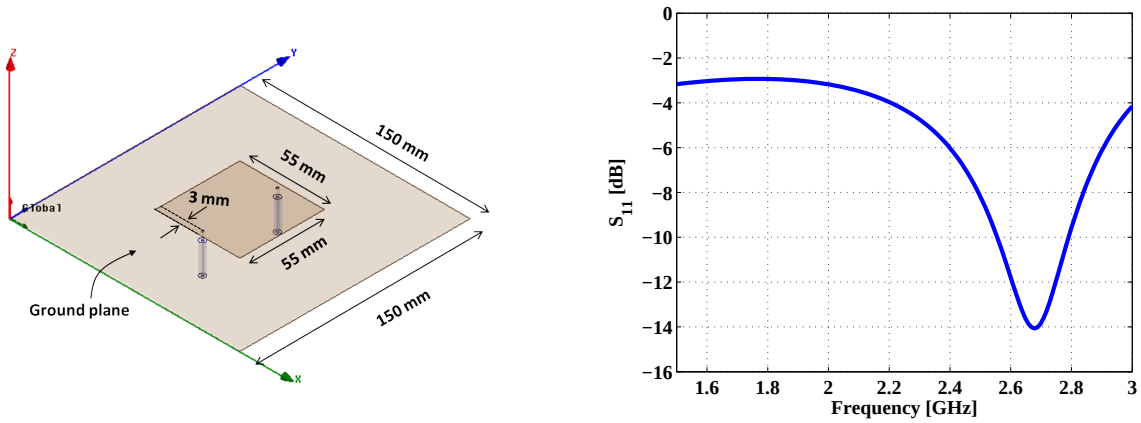

(a) Differentially fed patch antenna under study

(b) S_{11} response of the differentially fed patch antenna

Figure 2.16: Differentially fed patch antenna and its return loss response.

To understand the reasoning behind reduction of cross-pol in differentially fed patch antenna design, a differentially fed configuration has been considered with dimensions as shown in the Figure 2.16a. The thickness of the patch antenna is 5 mm and the dielectric chosen is air. The resonance of the antenna is obtained at 2.68 GHz, as shown by S-parameter response in Figure

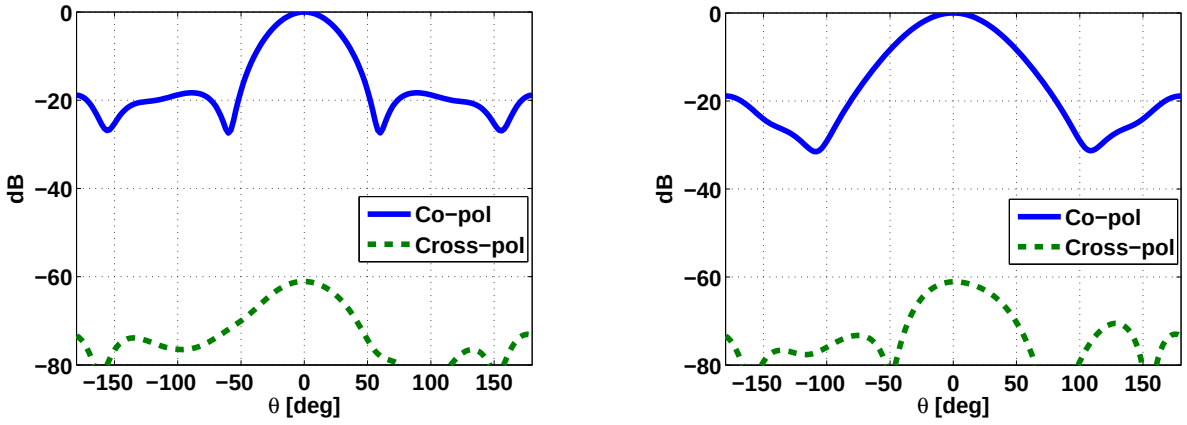

(a) E-Plane **(b)** H-Plane

Figure 2.17: The simulated far field radiation patterns for differentially fed patch at 2.68 GHz.

2.16b (identical for both the ports.). The far-field patterns at the resonance frequency show that antenna shows excellent cross-pol response in both the principal planes (Figure 2.17).

The RF operation of this topology can be easily understood, if the excitation of individual ports is considered separately. Figure 2.18 shows near-fields on the observation plane of the antenna when only port one (shown as encircled port in the Figure) is excited. The frequency of operation is chosen to be the resonant frequency of the antenna, i.e. 2.68 GHz. It can be observed that amplitude errors are small, since the port position is very near to the edge of the patch, as discussed in the previous sections (Figure 2.12b). The phase errors are quite large, which would create high cross-pol in the far-field.

Similarly, Figure 2.19 shows the near-field plots of the antenna when only port 2 (shown encircled) is excited with 180° phase shift. It can be seen that amplitude and phase distributions in two cases is juxtaposed and two fields are exactly anti-symmetrical. When both the ports are excited simultaneously, these two field distributions will be superimposed and added. The phase and amplitude errors present in each field distribution compensate for each other and create a field which does not have any errors. Figure 2.20 shows the field distribution on the observation plane when both the ports are excited. The phase and amplitude errors are reduced to almost

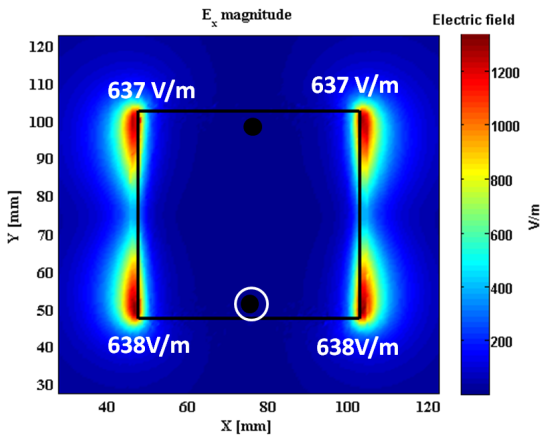

(a) Amplitude error = -0.0084

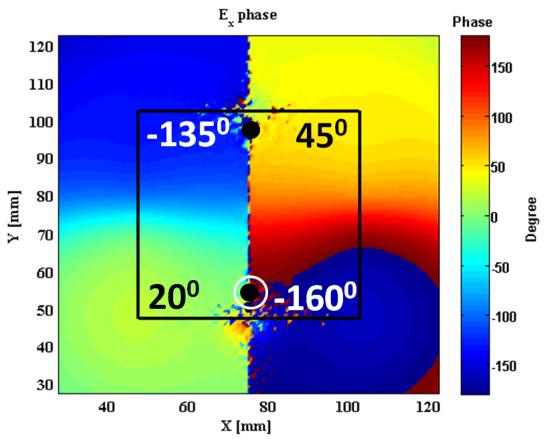

(b) Phase error = -25°

Figure 2.18: The amplitude and phase distribution with calculated phase and amplitude errors in differentially fed patch antenna when only port one excited.

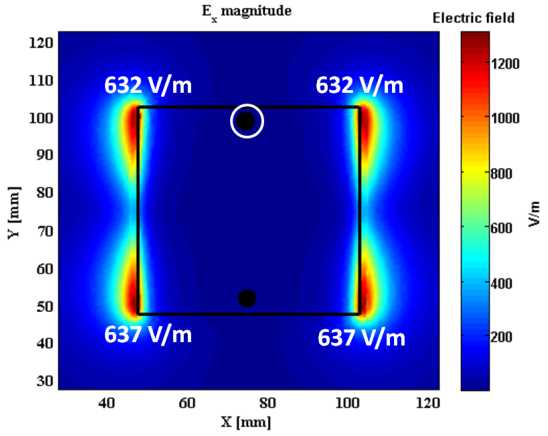

(a) Amplitude error = 0.07

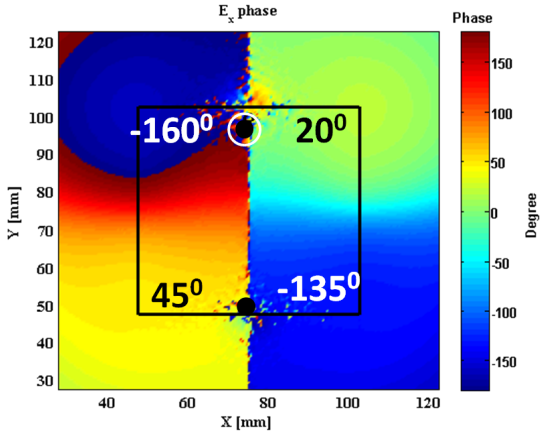

(b) Phase error = 25°

Figure 2.19: The amplitude and phase distribution with calculated phase and amplitude errors in differentially fed patch antenna when only port two excited with 180° phase shift.

zero. In phase plot each lobe has 180° phase shift with respect to neighbouring lobe in x and y directions. Here the lack of exact anti-symmetry in each port excitation has been restored by excitation of both the ports with phase shift.

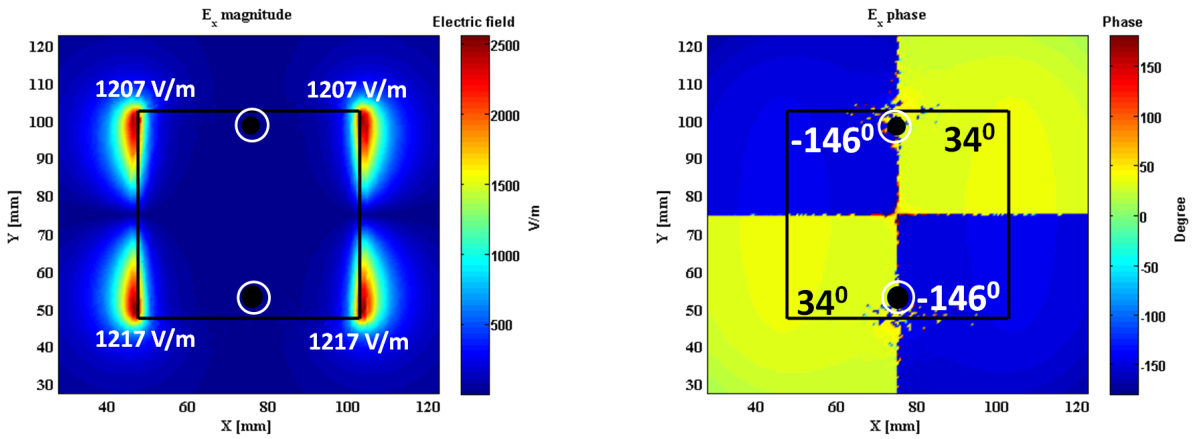

(a) Amplitude error = -0.07

(b) Phase error = 0°

Figure 2.20: The phase and amplitude in the near-field when both the ports are excited. The errors are reduced almost to zero.

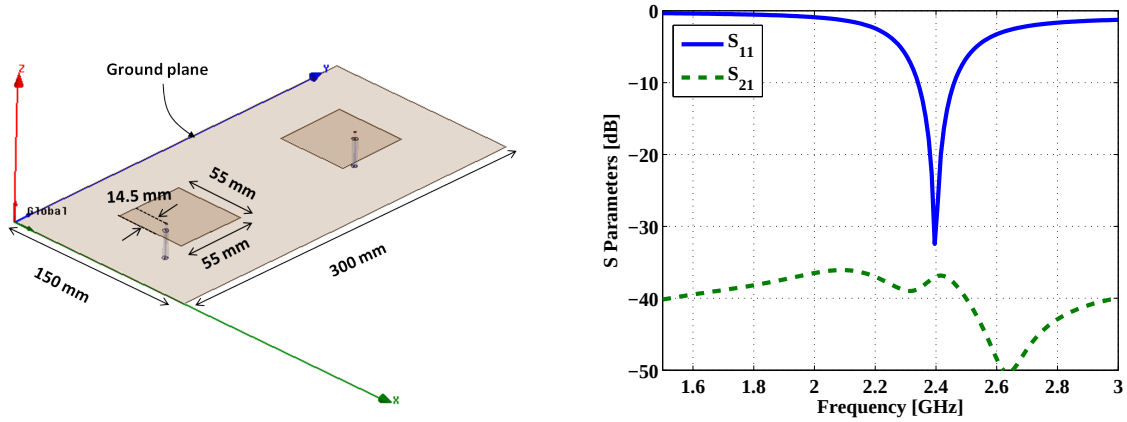

(a) An array of 2 by 1 rotationally fed patch elements

(b) S_{11} response of the each element of the array

Figure 2.21: A 2 × 1 array of patch antennas considered for the study.

2.4.2 Rotating feeding

For arrays, the H-plane symmetry can be restored using the concept of rotating feed network. The technique is very similar to differential feeding except for its extension to multiple elements in an array instead of one element. In order to study the operation of this technique in terms of near-field model, a rotating feed array of 2 × 1 is considered as shown in Figure 2.21. Element

dimensions and its S_{11} (Figure 2.21b) response is same as what was chosen before in Figure 2.5a. Again, the antenna shows excellent cross-pol performance in both the principal planes as shown in Figure 2.22.

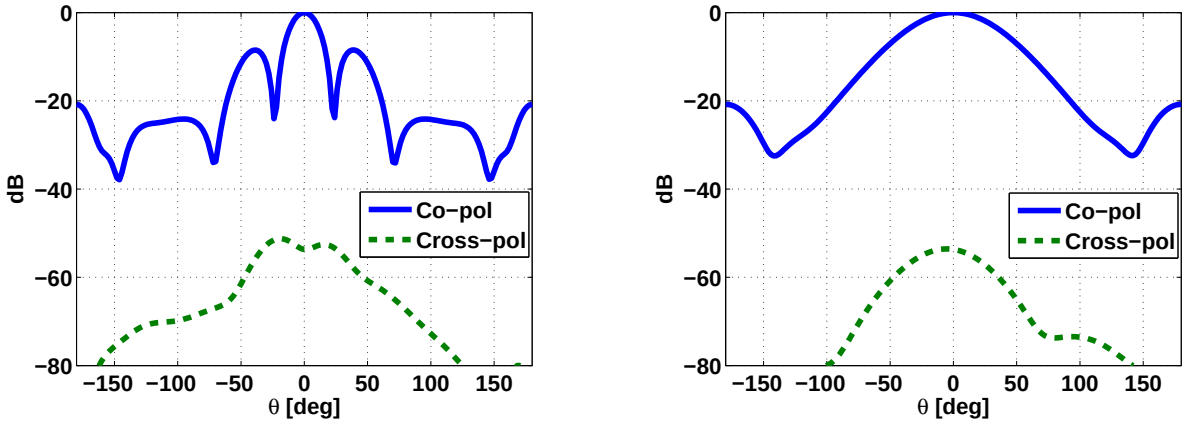

(a) E-plane radiation pattern

(b) H-plane radiation pattern

Figure 2.22: Radiation patterns of 2 × 1 array of rotationally fed patch antennas.

The near-field E_x component plots of this antenna are shown in Figure 2.23. Each of the individual elements have amplitude and phase errors. But these errors are anti-symmetrically located with across H-plane (i.e. plane y=150 mm). For example, the fields at the points (55,102) and (55,198) are $818\angle -127°$ and $818\angle 53°$ respectively. These fields are equal in magnitude and exactly 180° out of phase, which means they will cancel out in the far-field H-plane. Similar conclusions can be drawn for other regions where high electric field is present. This explain how the H-plane cross-pol is reduced for arrays using a rotating feed network.

2.5 Conclusion

A novel approach of understanding the cross-pol in patch antenna has been presented. The model based on the near-fields of the patch antenna, has been used to explain high H-plane cross-pol in rectangular patch antennas. Various parametric studies reveal that, the trend in the cross-pol in the far-field closely follows the trend in the near-field errors in the observation plane. These results are compared with previously published results and a good agreement has

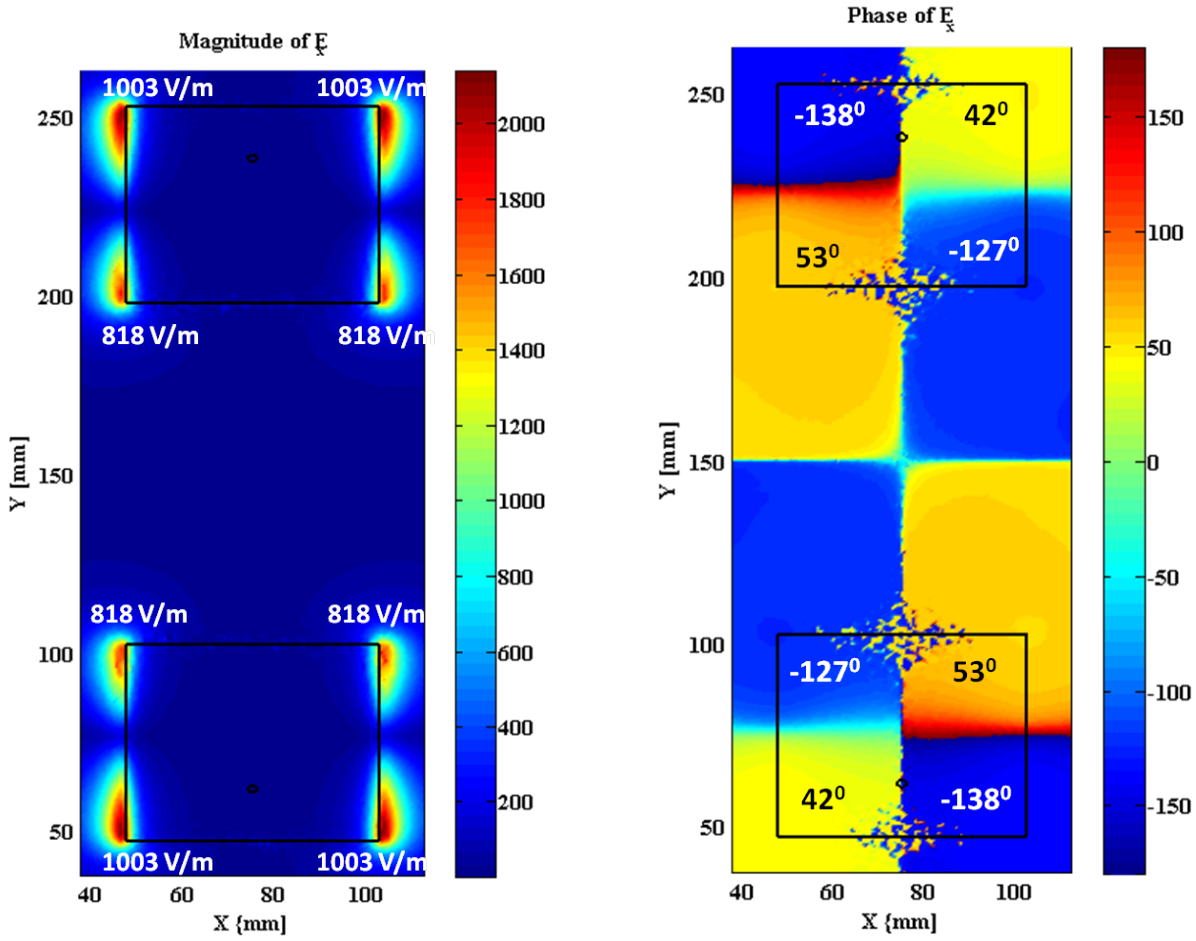

(a) Amplitude distribution in the near-field

(b) Phase distribution in the near-field

Figure 2.23: The phase and amplitude in the near-field for a 2 × 1 rotationally fed array, when both the ports are excited. Near-field errors of the individual elements are anti-symmetrically located.

been found. It has been concluded from this study, that near-field errors are a function of patch dimensions and frequency of operation and there is a potential for improving the H-plane cross-pol performance of the antenna by optimizing the frequency of operation or the dimensions. Finally, this technique has been used to understand the mechanism of the cross-pol reduction for two popular configurations of patch antennas - differentially fed patch antenna and patch

antenna array with rotating feeding.

It should be noted that, the current work focuses on understanding the reason for H-plane cross-pol in terms of the near-field generated from the non-radiating edges. Another interesting application of this near-field model would be understanding the effect of the near-field errors on the cross-pol radiation of the antenna in cross-plane ($\phi = 45°, 135°$), since reduction cross-pol radiation in these planes is critical for weather radar applications. However, such a study was not pursued in this work and would be an interesting topic for future work.

This analysis proves very helpful in providing a physical insight into the generation of cross-pol in rectangular patch antennas. It can be directly concluded that patch antenna asymmetry manifests itself in terms of near-field phase and amplitude errors, which is nothing but a deviation from theoretically predicted near-field distribution. Clearly, such errors in the near-field cause high H-plane cross-pol in the far-field. This analysis would be helpful in understanding the cross-pol in patch antennas and to potentially develop patch antenna structures with low cross-polar radiation.

CHAPTER 3

A Comprehensive Review of C-Shaped, E-Shaped and U-Slotted Patch Antennas

Slotted antennas have been widely popular for the application of wide-band and/or miniaturized antenna [29–34]. In the current application, achieving wide-band response is one of the prime objectives and hence there is a possibility that these antenna types can be utilized here. In order to study and understand the applicability of slotted antennas, a comparative study among some popular types of slotted antennas is conducted and presented in this chapter.

Here, four popular types of slotted antenna are chosen for comparison for their performance within same operation bandwidth of wireless communication frequency band 1.9 - 2.4 GHz. These configurations are: C-shaped [29], double C-shaped [30], U-slotted [31], and E-shaped [32] antennas. Since, these topologies have been prototyped and measured in past [29–32,35,36], this study is focused on comparatively analyzing these configurations, through full wave simulations. A brief introduction of these configurations is presented in next section, followed by comparison in subsequent sections.

The main distinction of this study is analysis of near-field plots in these antennas. These near-field plots reveal interesting feature about the nature of radiation from these antennas. Since conventional thought process about these antennas relies primarily on the current patterns on the surface of the patch, this analysis adds a new dimension by exploring the radiation from slotted structures.

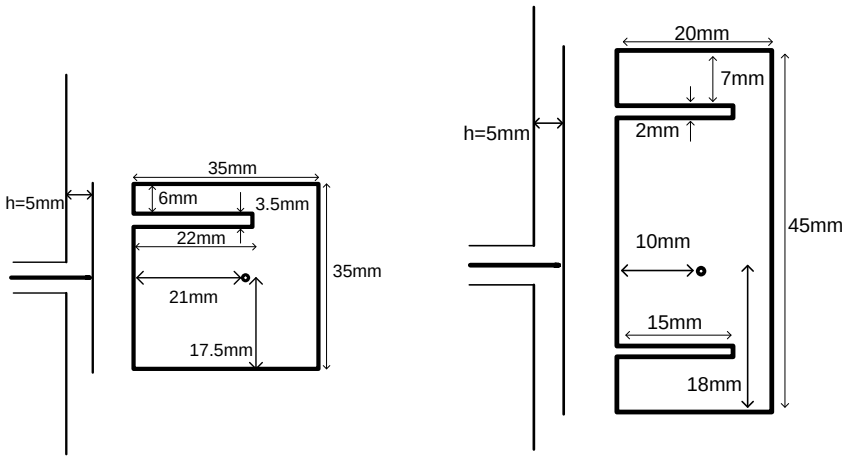

(a) C-shaped **(b)** Double C-shaped

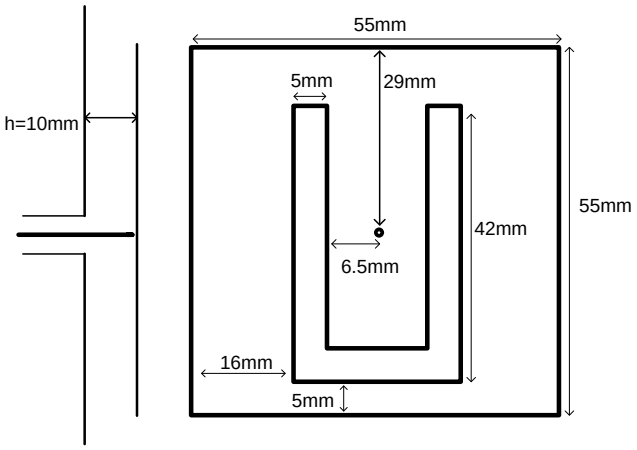

(c) U-shaped

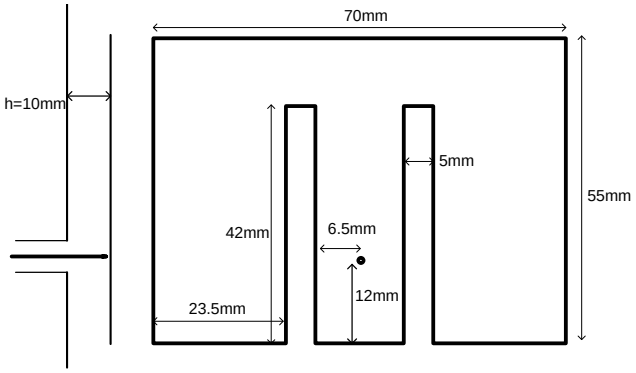

(d) E-shaped

Figure 3.1: Various topologies of slotted antennas under under study along with their dimensions.

3.1 Antenna Topologies Under the Study

A C-shaped patch antenna as shown in Figure 3.1a, is obtained by introducing a rectangular slot parallel to radiating edges of a conventional rectangular patch antenna. Double C-shaped patch antenna can be obtained by introducing two slots located on either side of feed, parallel to radiating edges of a rectangular patch antenna (Figure 3.1b). In Figures 3.1a and 3.1b, the orientation of the antennas can be rotated by 180^o to see the C and double C shape. In order to keep symmetry in figures, the shown figures of the antenna are rotated to keep the radiating edges in the same direction (i.e. horizontal direction). The U-slotted antennas, first reported in [37], are derived from rectangular patch by introducing a U-shaped slot such that the parallel arms of U are parallel to non-radiating edges of the patch (Figure 3.1c). In recent years, E-shaped patch antennas have gained popularity for wireless communications bandwidth 1.9 2.4 GHz and 5 6 GHz [32, 35, 36]. E-shaped patch antenna is obtained by introducing two slots, located symmetrically on either side of feed, parallel to non-radiating edges of a rectangular patch (Figure 3.1d). In Figure 3.1d, the orientation of E shape is rotated to keep the radiating edges (horizontal edges) in the same direction as other antennas. In general, the shape of the double C- and E-shaped patch antennas is similar, but it has been pointed out in [38] that these antenna configurations are indeed quite different in their RF-mechanism. It has been shown in this study that due to difference in specific orientation of slots in E-shaped patch antenna, this antenna has lower level of cross polarized radiation than C and double C-shaped patch antenna in its E-plane. The shape of E-shaped patch antenna is also comparable to U-slotted patch antenna. U-slot in Figure 3.1c, can be interpreted to be shifted all the way down to lower radiating edge in Figure 3.1d to create an E shape. This similarity of shape in E-shaped and U-slotted antennas is cause of similarity in properties in these antennas, as discussed in Sections 3.2.1 and 3.2.2. Figure 3.1 shows the dimensions chosen for the comparison. These dimensions were achieved after optimization for obtaining resonance within the given band of frequencies. The simulations are done with standard SMA connector at input ports. A conventional square patch antenna (not shown in Figure) with side 55 mm, and 5 mm thickness, resonating at $f_c =$ 2.40 GHz, has also been chosen as a reference design for comparison. A ground plane of size

10×10 cm^2 and air ($\epsilon_r = 1$) as substrate are chosen for all the designs. Ansoft HFSS is used for simulating theses designs.

In the current study the thickness of the patch antennas considered for the C-shaped, double C-shaped patch antenna topologies (h = 5 mm) differs from the U-slotted, E-shaped topologies (h = 10 mm). The reasoning behind this choice is to give advantage to different antenna types based on their strong points in different areas.C and double C-shaped designs were reported as compact and miniaturized designs [29, 30]. In these configurations, for high thickness values, the probe inductance severely affects the impedance matching due to small patch size. On the other hand, the E-shaped and U-slotted patches have high impedance bandwidth even at higher thickness values. Also, in E-shaped and U-slotted designs, the height to length ratio plays a role in deciding the ratio of its two resonant frequencies. Since, to achieve wide band operation the two frequencies should be close to each other, it is difficult to optimize a design for 1.9 – 2.4 GHz frequency band with thin substrate thickness (e.g., h = 5 mm). Broadband thin E-shaped designs (<7 mm) have been reported in past [36], but they operate for 5 – 6 GHz frequency band. Keeping these factors in mind, the thickness for C and double C-shaped patch was chosen as h = 5 mm and for E-shaped and U-slotted patch as h = 10 mm. This choice justifies advantages of respective designs in their own thickness domains. Also, the square patch antenna has been chosen with lower thickness (h = 5 mm), since again, with increasing thickness, the impedance matching is degraded due to increasing probe inductance.

3.2 Comparative Study

There are three main categories in which this comparative study can be subdivided. These parts are:

1. S-parameter response
2. Radiation mechanism
3. Far-field properties

These aspects of the comparison hae been discussed in detail in following subsections.

3.2.1 S-Parameter Response (Miniaturization v/s Bandwidth)

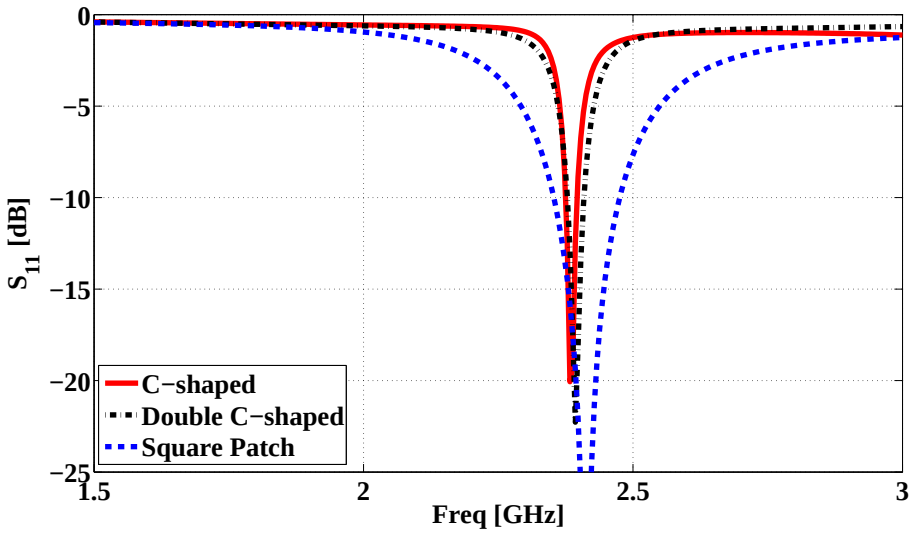

(a) C-shaped, double C-shaped and square patch antenna

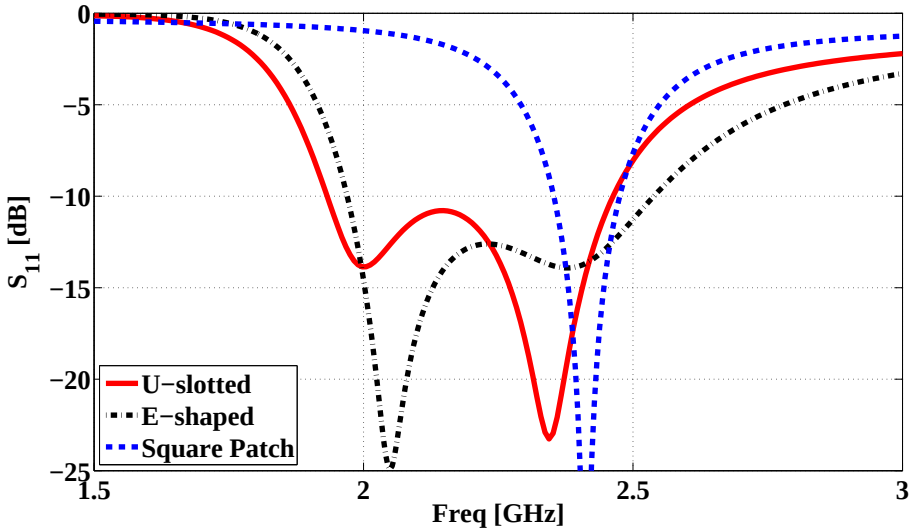

(b) U-slotted, E-shaped and square patch antenna

Figure 3.2: S_{11} response of the four chosen antenna topologies compared with simple square patch antenna.

The position and orientation of the slot with respect to the probe feeding position can change

the S_{11} response of the antenna. The slot can either create a miniaturization effect by effective increase in the current path on the surface of the patch antenna or can create a wide-band response by creating an alternate path of current while maintaining original path, creating a dual-resonance type response of the antenna. These points have been discussed in this section.

A comparison of S_{11} response of the four antenna types is presented in Figures 3.2. In this discussion, the convention of defining bandwidth is $S_{11} < -10dB$. The C-shaped antenna and double C-shaped antennas show a bandwidth of 0.84% ($f_c = 2.38$ GHz) and 1.25% ($f_c = 2.39$ GHz). This is narrow as compared to square patch operating at the same frequency, which gives a bandwidth of 5% ($f_c = 2.4$ GHz) 3.2a. U-slotted antenna shows a dual resonance behaviour with resonance at frequencies 2 and 2.34 GHz with a bandwidth of 24%. E-shaped patch antenna shows the similar behaviour with resonance at 2.05 and 2.39 GHz and bandwidth of 25%. The bandwidths in latter two antennas can be enhanced to as large as 30% with further optimization of geometrical parameters [35, 37], however such a study is not pursued here. The introduction of slot in general can be used either to decrease the size of the patch [29, 30] or to increase the bandwidth [31, 32]. Among the antennas under consideration, C-shaped and double C-shaped patch antenna use slots as device to increase in the current paths. Because of this increase in the current path, effective guided wavelength increases, enabling size-miniaturization. This effect can also be seen as increase in effective inductance due to increase in current path on the patch surface, and hence a decrease in resonance frequency ($f_c = \frac{1}{2\pi\sqrt{LC}}$). The simulated current-flow on the surface of the patch at respective resonant frequencies for C-shaped and double C-shaped patch antennas is shown in Figure 3.3. Clearly, due to slots, the current moves around the slots and effective path of current is increased providing size-miniaturization. Figure 3.4 shows the surface currents of U-slotted patch antenna at resonant frequencies 2.0 and 2.34 GHz. The higher frequency current plots are similar to surface currents on a simple square patch. The lower frequency resonance is created due to introduction of slot, which adds a new current path around the slots (Figure 3.4a). Similar observations can be made about E-shaped patch antenna (Figure 3.5), where currents in higher resonant frequency mode are similar to simple square patch (Figure 3.5b), whereas for lower frequency resonance, we see an increased current path around the slots (Figure 3.5a). The combination of these current paths at two resonances gives the dual

mode wide-band operation. C and double C-shaped patch antennas can be very effectively used for compact designs, because of their miniaturized size [39, 40]. For the dimensions considered under the study, C-shaped patch and double C-shaped patch antennas offer a size reduction of 60 and 70%, respectively as compared to simple square patch. A double C-shaped antenna can be further miniaturized into a more compact design either by folding the patch along the central line parallel to the radiating edge [41] or by shorting one of the radiating edge of a C-shaped design to ground plane and hence generate a double C-shaped structure using ground plane image [39]. For high bandwidth applications, U-slotted antenna and E-shaped antennas are suitable solutions, since they give around 25% increase in bandwidth, with marginal increase in size with respect to simple square patch.

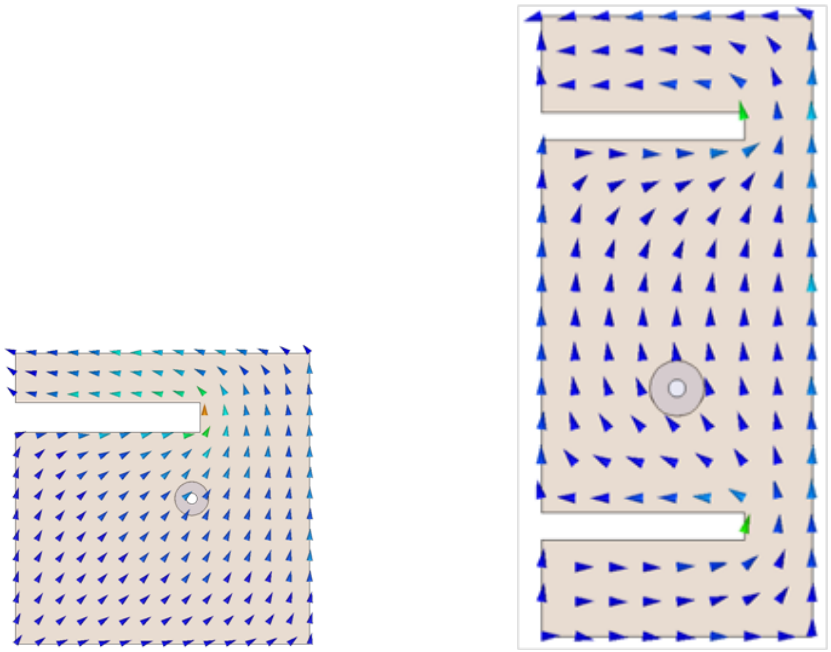

(a) C-shaped ($f_c = 2.38$ GHz)

(b) Double C-shaped ($f_c = 2.39$ GHz)

Figure 3.3: Simulated current-flow at resonant frequency.

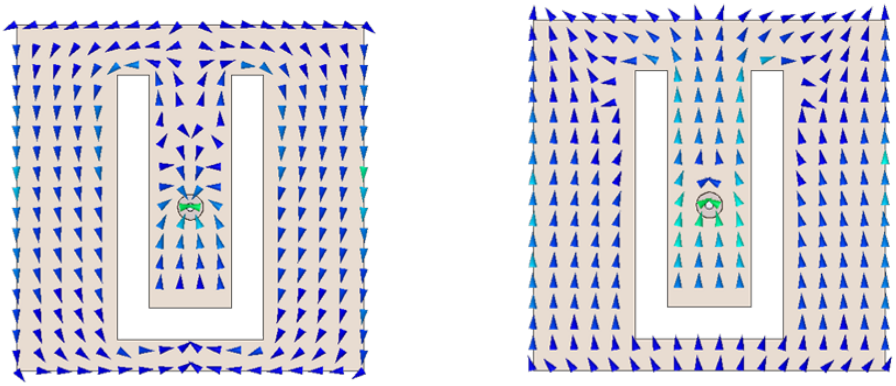

(a) Lower resonance ($f_c = 2.0$ GHz)

(b) Upper resonance ($f_c = 2.34$ GHz)

Figure 3.4: Simulated current-flow for U-slotted patch antenna.

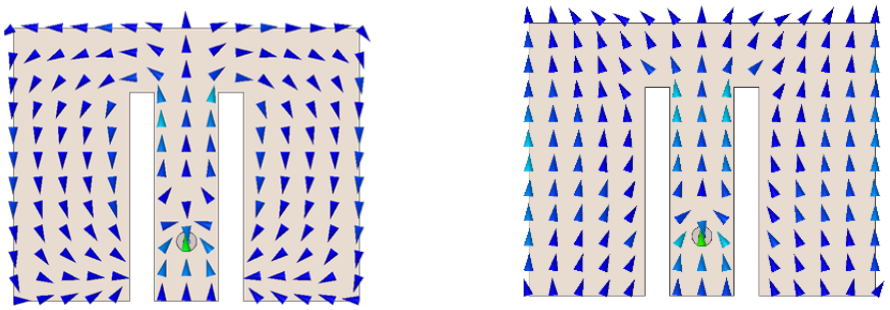

(a) Lower resonance ($f_c = 2.05$ GHz)

(b) Upper resonance ($f_c = 2.39$ GHz)

Figure 3.5: Simulated current-flow for E-shaped patch antenna.

3.2.2 Radiation Mechanism

Conventionally, the current flow on the surface of the patch antenna is used to understand the effect of slot on the performance of the patch antenna [29, 31, 32]. This approach is successful in predicting the circuit related features of the antennas (e.g., S_{11} response), but is not sufficient to give much insight into the effect of slot on the radiation pattern. Reason for this is the fact that radiation from patch antennas depends on the fringing fields at the edges of the patch. Introduction of slot on the patch antenna creates new edges and hence new fringing fields. To understand the effect of these fringing fields on the far-field radiation pattern, here a novel

strategy of looking at the antenna near-fields is presented and utilized. In order to look at the near-fields of each of the topology under consideration, coordinate system shown in Figure 3.6 has been utilized. The patch antenna shown in the figure can be any of the slotted topologies under consideration, depending on whichever topology is being analyzed.

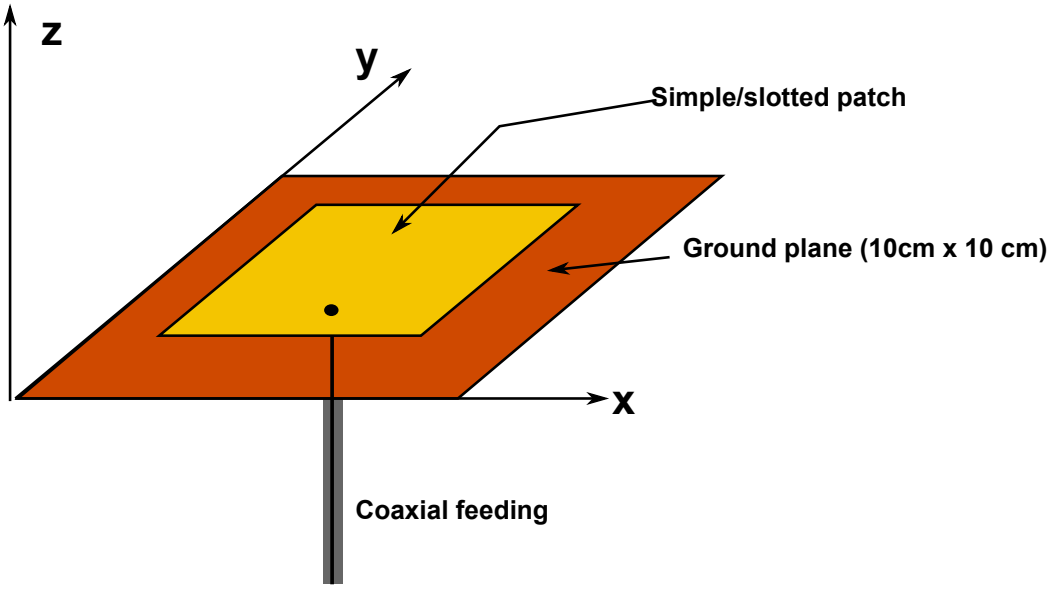

Figure 3.6: Antenna configuration and coordinate system used for the analysis of the all four types of the antennas.

It can be shown by vector potential formulation approach that for a y-polarized linearly polarized antenna (as shown in Figure 3.6), oriented in xy plane, the far-field co-pol radiation component depends on near-field E_y component and cross-pol component depends on near field E_x component of the antenna. An xy plane 2 mm (approx. $\frac{\lambda_0}{75}$) above the surface of the patch has been chosen for plotting the E_y and E_x component of the field.

As a reference, Figure 3.7 shows the plots of the antenna near-fields over a simple square patch antenna. A strong E_y component of the field is observed over x-directed edges and E_x component of the field is observed over y-directed edges of the antenna. Also, the E_y component has same phase on both the radiating edges, which means these fields interfere constructively in broadside to generate a far-field co-pol maxima, whereas the E_x component of the field has a four-lobed pattern such that phases of the field are flipped in each lobe, creating a broadside null. Such a near field pattern would create high co-pol (generated from E_y) and lower cross-pol

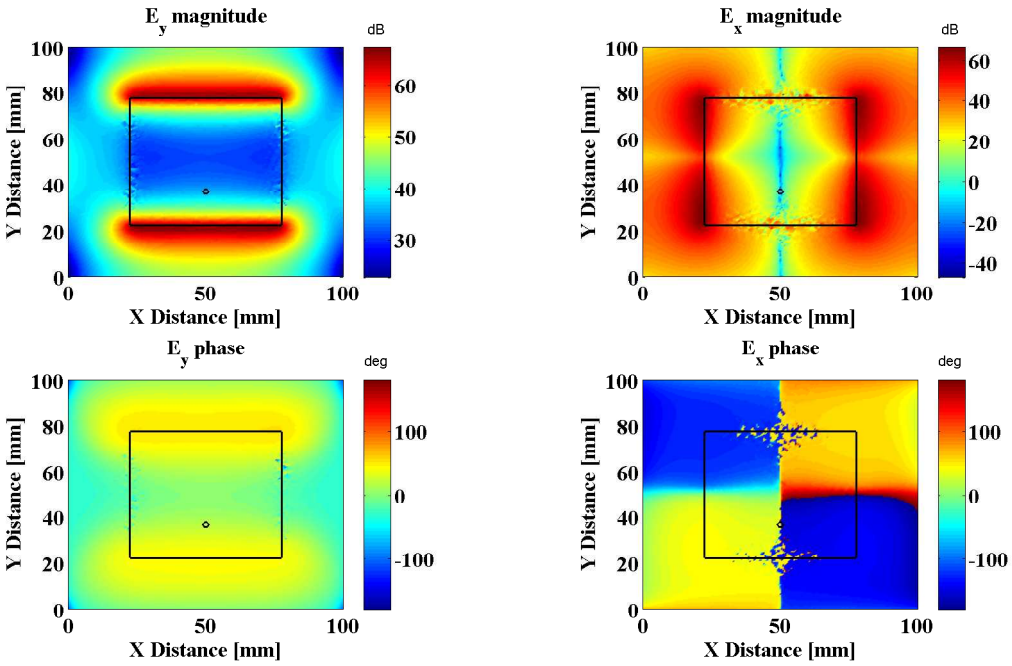

Figure 3.7: Simulated E_x and E_y components of the electric field in a xy plane 2 mm away over the simple rectangular patch antenna ($f_c = 2.4$ GHz).

(generated from E_x) pattern in far-field. This plot also highlights the notion of radiating edges (x-directed) and non-radiating edges (y-directed) in a simple square patch antenna. A similar analysis has been used to understand the radiation mechanism of the slotted antennas.

Figure 3.8 shows the near-field of C-shaped patch antenna under the study. The E_y component of the field, dominant just over x-directed edges of the antenna, is having approximately same phase value at all points in the aperture, and hence contributes to a broadside beam. E_x component has four-lobed pattern with flipped phases creating lower cross-polar component in the far-field. It can be seen that four lobes of E_x component in the near-field for a C-shaped antenna are not exactly antisymmetric since y-directed edge near the slot has high electric field. This lack in antisymmetry in E_x field as compared to simple square patch, causes higher cross-pol level in the far-field for Cshaped patch antenna. This is discussed in more detail in Section 3.3.

The near field plots in case of C-shaped patch antenna carry special importance, since in this type of antenna radiating and non-radiating edges are not clear by jus looking at the antenna geometry or the current flow path. Conventional method of deciding the radiating edges, by

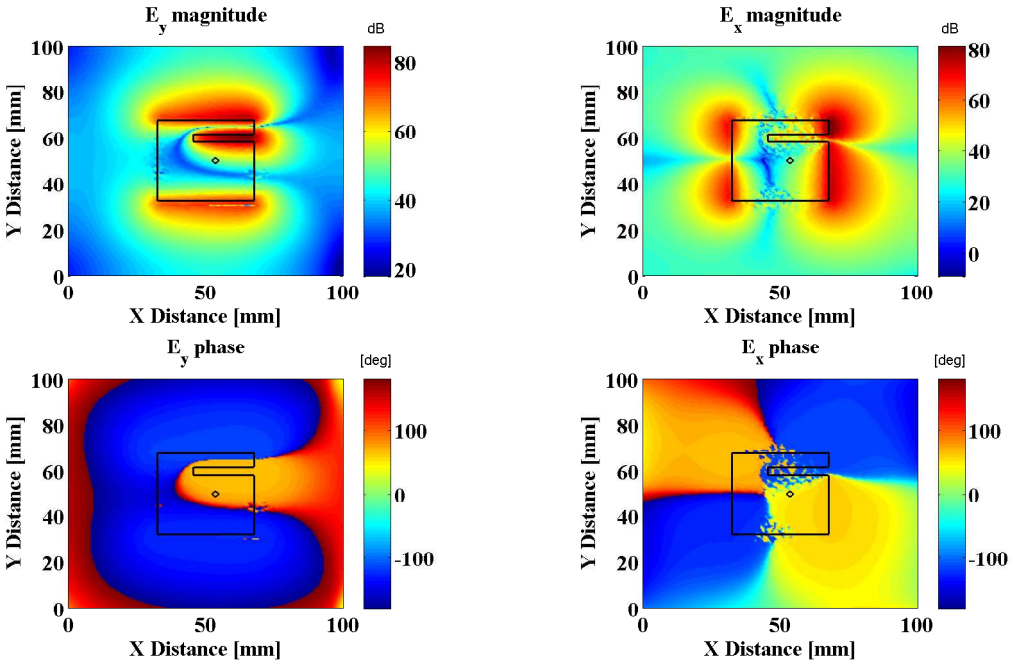

Figure 3.8: Simulated E_x and E_y components of the electric field in a xy plane 2 mm away over the C-slotted patch antenna ($f_c = 2.38$ GHz).

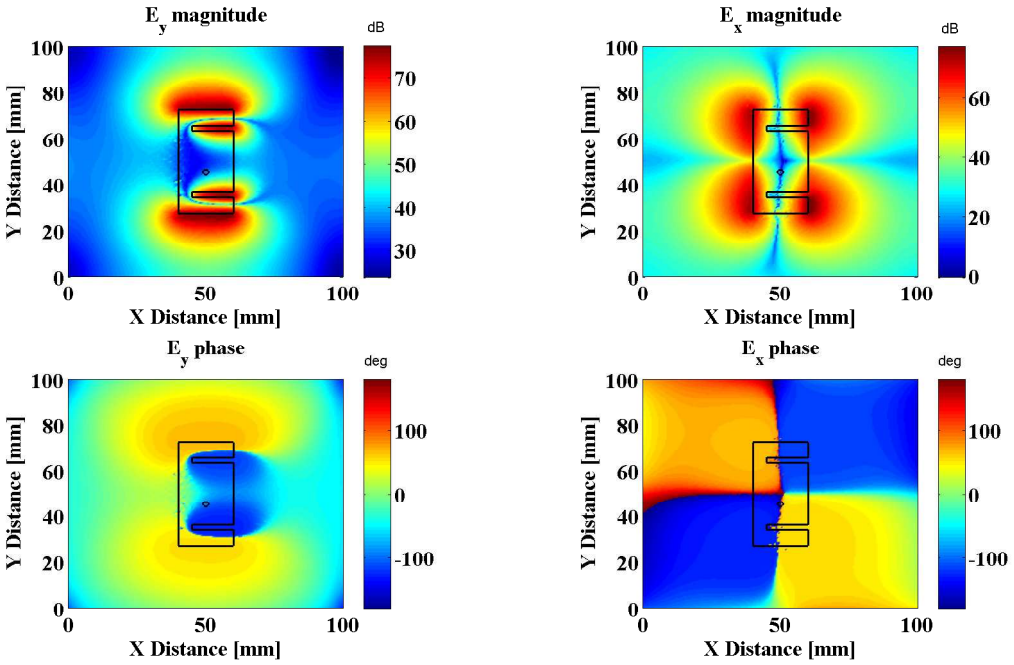

Figure 3.9: Simulated E_x and E_y components of the electric field in a xy plane 2 mm away over the double C-slotted patch antenna ($f_c = 2.39$ GHz).

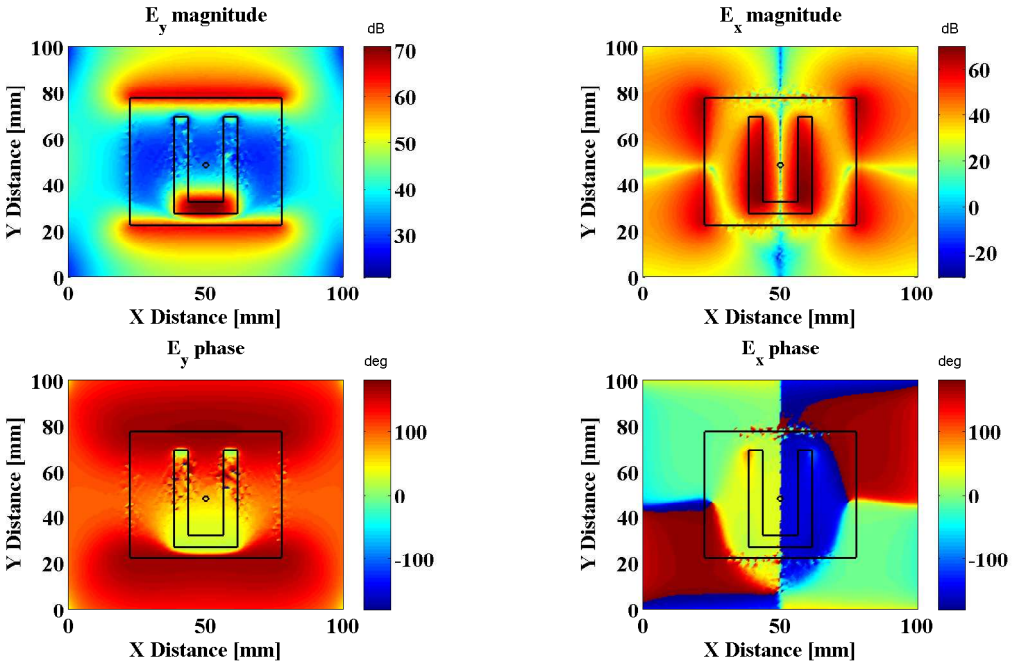

(a) Lower resonance ($f_c =$) 2.0 GHz

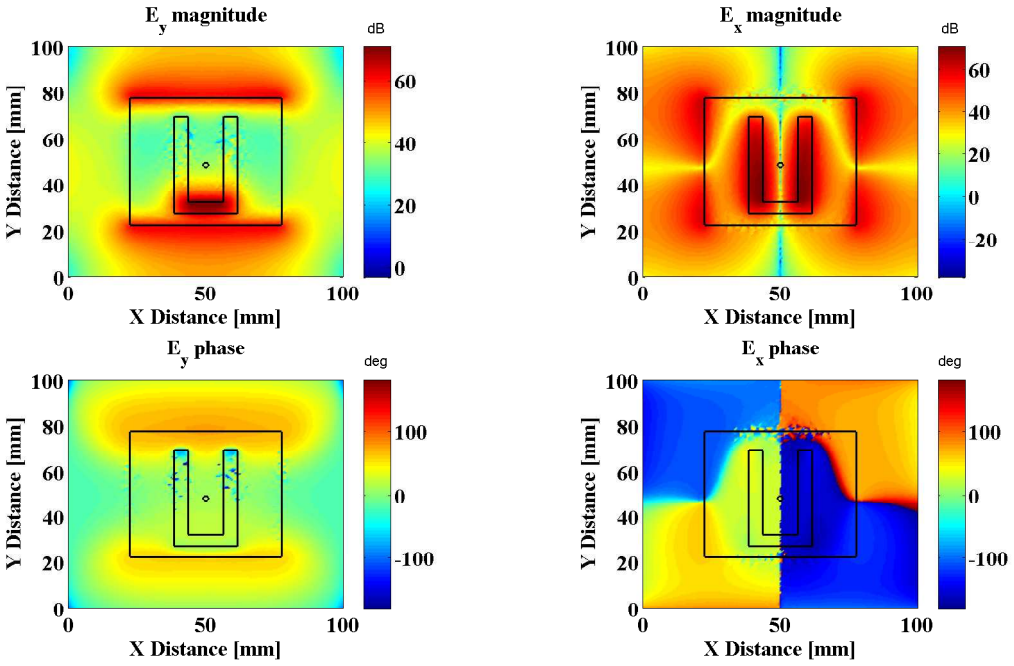

(b) Upper resonance ($f_c =$) 2.34 GHz

Figure 3.10: Simulated E_x and E_y components of the electric field in a xy plane 2 mm away over the U-slotted patch antenna (dimensions as shown in Figure 3.1).

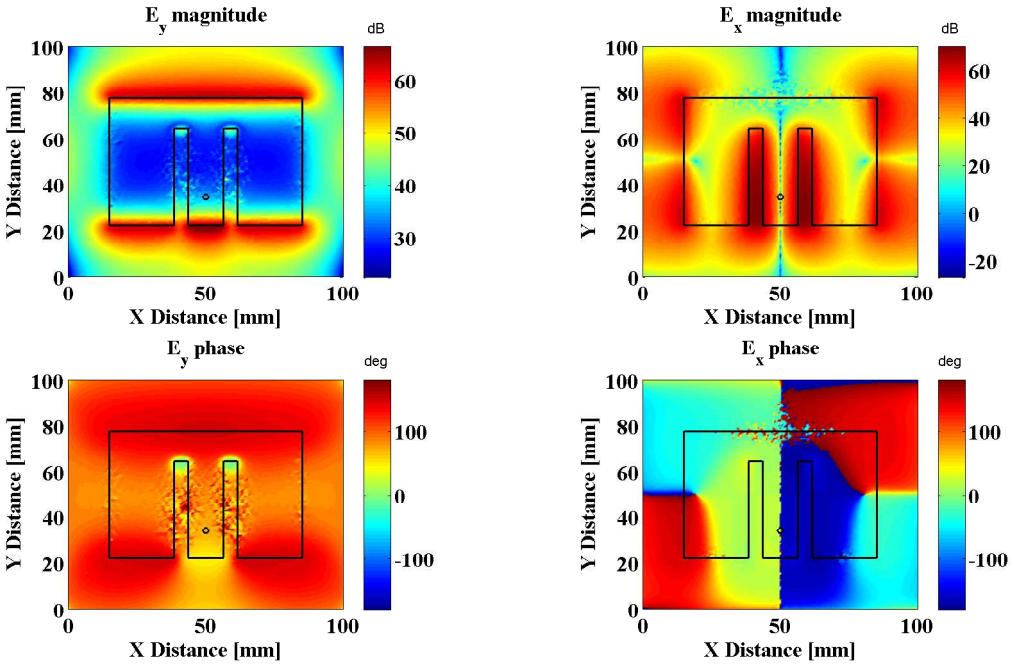

(a) Lower resonance (f_c =) 2.05 GHz

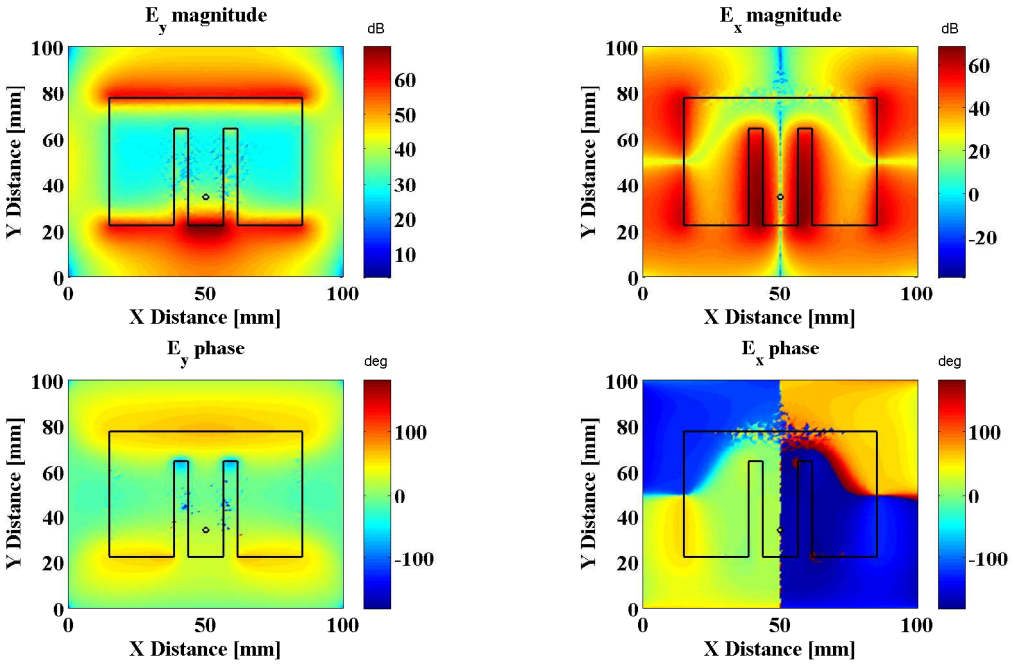

(b) Upper resonance (f_c =) 2.39 GHz

Figure 3.11: Simulated E_x and E_y components of the electric field in a xy plane 2 mm away over the E-shaped patch antenna (dimensions as shown in Figure 3.1).

using the location of the feed (usually location of feed is at midpoint in the direction along the radiating edge), will also fall short in this case, since the feed can be situated offset from central line in both directions.In such a scenario, these plots (Figure 3.8) very clearly point out that radiating edges are the ones parallel to slot, since other edges have fields with flipped phases which generates lower component of the far-field which becomes cross-pol.

Similar reasoning can be applied to double C-shaped patch antenna to understand the radiating and nonradiating edges. From Figure 3.9, it is clear that x-directed edges are radiating edges, since they have fields interfering constructively in far-field. Also, it can be inferred that cross-pol level in H-plane will be improved for this antenna, as compared to a C-shaped patch antenna, since the E_x magnitude and phase has the desired antisymmetry better than C-shaped patch antenna.

For the U-slotted antenna, the near-field distribution at the aperture plane for two resonant frequencies has been plotted in Figures 3.10a and 3.10b. Looking at the E_x and E_y components' magnitude and phase, it is clear that radiating edges are the ones orthogonal to the direction of longer arms of U-slots. It can be seen that the presence of slots creates new sources of radiation on the aperture. A high E_x field is observed at the longer arms of shape "U". Note that these new E_x fields, unlike a simple patch, are not antisymmetric about the central line parallel to x-axis, and hence do not create a null in H-plane. This gives rise to higher cross-pol in far-field for both resonance frequencies as compared to simple square patch.

There are many interesting features that can be observed from Figure 3.10. The shorter arm of slot produces a new E_y component of the field in the aperture. This field is in phase with the rest of the E_y field for higher frequency operation ($f_c = 2.34$ GHz), but has phase flipped for the lower frequency operation ($f_c = 2$ GHz). This is in agreement with current mechanism shown in Figures 3.4a and 3.4b, where the lower frequency operation dictates currents to move around the slots creating a phase flip at the end points of path i.e., at the shorter arm of "U". Same can be inferred by comparing the phases of cross-pol field (E_x) for lower and higher resonant frequencies. In terms of far-field radiation, E_y component, which is responsible for co-pol field, due to its flipped phase at the slot at lower resonance, would decrease the gain at the broadside,

although this effect is minimal.

Figure 3.11 shows similar plots for E-shaped patch antenna, and it is clear that radiation mechanism of E-shaped patch antenna is very similar to U-slotted antenna, except for the slot at shorter arm in U-slotted antenna has moved down all the way to lower radiating edge. Again just like U-slotted patch a higher cross-pol value is expected in H-plane due to absence of anti-symmetry about central line parallel to x-axis in Ex phase plot at both the resonant frequencies. Comparison of Figures 9 and 11, shows a clear distinction in the radiation mechanism of a double C-shaped and E-shaped antenna, in spite of their similar geometrical shape. In E-shaped antenna, the edges orthogonal to the slots create fields which are in same phase, responsible for co-pol component in far-field, whereas in double C-shaped antenna the radiating edges are the ones parallel to the slots. This comparative difference is in agreement with analysis presented in [38].

3.3 Far-Field Properties

In this section far-field properties of the antenna under study- cross-pol and directivity have been considered. Cross-pol is an important aspect of any small antennas, since they usually have high cross-polar radiation. In small antennas many times main focus is to optimize at the impedance matching of the antenna, and this aspect is many times neglected. As antenna with high cross-pol is basically radiating unwanted component of radiation and hence reducing the co-polar gain of the antenna. Also when the antenna is to be used in dual-polarization application, like the current problem objective, the cross-pol would be a deciding factor for choosing the correct antenna type for the design. As a reference, far-field radiation patterns for the square patch antenna for E- and H-plane are shown in Figure 3.12. In Figures 3.12-3.18, solid line represents the co-pol component and dashed line represents the cross-pol component of far-field patterns.

Figures 3.13 and 3.14 show the far-field patterns for C shaped and double C-shaped antennas respectively. Compared to simple square patch in H-plane, the cross-pol level in these antennas does not change substantially, however in E-plane, C and double C-shaped antennas show 36 and

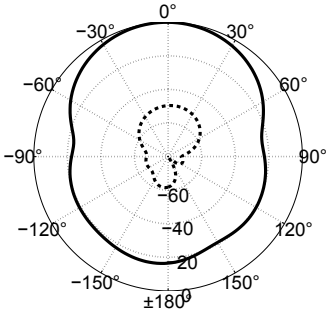

(a) E-Plane (y-z plane in Figure 3.6)

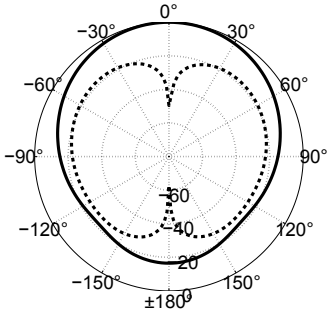

(b) H-Plane (y-z plane in Figure 3.6)

Figure 3.12: Far-field patterns of simple square patch antenna ($f_c = 2.40$ GHz).

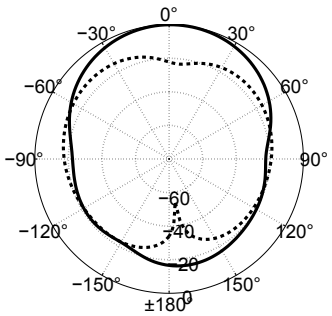

(a) E-Plane (y-z plane in Figure 3.6)

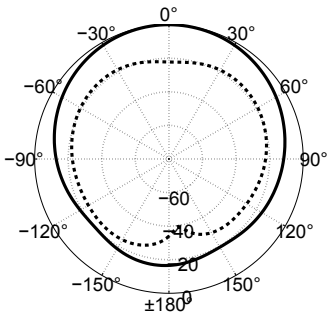

(b) H-Plane (x-z plane in Figure 3.6)

Figure 3.13: Far-field patterns of C-shaped patch antenna ($f_c = 2.38$ GHz).

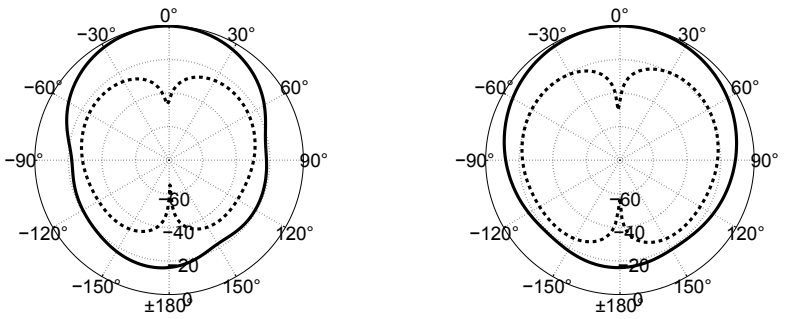

(a) E-Plane (y-z plane in Figure 3.6)

(b) H-Plane (x-z plane in Figure 3.6)

Figure 3.14: Far-field patterns of double C-shaped patch antenna ($f_c = 2.39$ GHz).

26 dB increase in cross-pol level, respectively. In C-shaped patch, the reason for high cross-pol in E-plane can be inferred from Figure 3.8. The E_x magnitude plot shows that the field near the slots have higher magnitude. Because of lack of antisymmetry, the E_x field components interfere to give high cross-polar field in far-field E-plane. Similar effect can be observed from Figure 3.9, although in double C-shaped patch this effect is less, causing lower cross-pol level as compared to C-shaped patch antenna. It should be noted that this asymmetry in both these antenna types is due to the fact that slots are introduced parallel to radiating edges. Therefore, size miniaturization in these antennas comes with the cost of high cross-pol level in E-plane.

U-slotted antenna and E-shaped antenna have low cross-pol in E-plane for both the resonance frequencies due to close antisymmetry of E_x components of the near fields across the central line along y-axis (Figure 3.11 and 3.10). But, both these antennas have higher cross-pol than square patch antenna in H-plane (3 to 6 dB higher). This can be explained by the fact that slots in these antennas, produce new E_x component of field just over the slots which are not anti-symmetric a across central line along x-axis. Figures 3.15 - 3.18 show the co-pol and cross-pol patterns of these antenna types in principal planes for lower and higher resonant frequencies. It should be noted that unlike C and double C-shaped patch, introducing slots along the direction of non-radiating edges does not disturb the antisymmetry of E_x field with respect to E-plane and hence has advantage for low cross-pol in E-plane. A summary of cross-pol levels in these antennas has

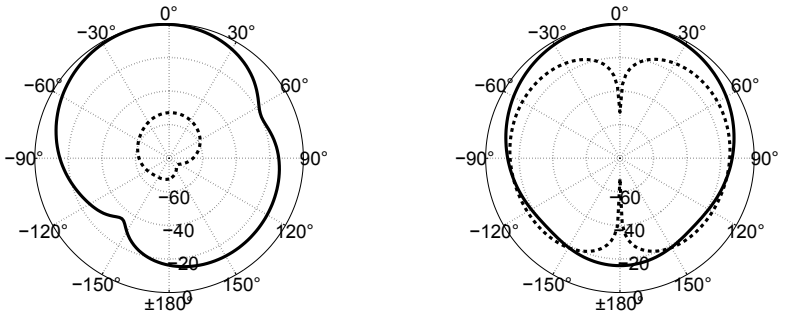

(a) E-Plane (y-z plane in Figure 3.6)

(b) H-Plane (x-z plane in Figure 3.6)

Figure 3.15: Far-field patterns of U-slotted patch antenna at lower resonance frequency (f_c = 2.00 GHz).

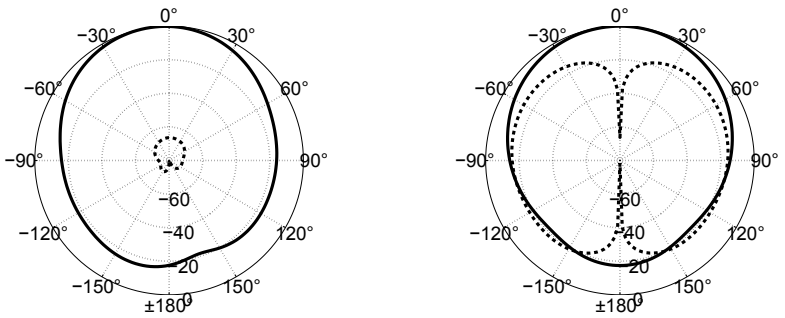

(a) E-Plane (y-z plane in Figure 3.6)

(b) H-Plane (x-z plane in Figure 3.6)

Figure 3.16: Far-field patterns of U-slotted patch antenna at higher resonance frequency (f_c = 2.34 GHz).

been presented in Table 3.1.

In terms of directivity, C-shaped and double C-shaped antennas have slightly better directivity of around 8 and 8.1 dB, respectively than U-slotted and E-shaped antennas. U-slotted and E-shaped antennas are found to have slightly lower directivity of 7.8 and 7.6, respectively.

An interesting feature of far-field patterns for U-slotted and E-shaped antennas is that, at lower resonance, the co-polar component in E-plane is not symmetric about zero degree direction

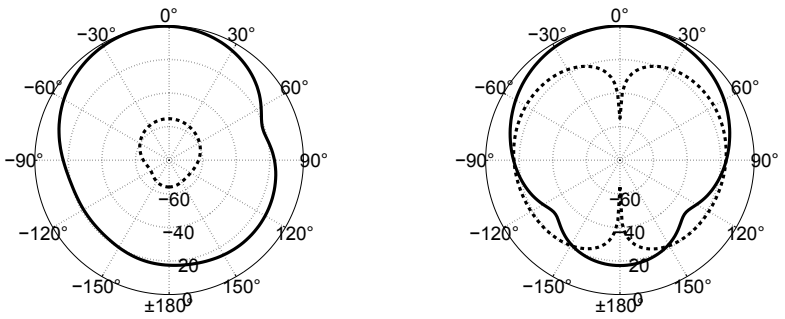

(a) E-Plane (y-z plane in Figure 3.6)

(b) H-Plane (x-z plane in Figure 3.6)

Figure 3.17: Far-field patterns of E-shaped patch antenna at lower resonance frequency (f_c = 2.05 GHz).

Table 3.1: Cross-pol Levels for the Antennas Under Study

Antenna Type	E-Plane (dB)	H-Plane (dB)
Simple Square Patch	-50	-18
C-shaped Patch	-14	-19
Double C-shaped	-24	-18
U-slotted (High/Low)	-55/-66	-12/-13
E-shaped (High/Low)	-55/-57	-15/-12

(Figures 3.15b and 3.17b). This can be explained from near field E_y plot of these antennas at lower resonance point. Because of movement of current around the slots, at lower frequency the phase of the E_y field is flipped near the slot. (Figures 3.10a and 3.11a). This can be observed over the smaller arm in U-slotted and over the small central part of lower radiating edge in E-shaped patch). Because of interference of this additional source of E_y field with a flipped phase, the maximum of the co-polar far-field is shifted from broadside direction. Such a phenomenon is not observed for higher frequency co-pol pattern, because current pattern on the surface of these antenna is same as in simple square patch at higher resonant frequency and E_y field components have same phase at all points in aperture (Figures 3.16 and 3.11b). This asymmetry of co-polar

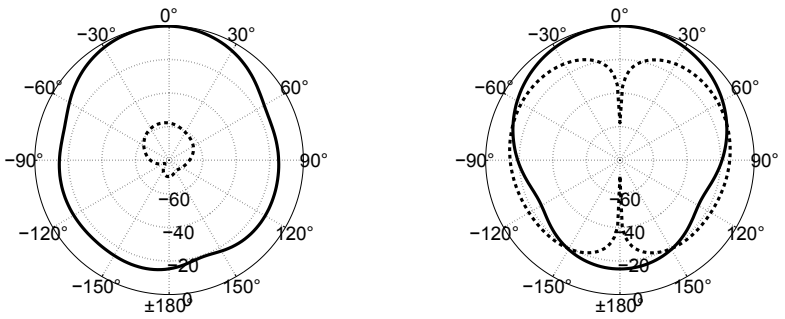

(a) E-Plane (y-z plane in Figure 3.6)

(b) H-Plane (x-z plane in Figure 3.6)

Figure 3.18: Far-field patterns of E-shaped patch antenna at higher resonance frequency (f_c = 2.39 GHz).

pattern in E-plane for lower frequency resonance has been observed previously in [35] and [40], but was not explained.

3.4 Conclusion

The idea of this study was to obtain a comprehensive insight into various types of popular slotted antenna types and understand their utility for the current design problem of the S-band weather array element design. A summary of the design results obtained for the four types of slotted

*E plane / H-plane

Table 3.2: Summary of Comparison of Slotted Antennas

	C-shaped	Double C-shaped	U-slotted	E-shaped
RF Mechanism	Single mode	Single mode	Dual mode	Dual mode
Bandwidth	0.8%	1.26%	24%	27%
Size Reduction	60%	70%	none	none
Cross-pol Level*(dB)	-14/-19	-24/-18	-55/-12	-55/-12
Directivity (dB)	8	8.1	7.6	7.6

antenna designs i.e., C-shaped, double C-shaped, E-shaped, and U-slotted, has been presented in Table 3.2. The study suggests that small size topologies such as C and double C-shaped patch antennas are good for narrow band compact size applications, while recently popular U-slotted and E-shaped patch antennas are good wideband solutions with minor penalty in size. Cross-pol comparison suggests C-shaped and double C-shaped designs come with a penalty of high cross-pol in E-plane, where as cross-pol level is within control for E-shaped and U-slotted patch antennas.

For the current application, the slotted antennas may not be a good solution, since either they present very narrow bandwidth or high cross-pol in one of the principal planes. These characteristics are not suitable for design objectives of wide bandwidth and low cross-pol. The study also gives intuitive understanding of the high cross-pol in E-shaped and U-slotted patch antennas, based on near-field plots of these antennas. The effect of slots on these near-fields and hence far-field is shown to be dependent on position and orientation of slot. Such a analysis should be very helpful for understanding the radiation mechanism in slotted antenna in general.

CHAPTER 4

Dual-Polarized Stacked Patch Antenna: Meeting the Bandwidth Requirements

One of the major requirements of the current design is achieving the required bandwidth of 10 percent (-10 dB bandwidth from 2.7 GHz to 3.0 GHz). The bandwidth of simple rectangular patch antenna can be increased using various methods such as slot loaded antennas; e.g. E-shaped [35] and U-shaped patch antennas [37], however these configuration can not be used for dual-polarized designs because of their asymmetry in two orthogonal planes. Another possibility of design configuration could be using two different antennas (each wide band) for two orthogonal polarizations, but the space assigned for each element is relatively small to accomplish this. Also, in wideband slot-loaded antennas, the bandwidth comes with the price of higher cross-polar radiation [42]. Therefore, the wideband response has to be achieved, while maintaining the symmetry in two orthogonal planes.

To start with, a number of simulations were conducted with simple square patch antenna utilizing different dielectric materials, to learn how much bandwidth can be achieved with simple square patch antenna. Three dielectric materials chosen for this study were air, honeycomb substrate and Rogers RT/Duroid-5880. Using air dielectric has an advantage of higher bandwidth for same thickness value, but would require additional arrangements for structural rigidity. Hence, with mechanics point of view, using honeycomb material should be preferred over using dielectric material, since it has dielectric constant close to one with added advantage of structural rigidity and lower weight. However obtaining honeycomb material for specified thickness value, would be expensive. This is why, it would be best if a design with commercially available RT-5800 can be achieved, which would be cost effective as well as mechanically rigid.

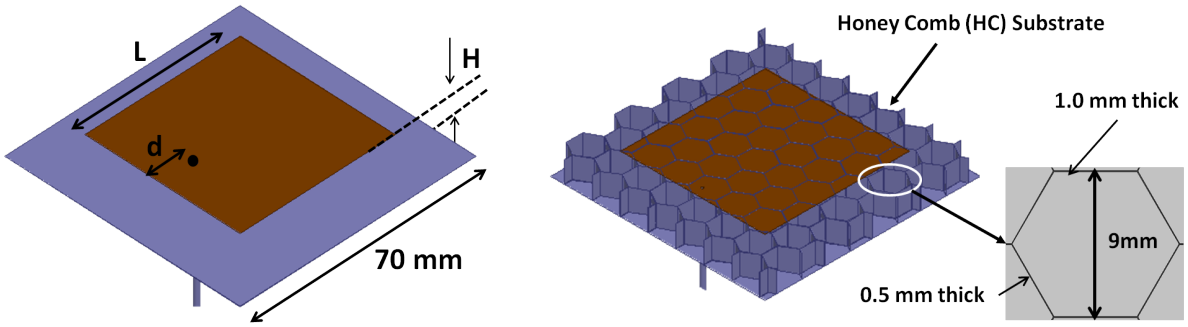

(a) Patch antenna with air dielectric

(b) Patch antenna with HC dielectric

Figure 4.1: Modelling of simple patch antennas with air and HC as dielectric.

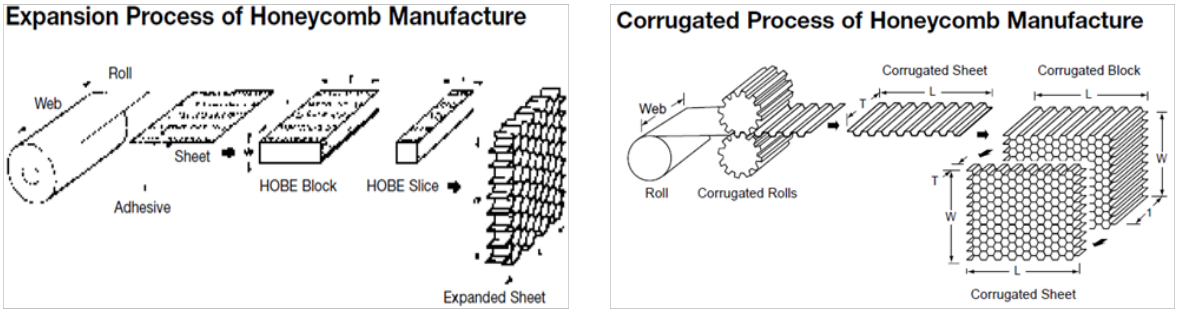

Figure 4.2: Two popular manufacturing processes for honeycomb material. notice that due to sticking together of two Aramid sheets, common side of hexagon will be twice as thick as compared to non-common side.

4.1 Preliminary Simulations

The model for simple square patch antenna under study with air as dielectric has been shown in Figure 4.1. The ground plane has been chosen to be 70 mm × 70 mm, for all cases. Simulations were also conducted with RT-5880 and honeycomb (HC) material as dielectric. For modelling honeycomb substrate (Figure 4.1b), regular hexagonal honeycomb unit cell was used with dimensions as provided in [43]. The material sheets used for making honeycomb material were modelled as Aramid (e.g Nomex^{TM}) fibre sheets (Loss tangent = 0.007, $\epsilon_r = 2$). The size of the cell was chosen as per commercially available Aramid honeycomb structures as shown in Figure 4.1b. Note that the thickness of the Aramid sheets is not same for all the sides of the hexagon. The two sides have been chosen twice in thickness, as compared to the other four sides. Such a

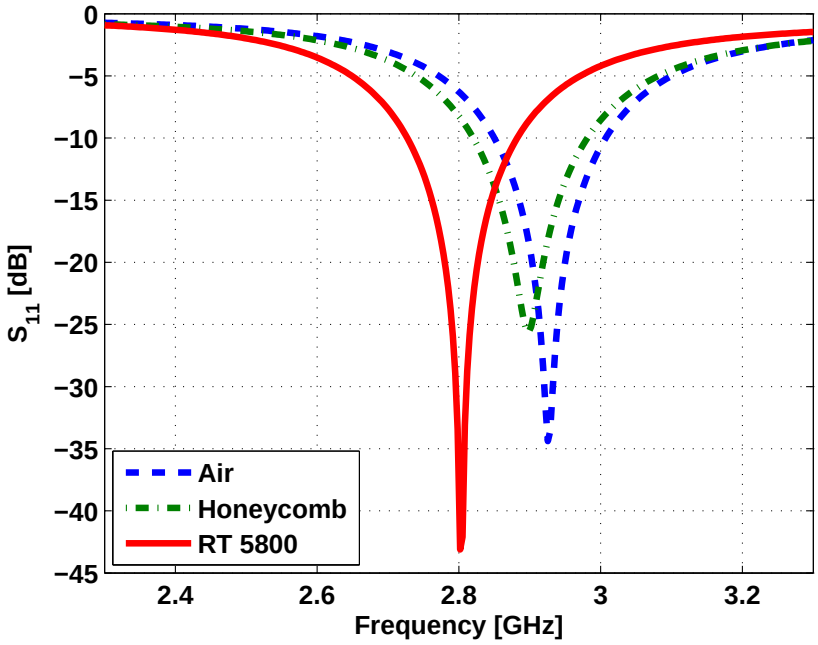

Figure 4.3: S_{11} Response of three antenna configuration. Dimensions in mm : L=45, d=10, H=5.

modelling has been done, since the manufacturing process for honeycomb material, as shown in Figure 4.2, involves binding of two layers of the Aramid sheets, such that the top and bottom sides have two times the thickness as compared to other sides.

Figure 4.3 shows the response obtained for three different dielectric substrates for same geometrical dimensions of the antenna. The bandwidth provided by the three cases is around 155 MHz, however, the resonant frequency is reduced for RT-5880 case, because of the higher dielectric constant ($\epsilon_r = 2.2$). There is slight reduction of resonant frequency for honeycomb case as compared to air, because of slight increase in the effective dielectric constant. It is clear that the required bandwidth of 300 MHz is not achievable using 5 mm thick designs.

The design bandwidth can be increased with the use of thicker dielectric substrates, however, thickness can not be increased beyond a limit, because for thicker substrates it is difficult to find correct matching point with coaxial feeding. This is because for a thicker substrate, the impedance variation is faster near the edges as compared to thin substrates [44]. Table 4.1 shows the varying position of coaxial probe with the thickness (air dielectric) of the patch. For a 10 mm

thick substrate, the coaxial probe has to be positioned right at the edge to achieve a resonance, but even then does not provide the required bandwidth of 300 MHz. There are some methods suggested for matching for thicker substrates using annular ring for coaxially fed case [45], but again such a measure will change the antenna radiation performance due to additional slots on the patch surface.

Table 4.1: Variation of parameter d (probe position) with changing H (thickness)

H (mm)	d (mm)
5	10
7	3
10	1

Since the required matching for the given thickness is not possible to be achieved using a coaxial feeding, edge feeding method can also be considered for designing the patch. Figure 4.4 shows the model with such feeding mechanism (using Honeycomb substrate) and its S_{11} response. A bandwidth of around 280 MHz can be achieved when the height of the substrate is increased to 10 mm. This feeding will also require microstrip line with appropriate width (shown as uw) for matching the impedance at the edge.

The studies conducted so far reveal that, with coaxially fed patch antenna, the required bandwidth of 300 MHz can not be achieved. Thicker substrates with edge feeding need to be used in order to achieve a bandwidth of 300 MHz. This configuration can be used along with honeycomb substrate, which can support stripline network. However, there are other potential cons of such design for the current application. First, exposing the stripline network to the radiation side of the antenna can create high cross-pol. Second, honeycomb substrate with customized thickness are costly. Because of these factors, other options for achieving high bandwidth have been explored.

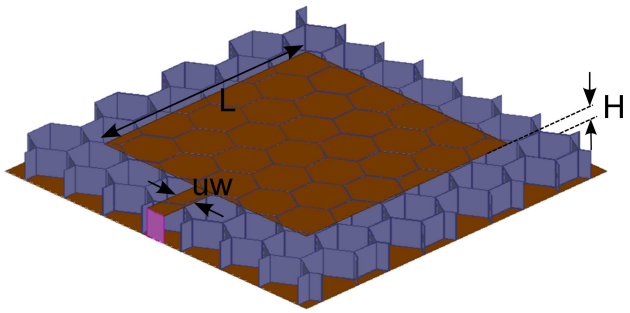

(a) The model of honeycomb substrate antenna under the study.

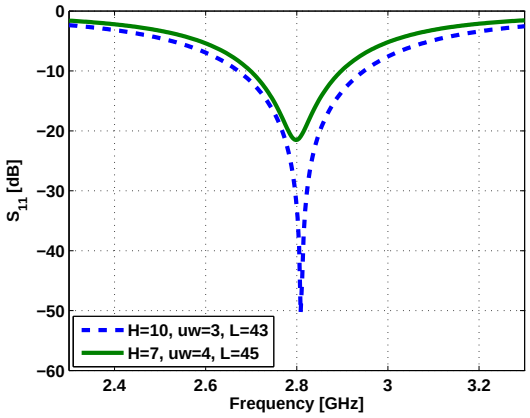

(b) S_{11} response of the strip line fed antenna. Dimensions in mm.

Figure 4.4: Modelling of HC patch antenna with strip line feeding.

4.2 Single Pol. Stacked Patch Antenna

In order to enhance the bandwidth of patch antennas while maintaining their conformal nature and symmetry in two orthogonal planes, stacked patch antennas can be utilized. Stacked patch antenna configuration has been studied and analyzed previously by various authors in past [46–49]. The basic configuration comprises of two layers of patch elements, stacked over one another such that lower one is directly fed by feeding mechanism and upper one is coupled capacitively to the lower one. Both patch elements have a common ground plane below the lower patch element. Because of different dimensions of the patch elements at two layers, the structure resonates at two different frequencies, which can be utilized to create a wide-band response.

Figure 4.5a shows the simulation model for the coaxially fed stacked patch antenna designed for the current application. Intention here is to design an element which can be fabricated from the commercially available dielectric materials, therefore the thickness of both layers was chosen to be 3.175 mm (125 mils thick Rogers RT/Duriod-5880 sheet can be used). Dimensions $L1$ and $L2$ were optimized to meet the bandwidth requirements of the design. The fabricated layers (using photo lithography), are shown in Figure 4.5b.

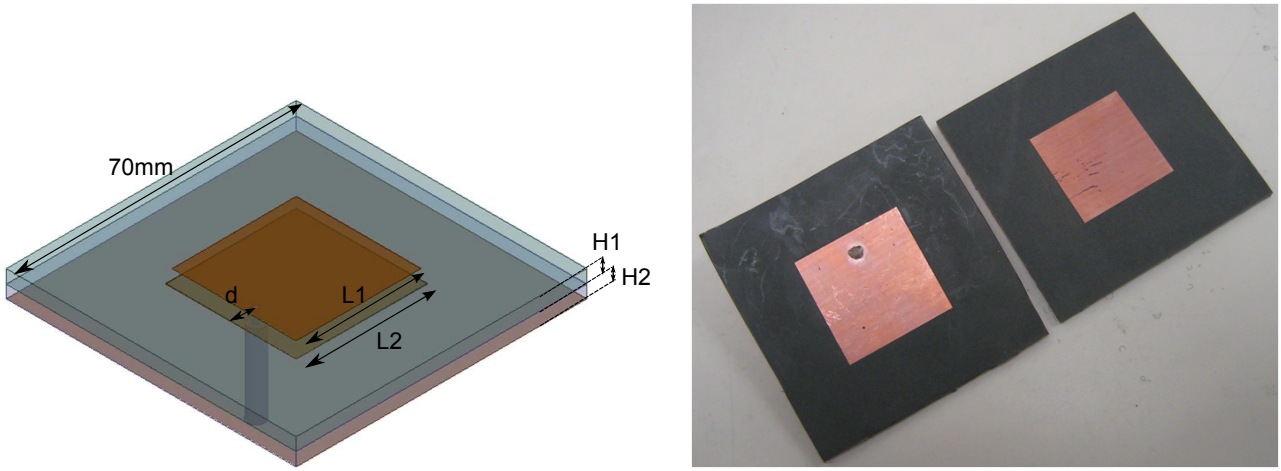

(a) The 3D Simulation model and dimensions

(b) Photo of fabricated layers

Figure 4.5: Simulation model and fabrication of stacked patch antenna.

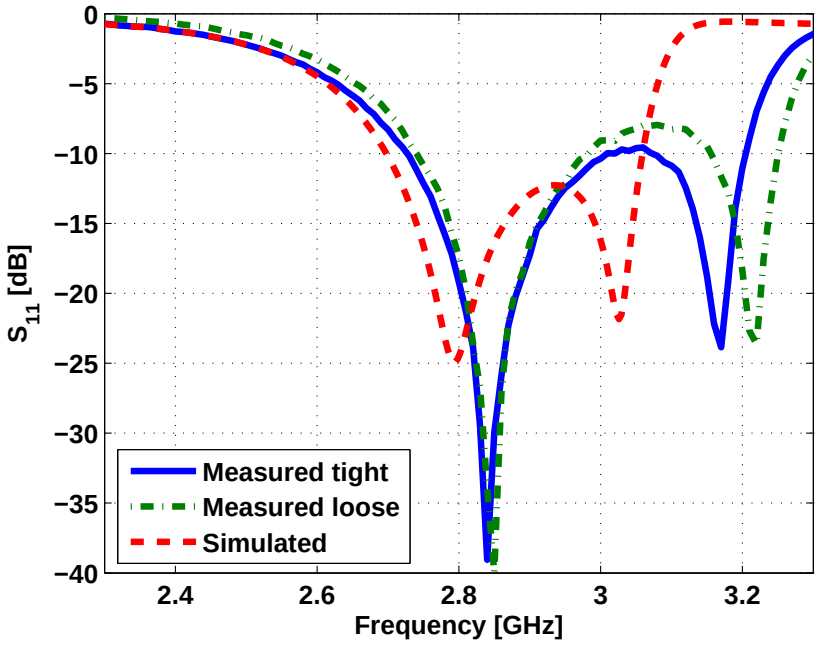

Figure 4.6: S_{11} Response of the single polarized stacked patch antenna (Dimensions in mm: L1=30, L2=31.5, H1=H2=3.175, d=6).

Figure 4.6 shows the simulated and measured response of the antenna shown in the Figure 4.5. The simulated S-parameter response of the antenna shows resonance at two frequencies 2.8 GHz and 3.0 GHz. The fabricated layers shown in Figure 4.5b , were tied together for the

measurement. It was observed that based on how tight the layers are tied together, the response of the antenna can changes. Two readings of S_{11} measurement were recorded for tightly and loosely bounded stacked patch cases (Figure 4.6). For tightly bounded case the higher resonance frequency shifts down as compared to loosely bound case. This phenomenon has been discussed in details in next section.

4.2.1 Sources of Errors is Fabrication

In the measured S_{11} response, the resonance frequency of the upper resonance point moves up the frequency band as compared to response obtained in simulation. This phenomenon of shift of upper resonance frequency is unfavourable, since due to separation of two resonance frequencies, condition of $S_{11} < -10$ dB is not maintained across the band. There may be two possible reasons for such 'walk-off' of higher frequency resonance point:

1. Misalignment of the two patch elements
2. Air-gap between the two dielectric layers

To understand the effect of these factors on the S_{11} performance of the antenna, further parametric simulations have been conducted, with intentionally introduced alignment or air-gap errors in the simulation model.

4.2.1.1 Alignment Error

An alignment error between the two layers of the patch, would mean that the two metal patch squares are not exactly one over another, rather shifted with respect to each other. Such an error can come into the system during the fabrication, since the cutting of the dielectric edges is manual work and can have human errors. To model the effect of such an error in the simulation, the top patch is shifted with respect to the bottom patch, as shown in Figure 4.7a. The offset parameter d has been chosen to be same for the misalignment in two directions. In the S_{11} response of the antenna, the misalignment is characterized by moving away of both the resonant

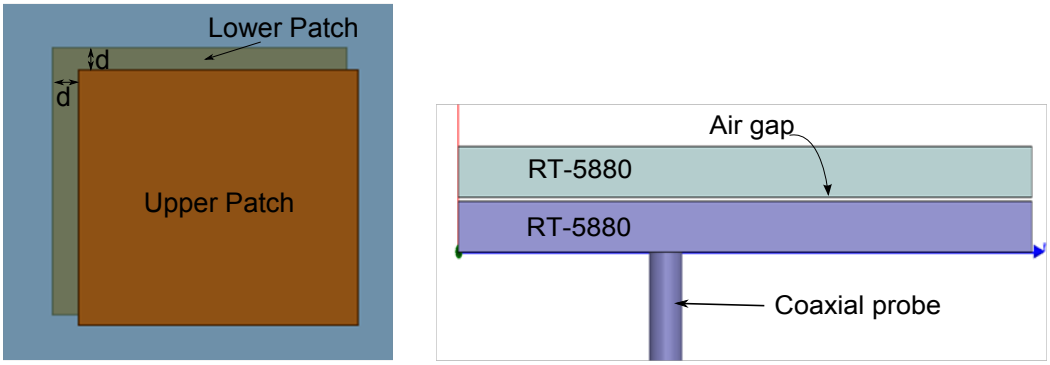

(a) Modelling of misalignment

(b) Modelling of air-gap

Figure 4.7: Two possible sources of errors in fabrication process.

frequencies from each other, with increasing offset of misalignment (Figure 4.8a). This 'walking-off' phenomenon of the two resonant frequency is relatively small.

4.2.1.2 Air-gap Error

The design also relies on the tightness with which the two layers of the patch antenna are bound together. In order to simulate the effect of the air-gap between the two layers of the dielectric, a uniform layer of air-gap is introduced between the dielectrics as shown in Figure 4.7b. Figure 4.8b shows the effect of changing the thickness of the air-gap for the design. With changing air-gap, the lower resonance frequency remains almost same, while the upper resonance frequency point moves up the band. the shift is the resonance frequency is considerable with changing air-gap between the layers of dielectric.

From the results of forced simulation errors in the simulation model, it is clear that the differences between the measured and the simulated S-parameter response in the antenna (Figure 4.6) are primarily due to the air-gap between the layers, since in the measured results, the lower resonance point has slightly changed while the upper resonance point has moved up considerably. As discussed, the air-gap errors affect specifically the second resonance frequency, which has been observed in the measurements too (tight and loose case in Figure 4.6) . In conclusion, to improve the performance of the antenna and achieve the continuous -10 dB band of frequency, the air-gap

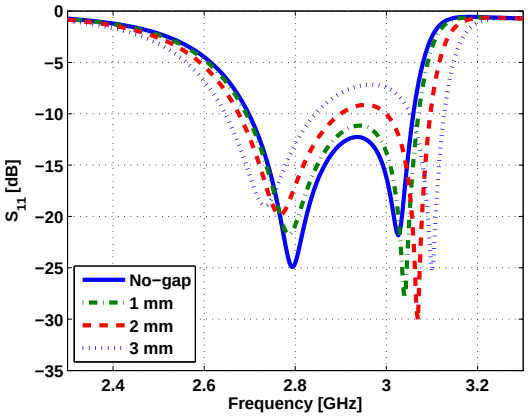

(a) Changing S_{11} response with changing misalignment

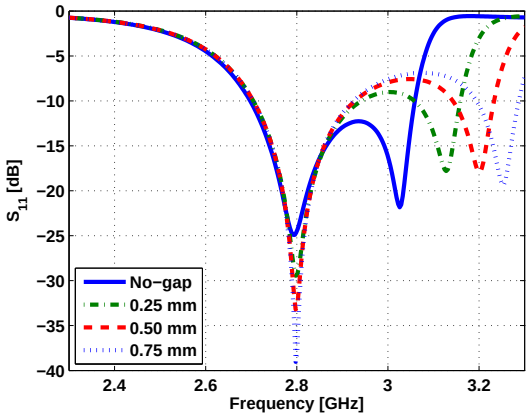

(b) Changing S_{11} response with air-gap

Figure 4.8: Effect of fabrication errors on the return loss of the antenna.

between the layers of dielectric needs to be eliminated. There are possible ways of countering the air-gap errors by closely packing the dielectric layers by using glue or using nylon screws, as will be discussed in further sections.

4.3 Dual Pol. Stacked Patch Antenna

With stacked patch configuration, the required bandwidth of 300 MHz can be achieved with the use of commercially available dielectric substrates. Next, a patch antenna with stacked patch configuration with dual-polarization was designed. Using this design, the isolation between the ports for a stacked patch antenna configuration can be obtained. This exercise will also provide a number for W-parameters (introduced in Section - 1.2.2), which would give an idea of its applicability for weather radars. A dual-polarized stacked patch antenna was designed and fabricated to meet these goals. The model used for simulation and optimization of design is shown in Figure 4.9a. A stacked patch design with two ports feeding the patch antenna in two orthogonal planes was optimized and fabricated (Figure 4.9), with dimensions as L1=30.5mm, L2=32.75mm, H1=H2=3.175mm, d=6mm.

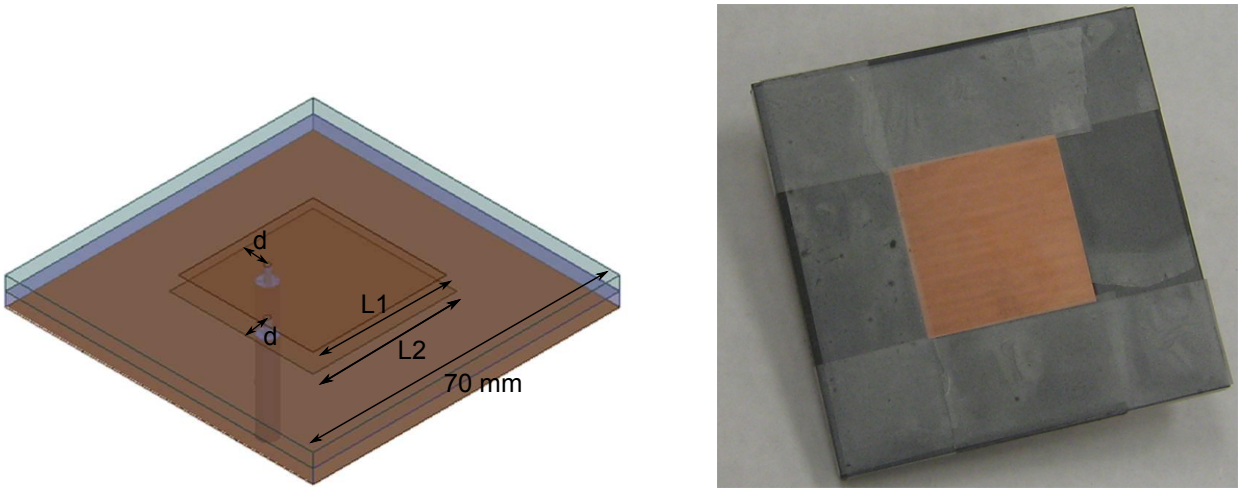

(a) Simulation model for dual-pol stacked patch element

(b) Fabricated antenna

Figure 4.9: Simulation model and fabricated design for dual pol stacked patch element.

4.3.1 Fabrication

As seen before, the air-gap between the dielectric layers can affect the performance of the antenna. One of the reasons for air-gaps between the dielectric layers is the presence of soldering bumps on the top surface of the bottom patch layer, which does not allow close packing of two dielectric layers. The lower layer of the patch is electrically connected to coaxial pin, which creates slight bumps on the top surface of the lower dielectric, due to protruding soldering iron points (Figure 4.10a). To ensure close packing, blank holes were drilled on the bottom face of upper dielectric substrate, which would accommodate the soldering iron bumps. Finally, The layers were tied together using scotch tape (Figure 4.9b).

4.3.2 S-parameter Performance

The simulated and measured performance of the designed antenna has been presented in Figure 4.11. The required bandwidth of 300 MHz has been achieved, but the measured S_{11} is just equal to -10 dB between the resonance points, since the higher resonance point moves up the frequency band. This trend is similar to as observed in single polarization case in previous sections, and

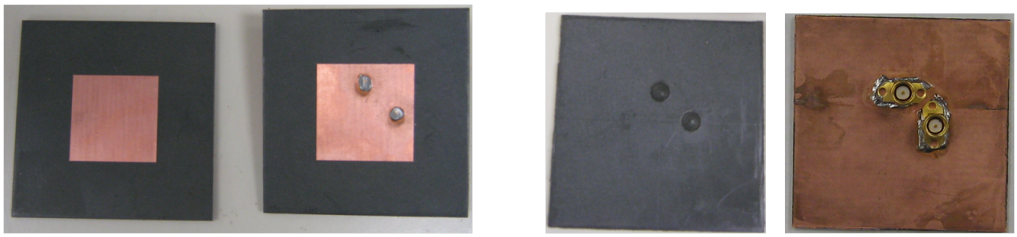

(a) Fabricated layers (front) **(b)** Fabricated layers (back)

Figure 4.10: Pictures of the fabricated layers of the dual polarized stacked patch antenna.

it shows that there is still some air-gap between the layers. There can be other methods for improving this performance, by gluing the two layers together or by using nylon screws, and will be discussed in future sections. The isolation between the two ports is better than 18 dB within the required bandwidth of 2.7 GHz to 3.0 GHz. This needs to be further improved since there is requirement to isolate the ports with better than 30 dB isolation.

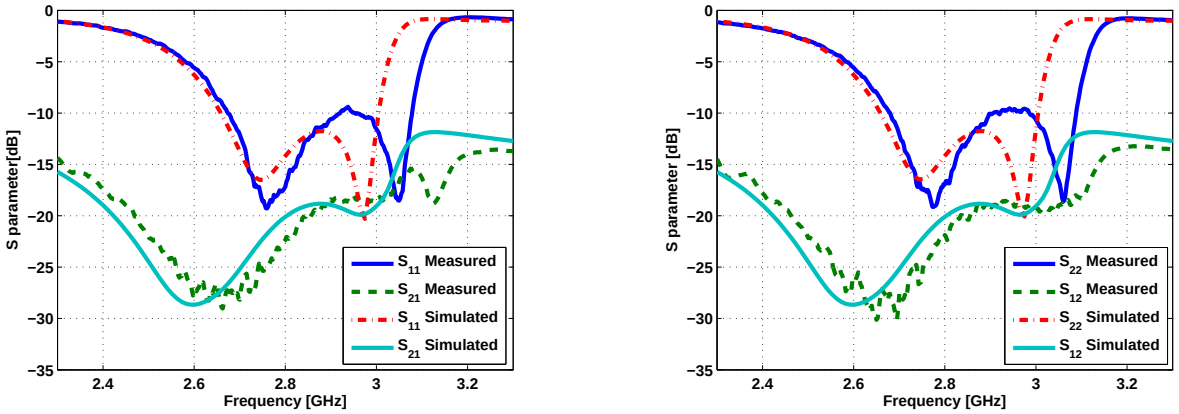

(a) Port 1 excitation **(b)** Port 2 excitation

Figure 4.11: S-parameter response of the dual-pol stacked patch element.(Dimensions in mm: L1=30.5, L2=32.75, H1=H2=3.175, d=6).

4.3.2.1 Using Adhesive

In order to reduce the 'walk off' of the higher resonant frequency, another method could be using a adhesive instead of taping the layers together. An epoxy adhesive was used to glue the layers

together to eliminate any air-gap between the layers. Fogure 4.12 shows the measured response of the antenna for two ports when epoxy adhesive was used to stick the two layers together.

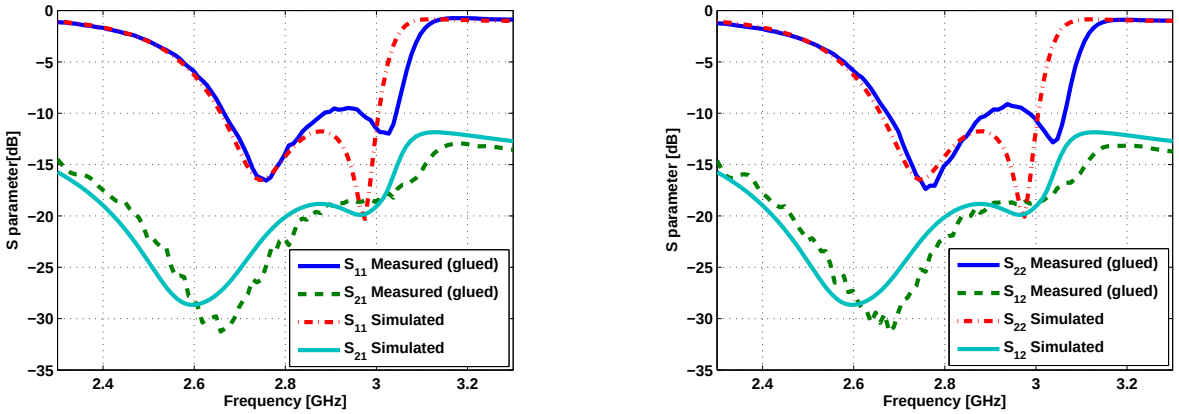

(a) Port 1 excitation

(b) Port 2 excitation

Figure 4.12: S-parameter response of the dual-pol stacked patch element with the use of adhesive between the layers. (Dimensions in mm: L1=30.5, L2=32.75, H1=H2=3.175, d=6).

It can be observed from the plot that, the higher frequency resonance walk-off is still present in the S_{11} measured response. Also, the matching of this resonance frequency is disturbed as compared to using tape to stick the two layers together. This could be happening because of the presence of additional layer of epoxy between the layers of the dielectric. It can be concluded that using epoxy adhesive may not be a solution for walk-off of the higher resonance frequency. However, this method can be used, if a design is optimized taking into account an additional layer of epoxy adhesive during simulation phase. Such a design was not pursued and other methods of packing the layers together were utilized (as discussed in next chapter).

4.3.3 Far-field Measurement

The simulated and the measured far-field patterns of the antenna for two frequencies 2.77 GHz and 3.0 GHz have been plotted in Figure 4.13a and 4.13b, respectively. The pattern measurements were done in UCLA *near-field anechoic chamber*. There is a good match between the measured and simulated patterns. A worst cross-pol of -20 dB has been measured for E- and

H-planes, whereas cross-pol as high as to -12 dB is recorded in diagonal planes. An important point of difference between the simulated pattern and measured pattern is the absence of any major radiation in the back lobe direction. This is happening because of the presence of the antenna mount structure right behind the AUT, which blocks any radiation in the back direction from the antenna.

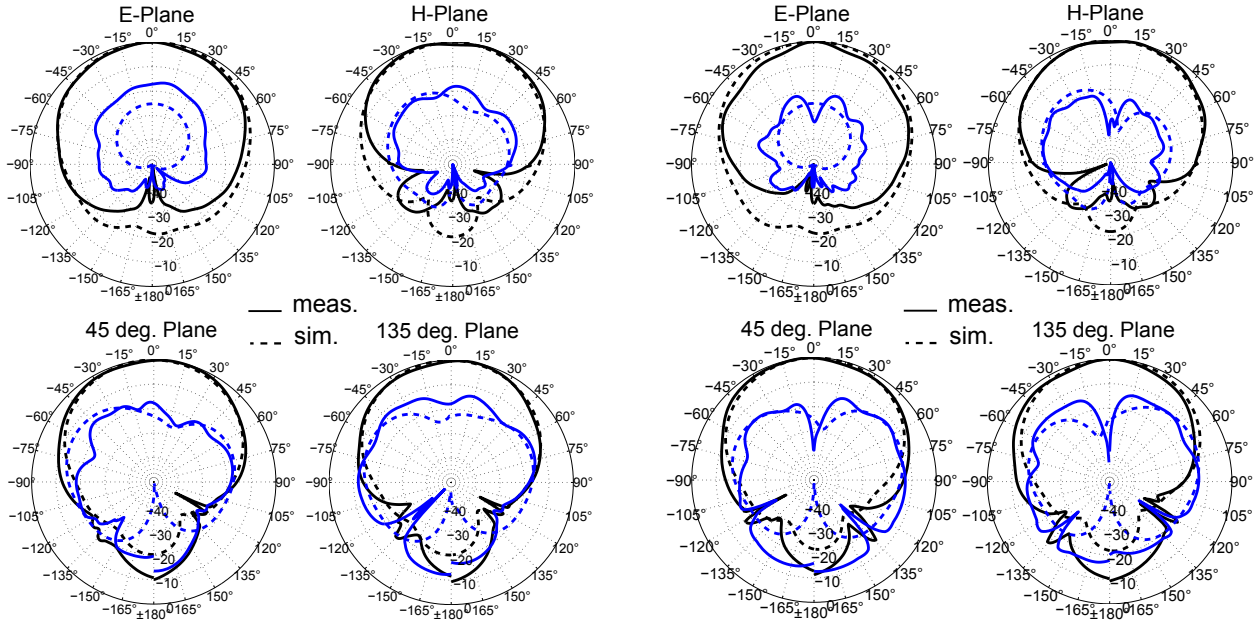

(a) At Freq = 2.77 GHz

(b) At Freq = 3.0 GHz

Figure 4.13: Measured and Simulated far-field patterns for dual-polarized stacked patch antenna element.

4.3.4 Far-field Patterns and W-Parameters

W-parameters are important performance parameters for the antenna element to be used for weather radar design, since they are directly related to the bias in differential reflectivity. As described in Section 1.2.2, the W-parameters can be reduced by reducing the cross-pol of the antenna for each polarization. Note that the calculation of W-parameters requires space integration of product terms of patterns, hence will depend on the cross-pol definition chosen. Here, the cross-pol has been defined based on Ludiwg's second definition of cross-pol [23]. In order to apply this cross-pol definition, orientation and position of the antenna with respect to the

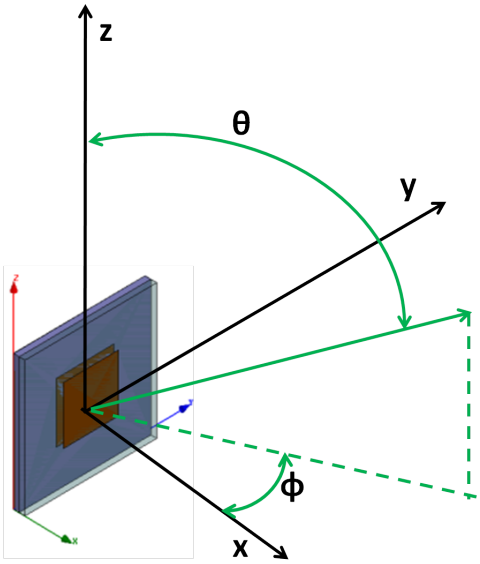

Figure 4.14: Coordinate system for calculation of W-parameters. Same coordinate system has been used for plots in Figures 4.15a - 4.18d.

coordinate system has been chosen as shown in Figure 4.14.

Since the W-parameters depend on antenna's far-field amplitude and phase distribution in the space, it is a good idea to have a look at the far-field patterns, i.e far-field (amplitude and phase) distribution in entire space. Figure 4.15 - 4.18, shows the simulated and measured far-field phase and amplitude plots at two frequencies. The x-axis of the plots is the ϕ variation of the space and y-axis shows the θ variation of the space. As mentioned before, the cross-polar patterns are based on Ludwig's second definition. Figure 4.15, shows the far-field phase and magnitude of co and cross-polar component of the radiation at frequency 2.77 GHz. It can be observed that co-polar pattern shows a main beam illuminating the broad side direction of the antenna, with uniform phase distribution. The cross-polar pattern shows deep nulls in principal planes, but high value in 45° planes with phase varying with direction of observation. The measured distribution of far-field (Figure 4.16), matches quite well with the calculated one. Similar observations can be made for higher resonant frequency, i.e. 3.0 GHz (Figure 4.17 and 4.18).

From the calculated and measured field distribution of the antenna far-field, W parameters have been calculated and presented in Table 4.2. The formula used for these calculations has been reiterated here:

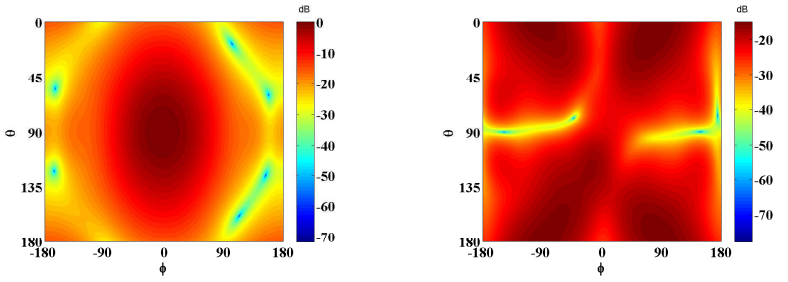

(a) Co-pol. mag.

(b) Cross-pol. mag.

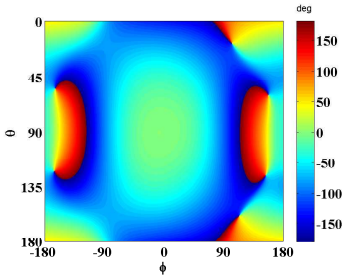

(c) Co-pol. phase

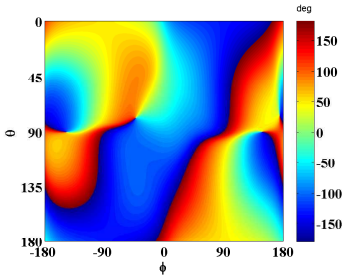

(d) Cross-pol. phase

Figure 4.15: Calculated far-field distribution at freq = 2.77 GHz.

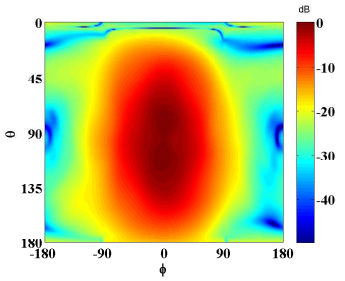

(a) Co-pol. mag.

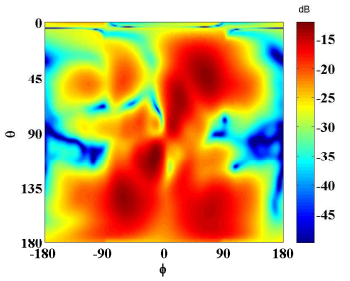

(b) Cross-pol. mag.

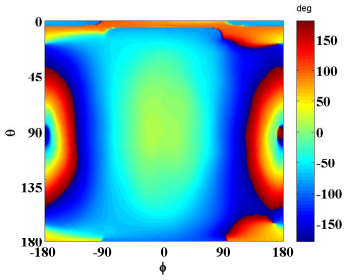

(c) Co-pol. phase

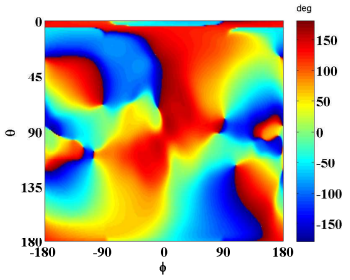

(d) Cross-pol. phase

Figure 4.16: Measured far-field distribution at freq = 2.77 GHz.

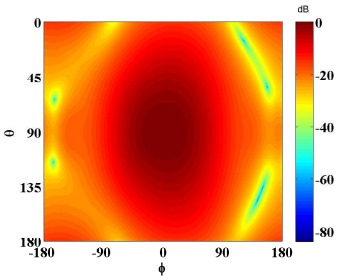

(a) Co-pol. mag.

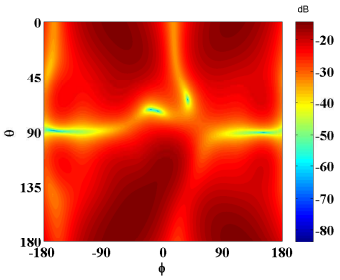

(b) Cross-pol. mag.

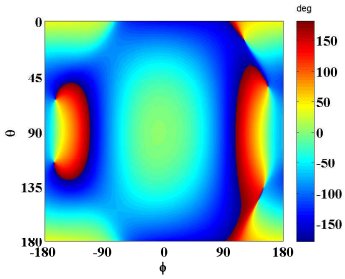

(c) Co-pol. phase

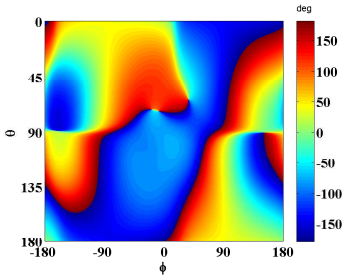

(d) Cross-pol. phase

Figure 4.17: Calculated far-field distribution at freq = 3.0 GHz.

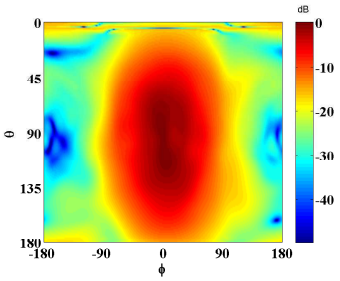

(a) Co-pol. mag.

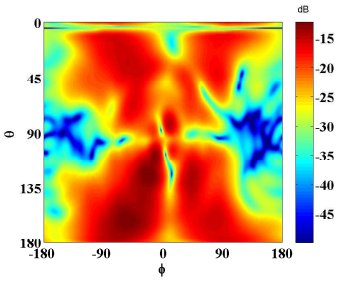

(b) Cross-pol. mag.

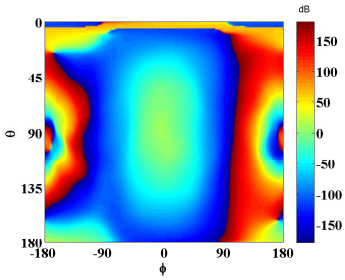

(c) Co-pol. phase

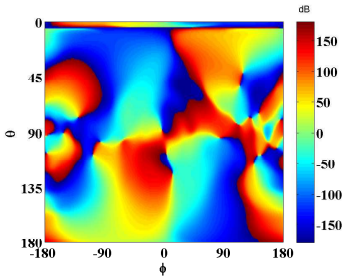

(d) Cross-pol. phase

Figure 4.18: Measured far-field distribution at freq = 3.0 GHz.

$$W_{hv} = \frac{\int_\Omega F_{hh}^2(\theta,\phi) F_{hh}^*(\theta,\phi) F_{hv}^*(\theta,\phi) d\Omega}{\int_\Omega |F_{hh}(\theta,\phi)|^4 d\Omega}$$

$$W_4 = \frac{\int_\Omega |F_{hh}(\theta,\phi)|^2 |F_{hv}(\theta,\phi)|^2 d\Omega}{\int_\Omega |F_{hh}(\theta,\phi)|^4 d\Omega}$$

Table 4.2: W_{hv} and W_4 parameters for dual pol stacked patch antenna.

Freq	W_{hv} (dB)		W_4 (dB)	
	Meas.	Sim.	Meas.	Sim.
2.77 GHz	-9.6	-9.8	-15.4	-18.5
3.05 GHz	-15.4	-10.6	-15.6	-19.2

Here the integration has been carried over entire space, with limits as θ = 0 to 90° and ϕ = $-180°$ to 180°. From the Table 4.2, it is clear that W_4 parameter is usually smaller than W_{hv}. This is expected, since calculation of W_4 involves the product term with second power of the cross-polar field as compared to first power for the case of W_{hv}. As the cross-pol values are normalized with the maximum co-pol value, cross-pol is usually a fraction (< 1.0). Due to which, the second power of cross-pol is considerably smaller number, leading to smaller W_4 as compared to W_{hv}. There is a reasonable degree of match between the measured and simulated values of these parameters. Still, there are noticeable differences between the measured and simulated values, specially at higher frequency. It has been noticed that, these parameters can be very sensitive to the variations of far-field amplitude and phase and small changes in radiated phase or amplitude can change these parameters significantly. This is expected since small differences in simulated and measured values of fields can accumulate into a large number, when integrated over the entire space. On the other hand, the variations in radiated phase and magnitude can arise due to slight differences in fabrication or measurement errors. A detailed discussion on sensitivity of W-parameters is conducted in Chapter 6.

4.4 Conclusion

Among the various options available to design the antenna, a stacked patch antenna configuration was selected for designing the required patch antenna element. Single polarized and dual polarized antennas were designed and fabricated. It was found that -10 dB bandwidth of 300 MHz can be achieved using stacked patch configuration, with the use of commercially available dielectric substrates (Rogers RT-5880). The measurements on dual-polarized antenna revealed that an isolation better than -18 dB can be obtained on stacked patch configuration without any other special arrangements for improving isolation. The cross-pol in the dual-polarized antenna was found to be around -20 dB in principal planes and -12 dB in diagonal planes. The W-parameters were also calculated from the simulated and measured far-field patterns of the antenna. These values revealed that there can be good amount of difference between the measured and simulated values of W-parameters, because of the variations of the phase and magnitude of far-field radiation patterns over the space.

CHAPTER 5

Dual-Polarized Stacked Patch Differentially Fed Patch Antenna

5.1 Introduction

In previous chapter, it was shown that a stacked patch topology provides enough bandwidth to meet the objectives of the design. However, it is required that the antenna has improved isolation between the ports and reduced cross-polarization level. A number of methods have been reported for improving the cross-pol performance in a patch antenna [50–52], but most of these cannot be applied for dual polarized configuration. In order to accomplish these objectives in stacked patch, dual-pol type configuration, a differential feeding mechanism can be utilized.

A number of designs have been reported which involve use of differential feeding to achieve low cross-pol and high isolation. In general, using a differential feeding mechanism, low cross-pol can be achieved, as reported in [27], [53] and [54]. But when cross-pol reduction problem combines with requirement of higher bandwidth and dual-polarization, it becomes challenging problem to solve. The bandwidth enhancement can be achieved, while maintaining the symmetry in two orthogonal planes, with the help of L-probe feeding mechanism, first reported in [55], analyzed in [56] and then later applied in differential feeding settings in [57]. A number of designs have also been reported the use of differentially fed L-probe in dual polarized configurations [58–60]. These designs provide wide band performance with reduced cross-pol and high isolation between the two ports. In particular, design in [59] utilizes additional posts to enhance the isolation between the ports and in [58] the bandwidth of the antenna is increased with the use of a broadband differential feeding network. These designs, although very effective, use air as dielectric and

will require additional arrangements for the structural rigidity when the elements are used in an array environment. This can be avoided using the honeycomb substrate as in [61], but again that solution would be expensive, since customized honeycomb substrates can be costly. Also, using L-probes in dielectric substrates (other than air) would require additional layers of dielectric.

It is clear that current application requires a simpler cost effective design with broadband performance, low cross-pol and high isolation between the ports, which can ultimately be a part of an array. As also shown in previous chapter, higher bandwidth can be achieved using stacked patch configuration utilizing the dual resonance. This design, along with cross-pol reduction mechanism of differential feeding can be utilized to reach a low cross-pol, wide-band configuration. In current design, the low cross-pol and high isolation has been achieved using differential feeding mechanism with the use of microstrip-line network and vias. Additional dielectric layer has been added below the ground plane to support the microstrip line network. Usually, a differentially fed design would require a phase shifter for the second feed, which can be avoided by providing phase shift by creating a $\lambda/2$ difference in the lengths of the microstrip lines feeding the ports. The design topology of a dual-polarized differentially fed stacked patch topology has been presented in next sections, followed by measurement results and calculation of W-parameters.

5.2 The Design

Figure 5.1 shows the 3-D model used for simulation and optimization of design. Two 125 mils RT-5880 layers are stacked one over other, with a common ground plane below the lower patch (Figure 5.1c). Another dielectric layer (31 mils RT-5880) has been introduced to support the feeding line network below the ground plane. The connection between the microstrip line and the lower patch has been made using four metal vias (0.445 mm thick), through the ground plane as shown in the figure. The microstrip lines are end-fed from the edge of dielectric substrate (Figure 5.1a), and additional length is added on the lowest layer of dielectric to leave some space for attaching end-launcher SMAs in the practical prototype. Different layers used in the design are combined together using four nylon screws at each corner of the substrate.

Microstrip network has been designed for 50 Ω SMA end launcher. Then the 50 Ω line

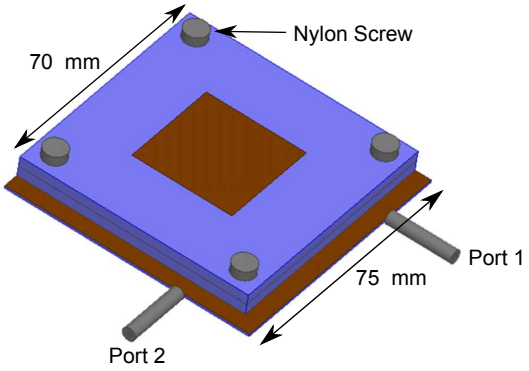

(a) 3D Model with dielectric and ground plane dimensions

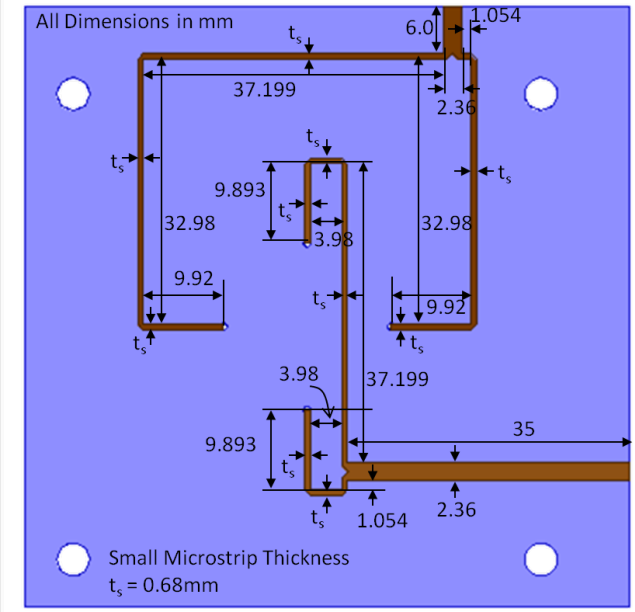

(b) Dual-pol differential feed network

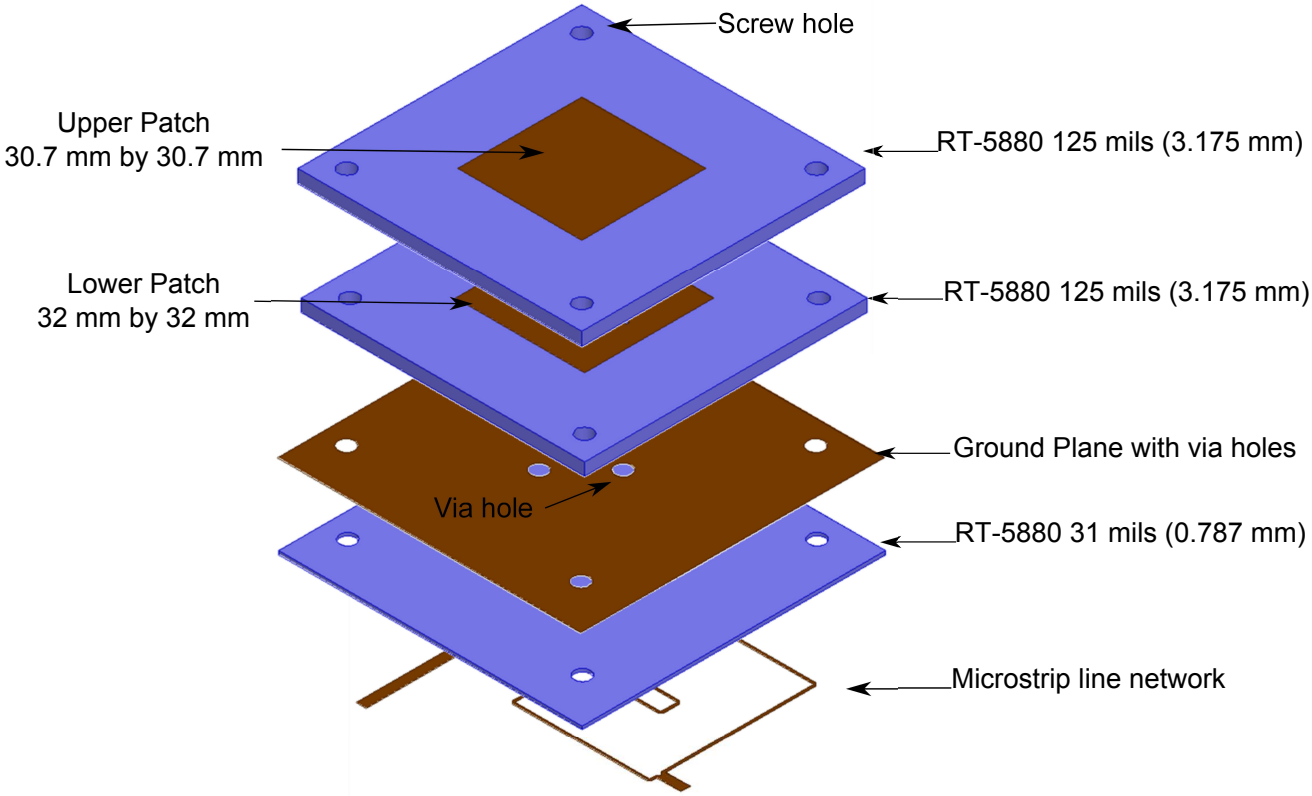

(c) 3-D Exploded view with patch dimensions

Figure 5.1: Design of dual-pol differentially fed stacked patch antenna.

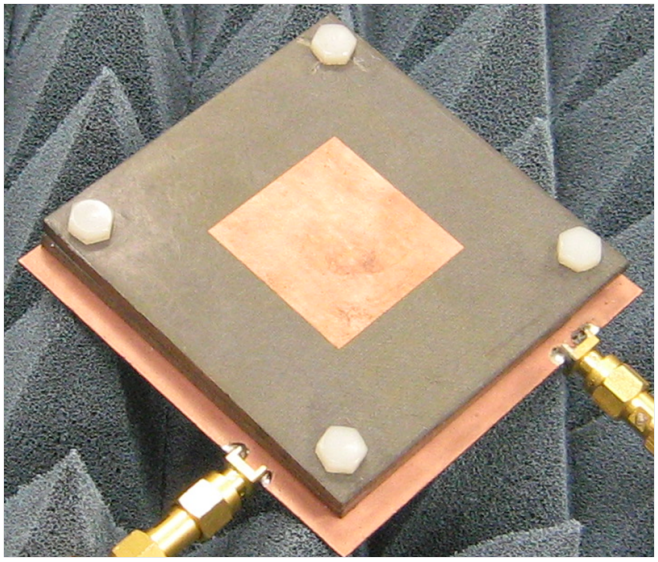

Figure 5.2: Dual-pol stacked patch antenna: fabricated design.

subdivides into two 100 Ω lines feeding the lower patch antennas. The microstrip lines feed the patch antennas at 100 Ω impedance points, which eliminates the requirement to transform the line back to 50 Ω (as done in [59] and [60]). Two symmetrically opposite lines feed one polarization from two symmetrically opposite points of the patch. A difference in the path of lengths of the lines feeding to two ends is intentionally added to create a 180° phase shift between the two fed signals. Same topology is designed for the other polarization. Figure 5.1b shows the details of the dimensions of the feeding network.

5.2.1 S-Parameter Measurements

The design optimized in simulation was fabricated as shown in Figure 5.2. The scattering parameter response antenna for the two ports has been shown in Figure 5.3. The simulated and measured responses show a very good match, but second resonance point in measurement moves up the frequency band, due to unavoidable air-gaps between the dielectric layers. However, this does not affect the antenna performance in negative manner. In fact, the measured bandwidth actually increases due to this effect. Also, it should be noted that, two ports show slight differences in S-parameter response, since feeding networks are not identical. It can be seen that the designed antenna provides a wideband response and covers the complete desired band of 2.7

GHz to 3.0 GHz ($S_{11} \leq -10dB$). An isolation of around 30 dB has also been achieved within this band. Hence, the antenna satisfies the required objectives of wide bandwidth along with high isolation between the ports.

As also discussed in previous chapters, the air-gap can create the walking off effect of the higher resonant point. A comparison of measured response with the simulated one, where simulation model was introduced with air-gap errors between each layer of dielectric, has been presented in Figure 5.4. It can be seen that resonance frequencies of the simulation and measurement results match more closely, when an air-gap error of 0.25 mm is introduced in simulation.

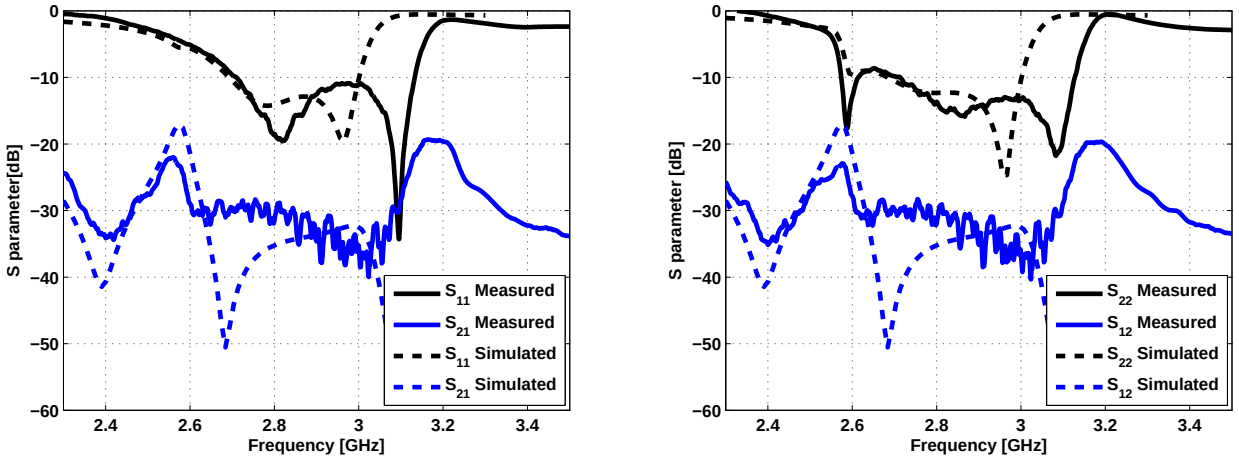

(a) Port 1 excitation

(b) Port 2 excitation

Figure 5.3: S-Parameter response of dual-pol differential feed stacked patch.

5.2.2 Far-field Radiation Pattern Measurement

The far-field pattern of the fabricated prototype was measured at the UCLA spherical near-field measurement chamber (Figure 5.5). The far-field radiation plots for the antenna for three frequencies within the band (2.7 GHz, 2.85 GHz, 3.0 GHz) have been plotted in Figure 5.6 (Port one excitation) and 5.7 (Port two excitation). There is good match between the simulated and measured patterns in principal and diagonal planes in the broadside direction. Towards the back direction, the mismatch between the simulated and measured patterns is due to the presence

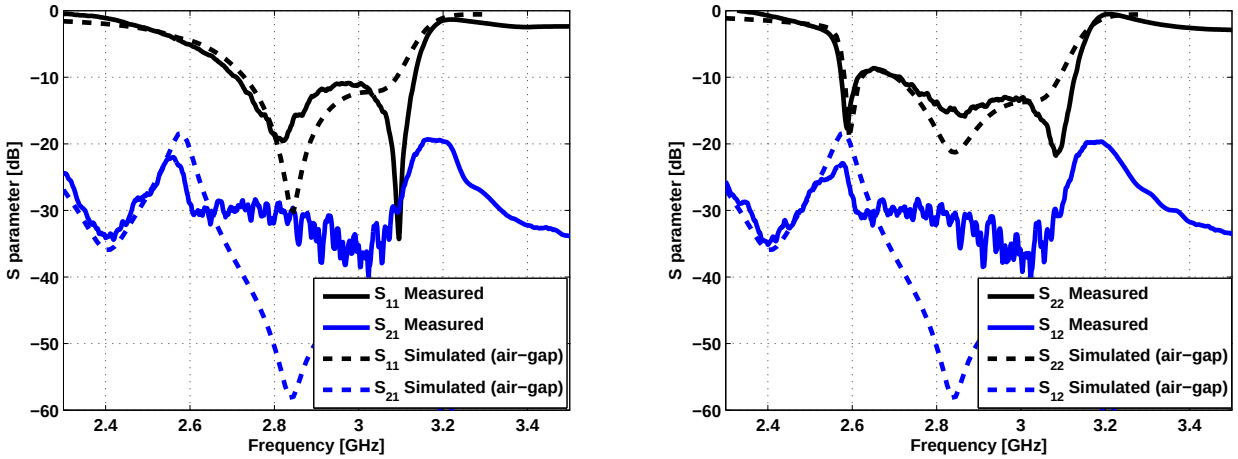

(a) Port 1 excitation

(b) Port 2 excitation

Figure 5.4: Comparison of measured v/s simulated. Simulation is conducted with introduced air-gap of 0.25 mm.

of antenna mount structure. It can be observed that there is an improvement in the cross-pol performance of the antenna, due to differential feeding configuration.

At 2.7 GHz, the cross-pol in all the planes is within -20 dB in the broad-side direction. In diagonal planes, this is an improvement over the previous configuration (non-differentially fed), where the diagonal plane cross-pol was found to be around -12 dB (Figure 4.13). The cross-pol numbers further improve with increasing frequency of operation. This is expected since the effective ground plane dimensions increase with increasing frequency [62]. At 3.0 GHz, the cross-pol is around -25 dB in most of the elevation angles, except for certain increase in some directions. In general the cross-pol performance of the antenna is improved as compared to the singly fed case of stacked patch element.

5.2.3 Far-Field Patterns and W-parameters

Simulated and measured far-field radiation from the antenna, with port one excitation for three frequencies across the band of interest, has been presented in Figures 5.8a – 5.13d. The general pattern of co and cross-pol field distribution measured has been found to be similar to the

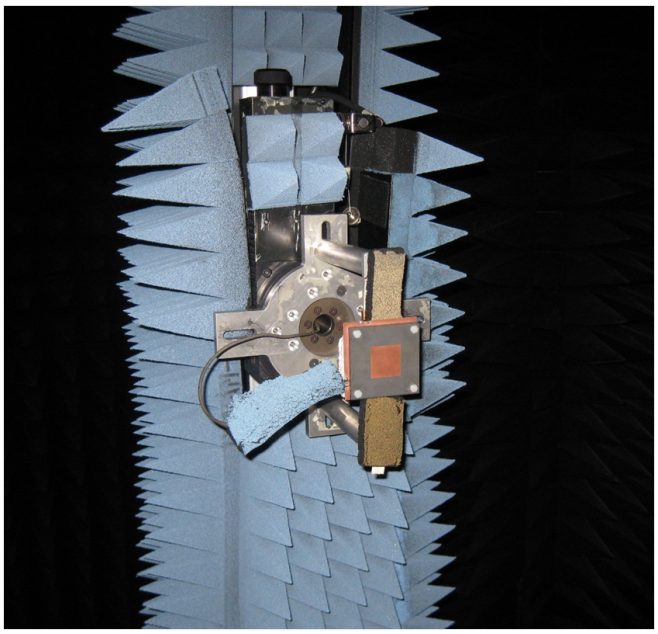

Figure 5.5: Far-field pattern measurement in the UCLA spherical near-field antenna chamber.

simulated one. The co-polar field pattern shows a broadside uniform phase beam, whereas, the cross-polar field contains four lobes with varying phase. These far-field distributions can now be used for calculation of W-parameters as defined in Chapter 1. Here, the definitions of the W parameters are re-iterated for convenience.

$$W_{hv} = \frac{\int_\Omega F_{hh}^2(\theta,\phi)F_{hh}^*(\theta,\phi)F_{hv}(\theta,\phi)d\Omega}{\int_\Omega |F_{hh}(\theta,\phi)|^4 d\Omega}$$

$$W_4 = \frac{\int_\Omega |F_{hh}(\theta,\phi)|^2|F_{hv}(\theta,\phi)|^2 d\Omega}{\int_\Omega |F_{hh}(\theta,\phi)|^4 d\Omega}$$

The calculated W-parameters from measured and simulated far-field patterns for the two ports has been presented in Table 5.1 and 5.2. Measured W_{hv} parameter for the antenna was found to be around -11 to -13 dB in the band of interest, whereas, W_4 parameter is found to be around -15 to -18 dB. W_{hv} is expected to be higher than W_4, since depends on first power of cross-pol pattern as compared to W_4, which depends on second power of cross-pol pattern.

The W-parameters calculated from simulation versus the measurements do have noticeable differences. These differences are expected, since even small variations in simulated versus mea-

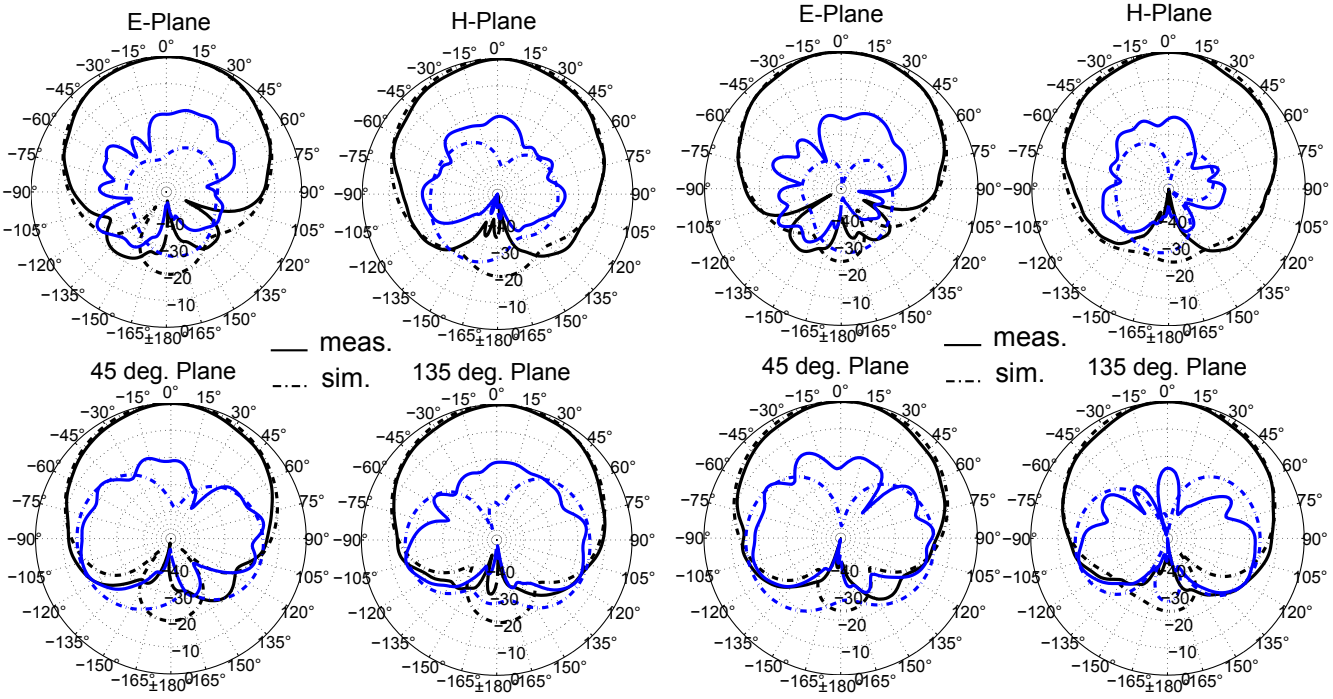

(a) Freq = 2.7 GHz

(b) Freq = 2.85 GHz

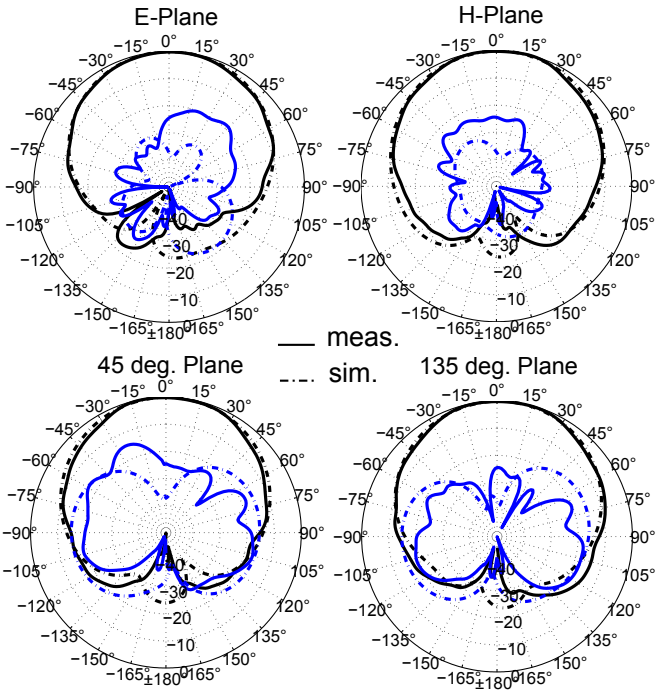

(c) Freq = 3.0 GHz

Figure 5.6: Far-field radiation pattern: port one excitation.

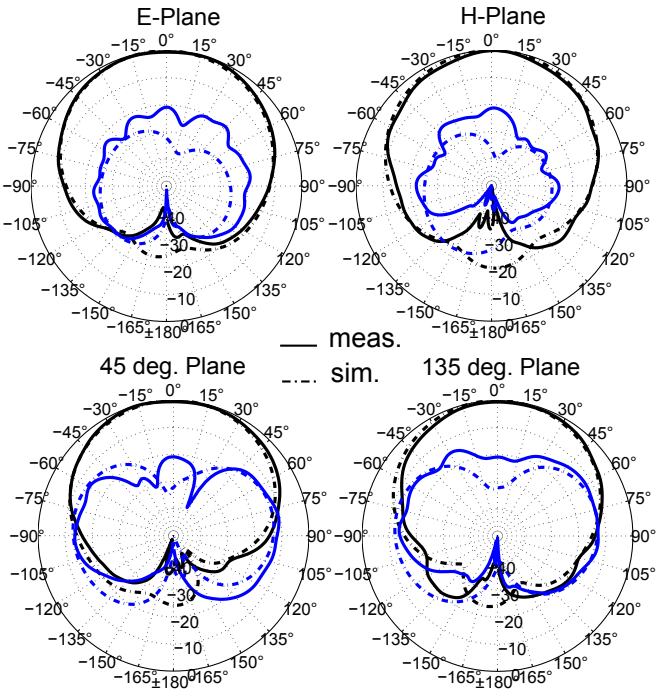

(a) Freq = 2.7 GHz

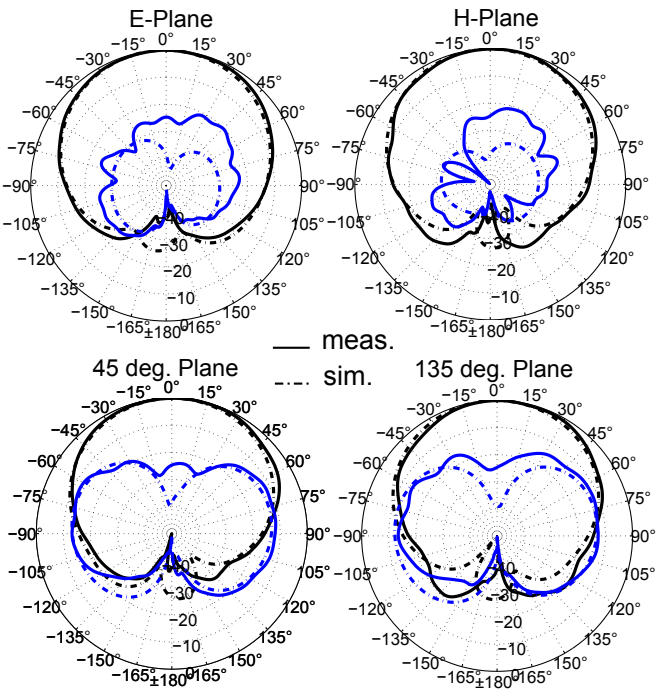

(b) Freq = 2.85 GHz

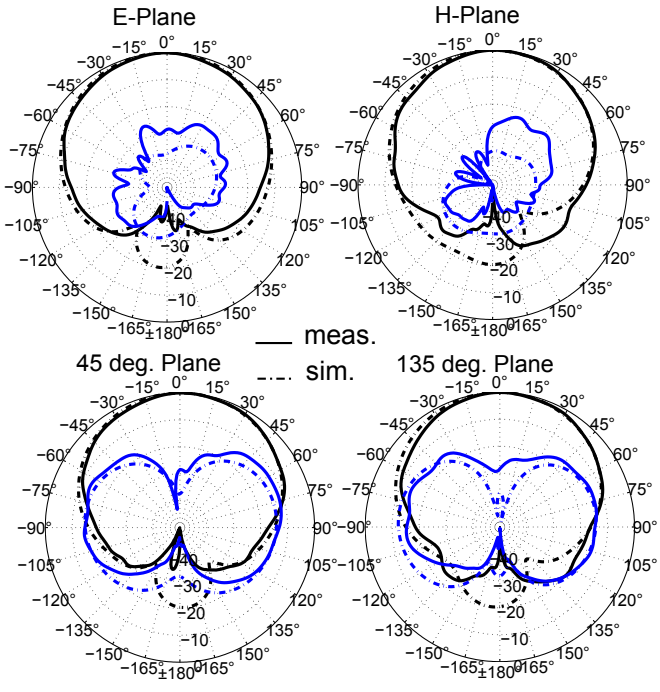

(c) Freq = 3.0 GHz

Figure 5.7: Far-field radiation pattern: port two excitation.

Table 5.1: W_{hv} and W_4 parameters for dual-pol differentially fed patch antenna. (Port one excitation)

Freq	W_{hv} (dB)		W_4 (dB)	
	Meas.	Sim.	Meas.	Sim.
2.70 GHz	-11.1	-18.4	-18.1	-19.9
2.85 GHz	-12.4	-22.4	-18.9	-20.4
3.00 GHz	-12.8	-20.1	-19.2	-18.7

Table 5.2: W_{hv} and W_4 parameters for dual-pol differentially fed patch antenna. (Port two excitation)

Freq	W_{hv} (dB)		W_4 (dB)	
	Meas.	Sim.	Meas.	Sim.
2.70 GHz	-12.8	-17.1	-15.3	-16.4
2.85 GHz	-12.9	-19.8	-15.4	-16.8
3.00 GHz	-13.3	-18.2	-16.0	-24.0

sured patterns in different directions can add to create an appreciable change in complete integrated number. From the table shown, W_4 parameter matches more closely to the simulated one for both the ports, as compared to W_{hv}. In Chapter 6, further analysis has been carried out to investigate the sensitivity of these numbers on radiation patterns.

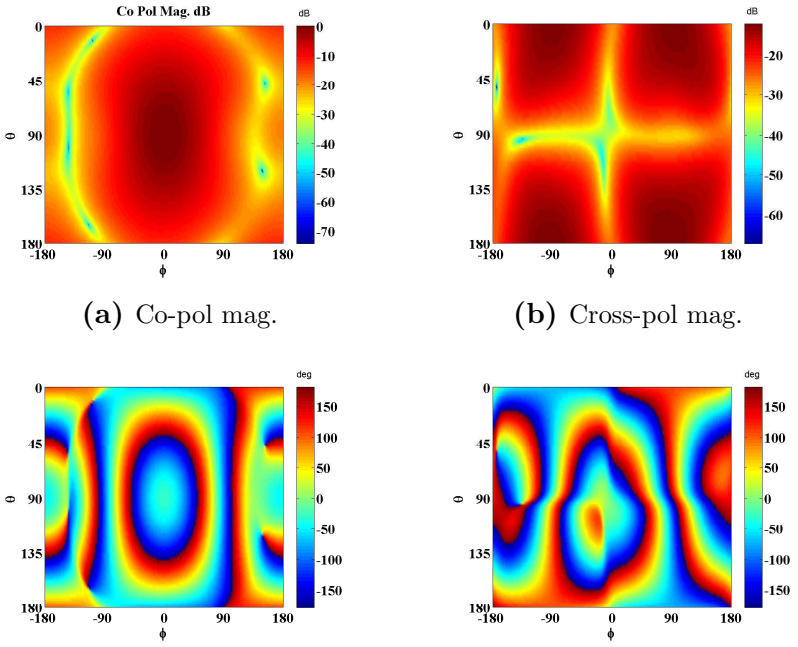

(a) Co-pol mag. **(b)** Cross-pol mag.

(c) Co-pol phase **(d)** Cross-pol phase

Figure 5.8: Simulated far-field radiation (Frequency = 2.7 GHz).

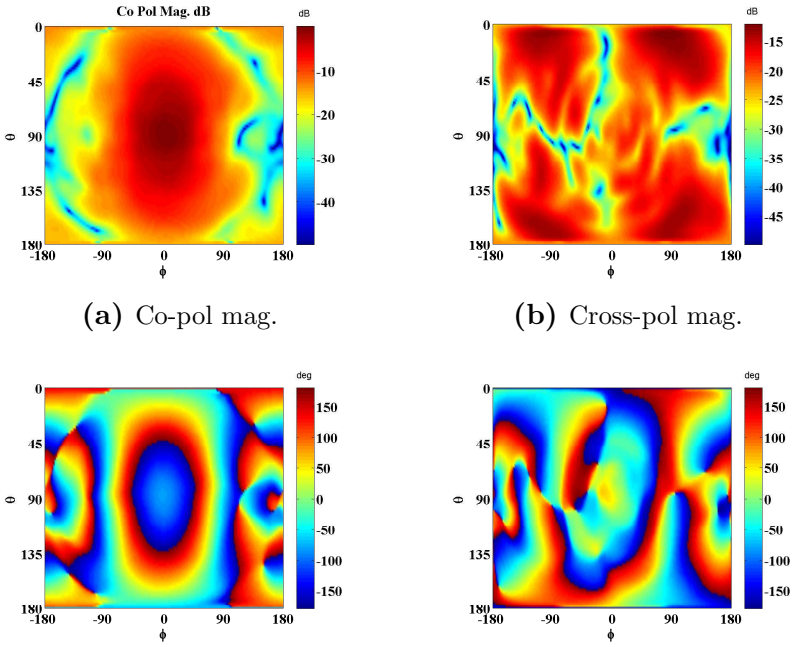

(a) Co-pol mag. **(b)** Cross-pol mag.

(c) Co-pol phase **(d)** Cross-pol phase

Figure 5.9: Measured far-field radiation (Frequency = 2.7 GHz).

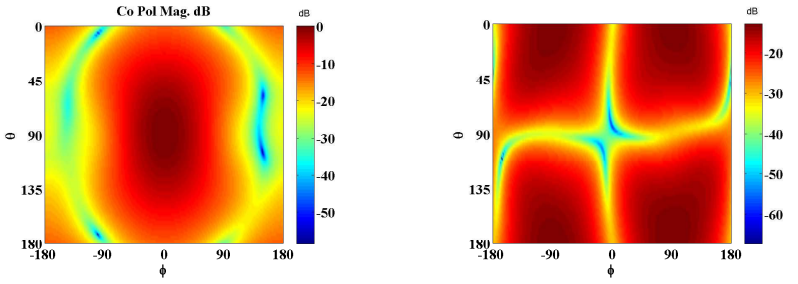

(a) Co-pol mag. **(b)** Cross-pol mag.

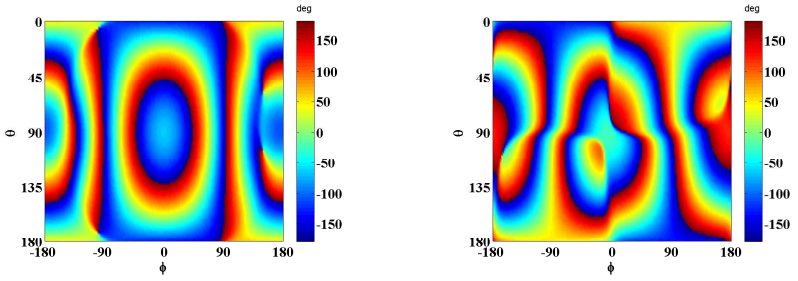

(c) Co-pol phase **(d)** Cross-pol phase

Figure 5.10: Simulated far-field radiation (Frequency = 2.85 GHz).

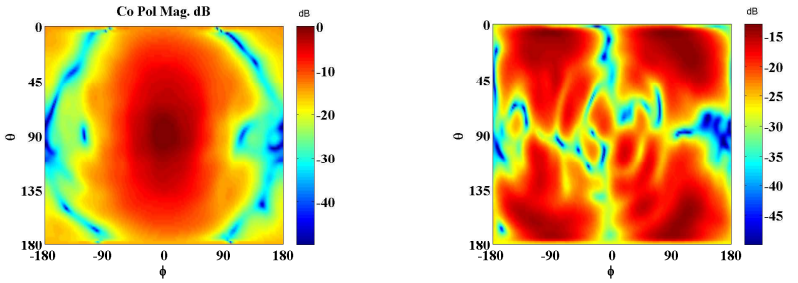

(a) Co-pol mag. **(b)** Cross-pol mag.

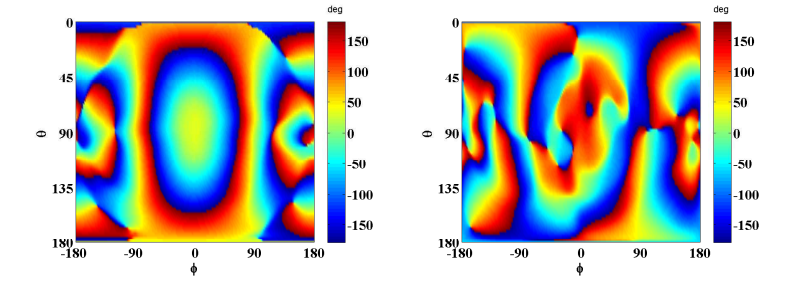

(c) Co-pol phase **(d)** Cross-pol phase

Figure 5.11: Measured far-field radiation (Frequency = 2.85 GHz).

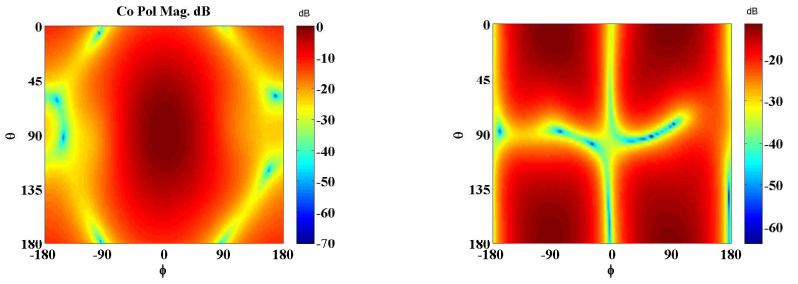

(a) Co-pol mag. **(b)** Cross-pol mag.

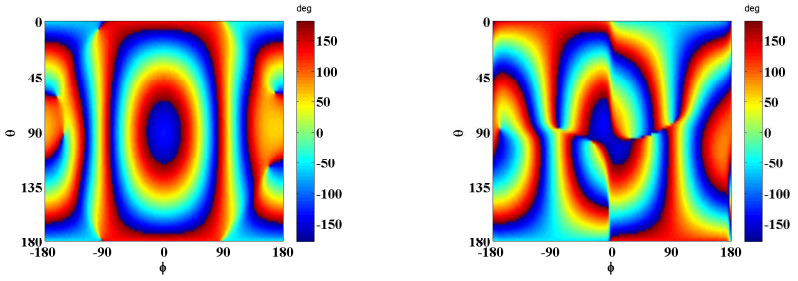

(c) Co-pol phase **(d)** Cross-pol phase

Figure 5.12: Simulated far-field radiation (Frequency = 3.0 GHz).

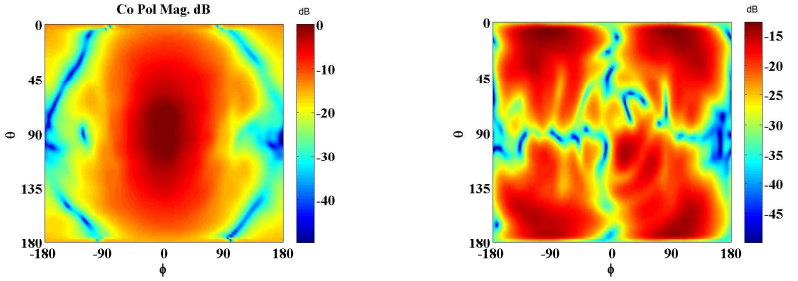

(a) Co-pol mag. **(b)** Cross-pol mag.

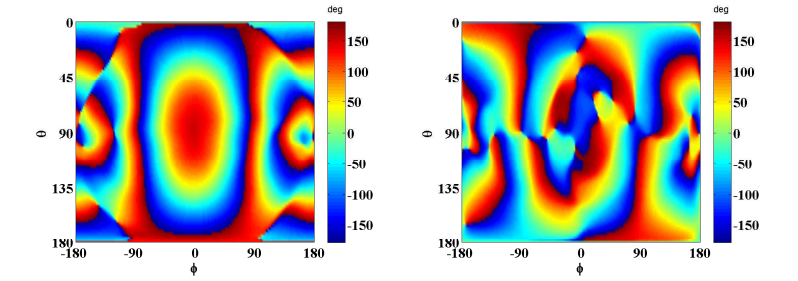

(c) Co-pol phase **(d)** Cross-pol phase

Figure 5.13: Measured far-field radiation (Frequency = 3.0 GHz).

Table 5.3: Various parameters of the array

Parameter	Sim	Meas.
Beamwidth	20°	20°
SLL*	-13.2 dB	-12.86 dB
Directivity	19.6 dB	19.5 dB
W_{hv}	-19.4 dB	-12.3 dB
W_4	-36.0 dB	-24.1 dB

5.2.4 Array Design

The final objective of the designed element is to be used in a 4×4 array for weather radar application. A general estimate of the radiation properties of the array can be made from the performance of the single element. In order to obtain a far-field pattern from an array, elemental pattern from a number of shifted elements (as according to the position of the array elements) can be summed in far-field. Figure 5.14 shows the schematic of the array considered for this exercise. The chosen distance between the two elements is specified 7 cm (same as the dimension of the element designed). As discussed in Chapter 2, the cross-pol in an array can be reduced with the use differential feeding. A differentially fed configuration in 2-D array, also known as rotating feeding configuration, can be employed here to reduce the cross-pol. But, since the elements are already differentially fed, it should not further reduce the cross-pol as compared to non-rotating feeding mechanism.

Tests were conducted to see, if rotating the elements in array would help in the further reduction of the cross-pol in 4×4 array. Figure 5.15 and 5.16 show the calculated far-fields from the elemental pattern of the single element in case of simulation and measurements at 2.85 GHz. Figure 5.15 shows the simulated patterns for the array for two cases- rotating and non-rotating feeding configurations. It is clear that rotating configuration does not help in reduction of the cross-pol in the broadside. In fact, in the off-broadside directions, the cross-pol radiation from the array increases in the rotating feeding case. Simulations show around -40 dB cross-pol level

*SSL means first side lobe level

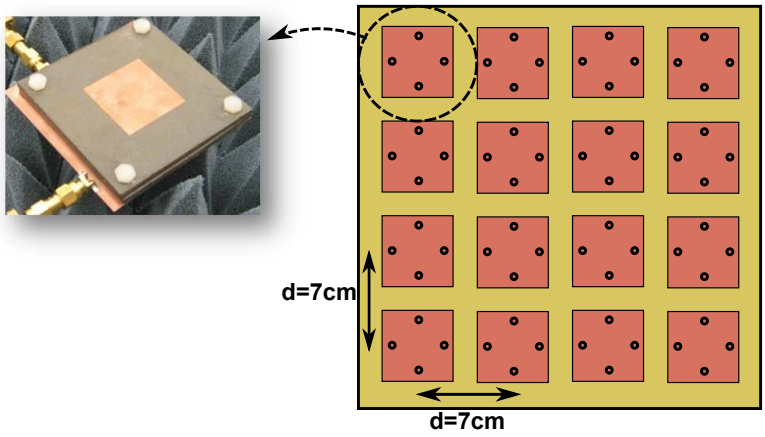

Figure 5.14: A 4×4 array generated from dual-polarized, differentially-fed patch element.

for non-rotating feeding.

Figure 5.16 shows the calculated radiation pattern from the array from the measured elemental pattern of the dual-pol, differentially-fed patch, with and without rotating feeding mechanism. Again, it is clear that the cross-pol does not improve in the broadside rather it becomes worse in the off-broadside directions when the elements are rotated. Measured patterns show -20 dB cross-pol level for the array. As discussed before, the cross-pol performance would improve when a larger ground plane is considered in the design [62].

Table 5.3 shows the simulated versus measured values of various parameters for the array in case of non-rotating feeding configuration. There is a good agreement between the simulated and measured values of these parameters. It can be concluded that, around 20 dB directivity, with 20° beam-width and -13 dB SLL would be achieved if an array is designed from the fabricated element. A noticeable improvement in W_4 parameter can be observed in the array (as compared to single element), but W_{hv} parameter remains almost same.

5.3 Conclusion

The shown design provides a cost effective and easily realizable solution for element which can used in developing S-band weather radar array. W-parameters, which are responsible for accurate measurement of differential reflectivity for weather radar, were calculated from the measured

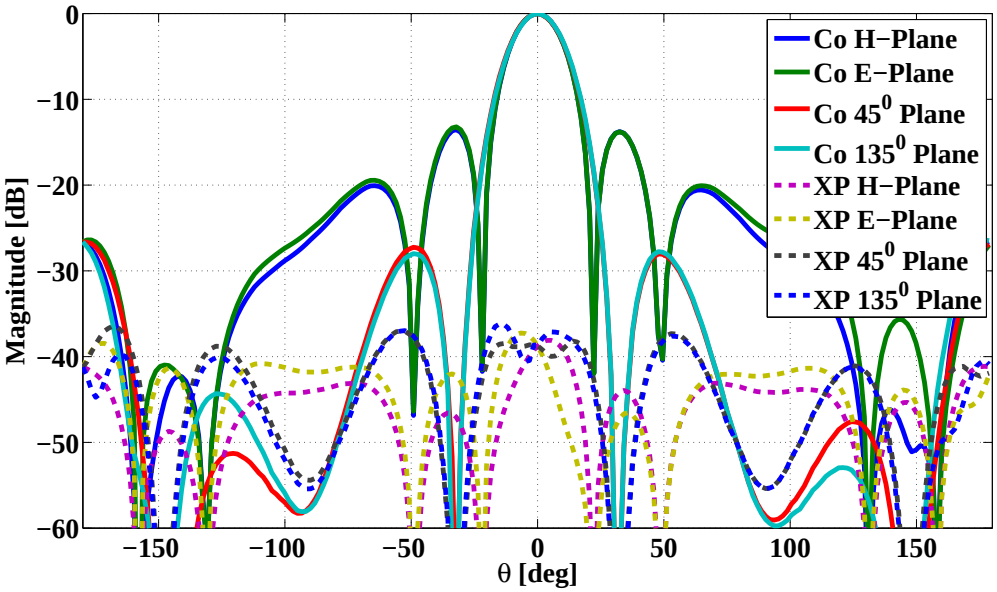

(a) Non-rotating feeding configuration

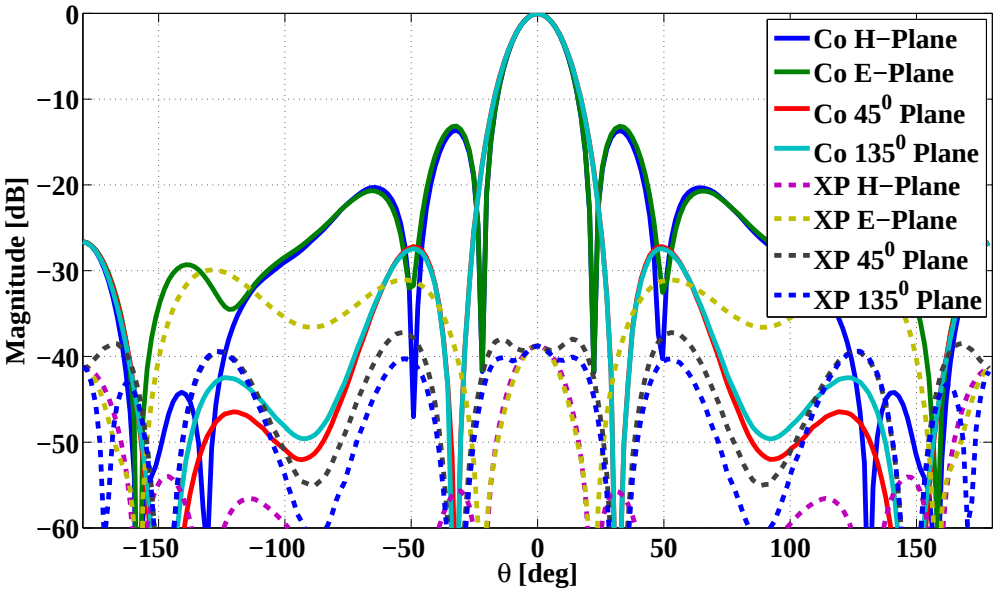

(b) Rotating feeding configuration

Figure 5.15: Synthesized array far-field pattern from simulated pattern of single element.

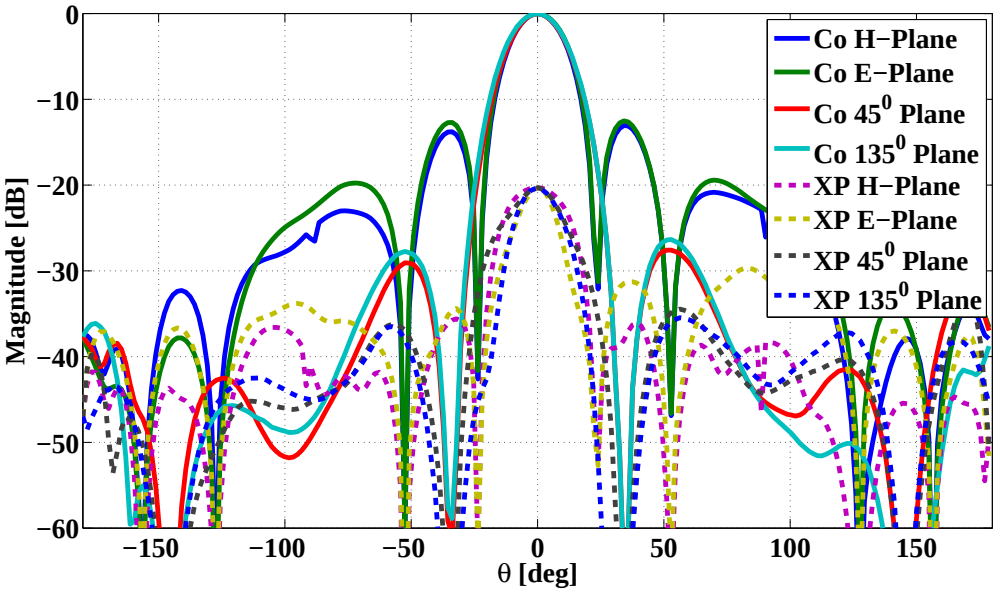

(a) Non-rotating feeding configuration

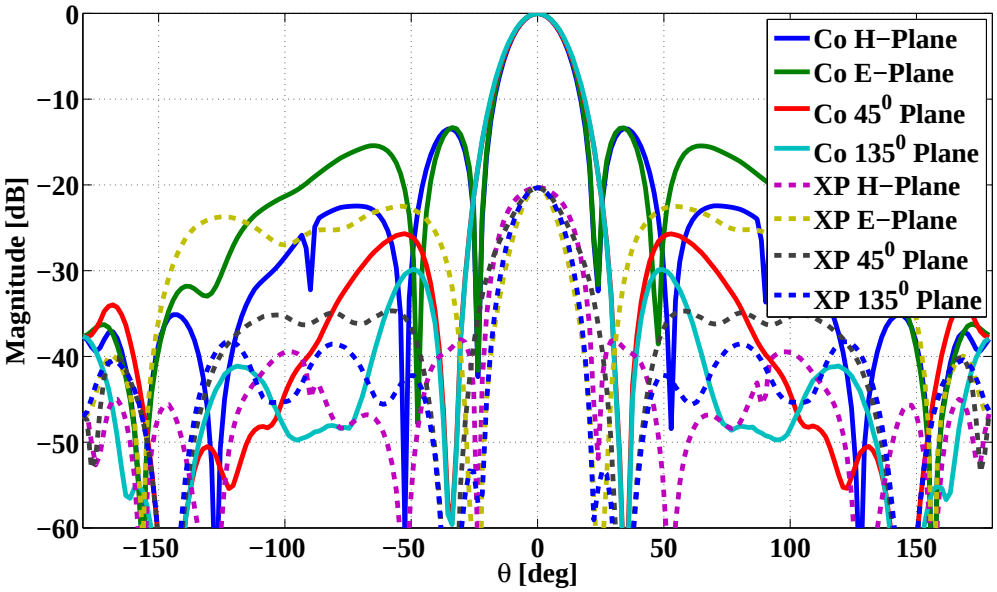

(b) Rotating feeding configuration

Figure 5.16: Synthesized array far-field pattern from measured pattern of single element.

Table 5.4: Summary of parameters of the realized design

Bandwidth:	400 MHz (2.7 GHz to 3.1 GHz)
Isolation:	$<$ -30 dB
Cross-Pol:	$<$ -20 dB
W_{hv}:	-11 dB to -13 dB
W_4:	-15 dB to -19 dB

radiation data. It was found that, there can be differences in the W-parameters calculated from simulated and measured radiation data, since small differences in pattern magnitude and phase can accumulate over the space and produce significant differences. A further study of various aspects of W-parameters has been conducted in the next chapter. W-parameters for this design also show some improvement over the singly fed stacked patch element shown in previous chapter. This is expected, since differential feeding mechanism reduces the cross-polar radiation decreasing the W-parameters.

The design shows a low cross-pol, high isolation performance with high bandwidth. The cross-pol of the element is further expected to decrease, when used in an array with larger ground plane [62]. A summary of the features of the realized design has been presented in Table 5.4.

Finally, to estimate the performance of a 4×4 array with demonstrated element, far-field pattern of the array has been calculated. General results of the array were obtained with simulation and measured elemental patterns. It is found that, 20 dB directivity with -13 dB side lobe level can be obtained with array made from the proposed element. Also, it has been verified that using rotation of element in the array will not help in reducing the cross-pol, since the individual elements are already differentially fed.

CHAPTER 6

Some Properties of W-Parameters

W-parameters (W_{hv} and W_4) as defined in [8], are the key parameters of any antenna which is to be used for polarimetry. These parameters are related to bias in differential reflectivity of the antenna, which is an important parameter for accurate prediction of weather conditions. In this work, these parameters have been calculated for two different types of patch antennas: (1) Dual-pol singly fed stacked patch antenna and (2) Dual-pol differentially fed stacked patch antenna. In previous chapters, the parameter W_{hv} has been found to be around -9 dB for the first antenna and around -12 dB for second antenna. Similarly, W_4 has been found to be around -15 dB and -19 dB respectively. The trend in reduction of W-parameters for the differentially fed stacked patch antenna is clear, however, some calculated numbers are out of the general trend. Also, when the simulated numbers are compared with the measured numbers, significant differences have been observed. In general, it appear that the W-parameters are sensitive to minor changes in the far-field distribution, which would explain the ambiguities in the general trend in the W-parameters and differences between the measured and simulated values. To investigate the sensitivity of the W-parameters on varying phase or magnitude of far-field distribution, study is conducted to observe the changes in W-parameters with changing phase or magnitude.

Another important aspect of the W-parameters is its dependence on the location of the antenna with respect to the origin. Since phase of the far-field is varying with changing position of the antenna and the integral for W_{hv} is a function of complex multiplication of the radiation patterns, this parameter may vary depending on position of the antenna near the origin.

A detailed study on these aspects of W-parameters have been presented in following sections.

6.1 Dependence of W-parameters on Far-Field Radiation Pattern

In order to observe the sensitivity of the W-parameters on the far-field radiation pattern, the cross-pol radiation of the antenna was modified such that now it had introduced errors. This exercise was conducted on the simulated field distribution of dual-pol, differentially fed stacked patch antenna presented in previous chapter. But the trends observed in this exercise should be true for any other designs too. The far-field and W-parameters are related by following relationship

$$W_{hv} = \frac{\int_\Omega F_{hh}^2(\theta,\phi)F_{hh}^*(\theta,\phi)F_{hv}^*(\theta,\phi)d\Omega}{\int_\Omega |F_{hh}(\theta,\phi)|^4 d\Omega} \tag{6.1}$$

$$W_4 = \frac{\int_\Omega |F_{hh}(\theta,\phi)|^2|F_{hv}(\theta,\phi)|^2 d\Omega}{\int_\Omega |F_{hh}(\theta,\phi)|^4 d\Omega} \tag{6.2}$$

The W_{hv} parameter depends on the phase antisymmetry and magnitude symmetry of the cross-polar pattern, therefore, the observed differences in simulated and measured values of the W-parameters may arise due to lack of exact antisymmetry of the fields. To simulate this effect, the errors were introduced by changing the magnitude or phase of one or two quadrants in the far-field (Figure 6.1 and 6.3). This introduces the antisymmetry of fields and the complete integral is expected to change.

6.1.1 Magnitude Errors

To understand the effect of magnitude errors, two cases are considered:(1) Modify the magnitude of the cross-polar field in one quadrant only (Figure 6.1a) (2) Modify the magnitude of the far-field in two quadrants (Figure 6.1b). Since modification of the field is in both ways - increasing as well as decreasing, these two cases cover the other two cases- when the cross-polar is modified in three quadrants or two other quadrants. The errors in particular quadrants are modified by multiplying by a factor M, which varies from 0.2 to 2, shown in following equation.

$$E_{new} = M.E_{old} \tag{6.3}$$

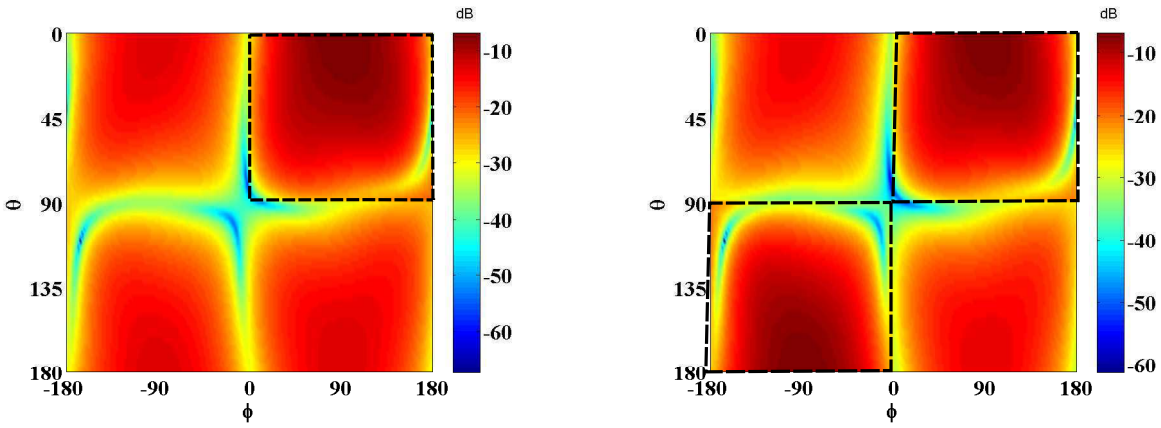

(a) Case 1: Magnitude Errors introduced in one quadrant

(b) Case 2: Magnitude errors introduced in two quadrants

Figure 6.1: Illustration showing regions where magnitude errors have been introduced.

For Case 1, range for applying above modification would be quadrant-one ($0 < \theta < 90, 0 < \phi < 180$) and for case 2, range would be quadrant-one ($0 < \theta < 90, 0 < \phi < 180$) and quadrant-three ($90 < \theta < 180, -180 < \phi < 0$). The W-parameters obtained by changing values of M are plotted in Figure 6.2. The trend of variation of W_{hv} and W_4 are similar for the two cases. W_{hv} increases when the M is changed from value one towards either directions, whereas W_4 monotonically increases on increasing M from 0.2 to 2. W_{hv} has phase component in its calculation and integral with phase component can change either way, when magnitude in one or two quadrants is changed. W_4, which depends only on the absolute value of cross-polar field, monotonically increases when cross-pol magnitude is increased in partial space. Finally, the variation in case 2 is stronger as compared to case one, since the variation is taking place in two quadrants as compared one.

It is clear that even minor changes of cross-polar field in one of the quadrants can create significant variations in the W-parameters. In plot shown in Figure 6.2a, a variation in M from 1 to 1.2 (1.6 dB change), can create almost 3 dB change in W_{hv}. In previous chapter, it was observed that there can be difference in simulated and observed values of cross-pol in different planes (Figures 5.6 and 5.7). This analysis here proves that such differences in magnitude can create appreciable differences in the W-parameters.

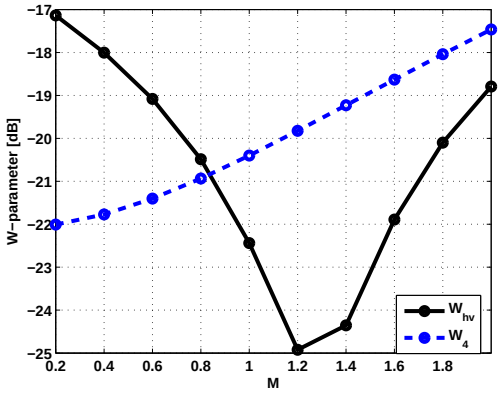

(a) Magnitude Errors introduced in one quadrant

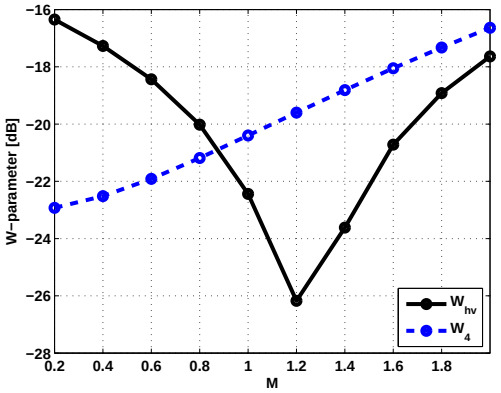

(b) Magnitude errors introduced in two quadrants

Figure 6.2: Variation of W-parameters with introduced magnitude errors in cross-polar field (Frequency = 2.85 GHz).

6.1.2 Phase Errors

Since W_{hv} parameter is dependent on the phase of the co and cross polar field, study is conducted to understand this relationship. It can be proven that W_{hv} depends on the difference of the phases of co and cross-polar field at each point in space (Equation 6.4), hence adding a linear error in phase of cross-polar pattern should be enough to simulate the error in phase of co and cross-polar field.

$$\begin{aligned} W_{hv} &= \frac{\int_\Omega F_{hh}^2(\theta,\phi)F_{hh}^*(\theta,\phi)F_{hv}^*(\theta,\phi)d\Omega}{\int_\Omega |F_{hh}(\theta,\phi)|^4 d\Omega} \\ &= \frac{\int_\Omega |F_{hh}(\theta,\phi)|^3 |F_{hv}(\theta,\phi)| e^{j\phi_{hh}-j\phi_{hv}} d\Omega}{\int_\Omega |F_{hh}(\theta,\phi)|^4 d\Omega} \end{aligned} \tag{6.4}$$

where ϕ_{hv} and ϕ_{hh} are the phases for the cross-polar and co-polar field components. Following formulation can be used to simulate the phase error in one quadrant (case 1) or two quadrants (case 2).

$$\phi_{hv}^{new} = \phi_{hv}^{old} + \phi_{err} \tag{6.5}$$

For Case 1, range for applying above modification would be quadrant-three ($90 < \theta < 180, -180 < \phi < 0$) and for case 2, range would be quadrant-one($0 < \theta < 90, 0 < \phi < 180$) and quadrant-three ($90 < \theta < 180, -180 < \phi < 0$), as shown in Figures 6.3a and 6.3b respectively.

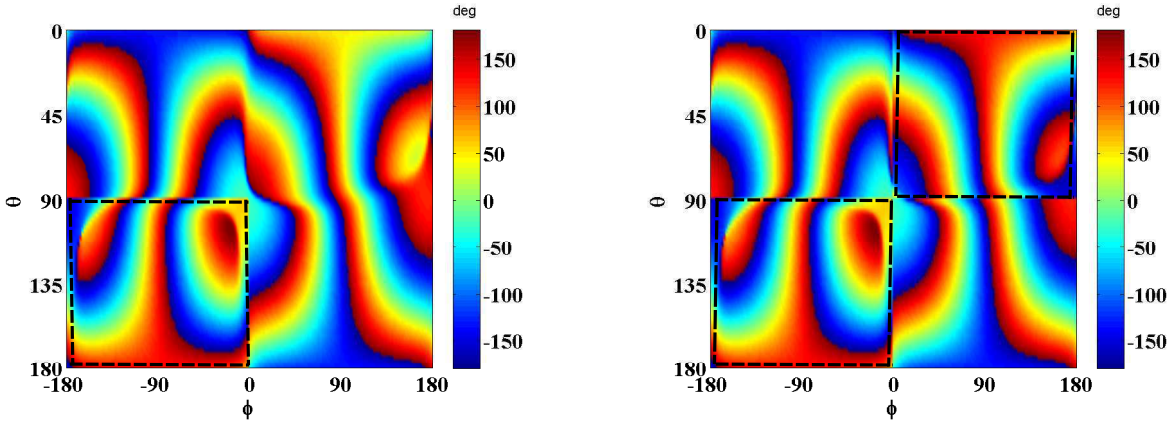

(a) Case 1: Phase Errors introduced in one quadrant

(b) Case 2: phase errors introduced in two quadrants

Figure 6.3: Illustration showing regions where phase errors have been introduced.

Figure 6.4 shows the variation in W_{hv} with changing phase error for the two cases. The variation is periodic with changing value of introduced phase error, since the phase variation can create constructive and destructive interference with the non-varying field in other quadrants. It can be observed that even a minor variation of $\pm$ 5 deg of phase can create a difference of 2 dB and 6 dB in W_{hv} for cases 1 and 2 respectively. The variation is more for two quadrant case, which means the W_{hv} variation keeps increasing till half of the complete space has uniformly added phase errors. After more than half the space has phase errors, W_{hv} should decrease, since it starts to converge to case 1.

The study reveals that these parameters are sensitive to changes in phase and magnitude variation in the the FF radiation. The study is conducted with uniformly added phase and magnitude errors, which is a simplified case and may not be practically relevant, but the study gives a qualitative idea how there can be wide differences in the W-parameters, due to relatively small variations in pattern measurements (as compared to simulation). In general, the differences in the measured and simulated values of W-parameters obtained in previous chapters can be

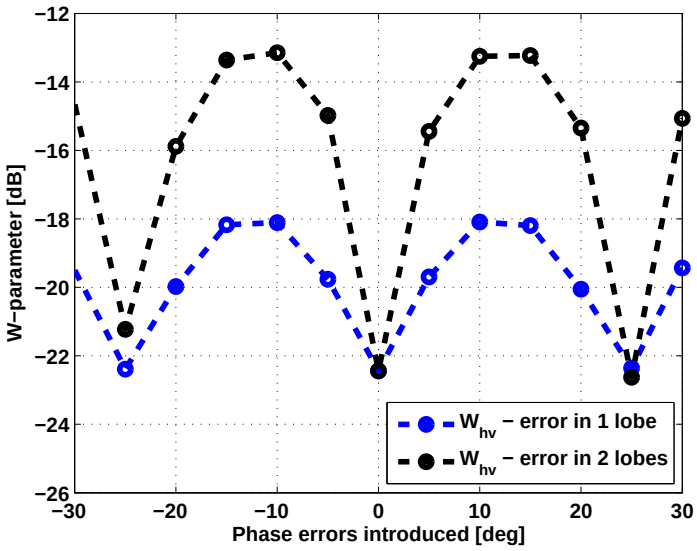

Figure 6.4: Variation of W_{hv} with introduced phase errors in cross-polar field (Frequency = 2.85 GHz).

explained and accounted for using this analysis.

6.2 W-Parameters with Changing Coordinate System

Magnitude of the far-field radiation remains same with small variations of the antenna position with respect to the origin, as long as the relative position of the antenna with respect to the origin is not in the far-field of the antenna. However, the phase of the radiated signal at a point in far-field can change with small changes in antenna position with respect to the origin. The parameter W_{hv} depends on the magnitude as well as the phase of the co and cross-pol of the antenna, hence is expected to change with changing antenna position. However, it can be proven mathematically that due to conjugate multiplication of the co and cross-polar fields, the parameter does not change with changing position of the coordinate system.

6.2.1 Mathematical Proof for Independence of Coordinate System

In general, an antenna can be represented by 3-D current source ($\vec{J} = J_x\hat{x}+J_y\hat{x}+J_z\hat{x}$), distributed in an aperture of area S. Figure 6.5 shows the antenna with coordinate system considered for this analysis. It will be shown that W_{hv} parameter calculated for the antenna situated at position vector $\vec{x}$ is same as for the antenna situated at the origin.

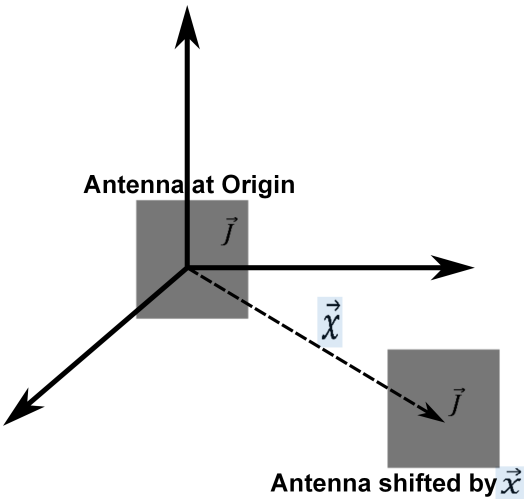

Figure 6.5: The shifting in the position of antenna to understand the dependence on the choice of coordinate system.

To start with, the antenna situated at the origin is considered. The radiated field from these components can be written as [63]

$$E_\theta = \frac{-j\beta e^{(-j\beta R)}}{4\pi R}\eta N_\theta \tag{6.6}$$

$$N_\theta = \int_S (J_x\cos\theta\cos\phi + J_y\cos\theta\sin\phi - J_z\sin\phi)e^{(j\beta\vec{r'}.\hat{r})}ds' \tag{6.7}$$

$$E_\theta = \frac{-j\beta e^{(-j\beta R)}}{4\pi R}\eta N_\phi \tag{6.8}$$

$$N_\phi = \int_S (-J_x\sin\theta + J_y\cos\phi - J_z\sin\phi)e^{(j\beta\vec{r'}.\hat{r})}ds' \tag{6.9}$$

$\hat{r}$ is the direction of observation, which can also be represented by (θ, ϕ), β is propagation constant in free space, and $\vec{r'}$ is the vector representing position of any point on antenna with respect to the origin. Considering Ludwig's second definition of cross-pol, for a horizontally

polarized antenna, E_θ can be considered cross-pol and E_ϕ can be considered co-pol component. Hence,

$$E_\theta = F_{hv} \tag{6.10}$$

$$E_\phi = F_{hh} \tag{6.11}$$

Here, for simplicity only the kernel of numerator of the integral shown in 6.1, since space integral is going to be same for both positions of the antenna. Also, denominator consists of absolute values of far-field which remain independent of the small changes in antenna position with respect to the origin. Hence the kernel of the inetegral would be,

$$Kernel = (F_{hh}(\theta,\phi))^2 (F_{hh}(\theta,\phi))^* (F_{hv}(\theta,\phi))^* \tag{6.12}$$

Now, if the antenna is shifted to a new position with respect to the origin, represented by position vector $\vec{x}$, the same formulation can be written as:

$$F^x_{hv} = E^x_\theta = \frac{-j\beta e^{(-j\beta R)}}{4\pi R}\eta N^x_\theta \tag{6.13}$$

$$N^x_\theta = \int_S (J_x \cos\theta\cos\phi + J_y \cos\theta \sin\phi - J_z \sin\phi) e^{(j\beta(\vec{r'}+\vec{x}).\hat{r})} ds' \tag{6.14}$$

$$F^x_{hh} = E^x_\phi = \frac{-j\beta e^{(-j\beta R)}}{4\pi R}\eta N^x_\phi \tag{6.15}$$

$$N^x_\phi = \int_S (-J_x \sin\theta + J_y \cos\phi - J_z \sin\phi) e^{(j\beta(\vec{r'}+\vec{x}).\hat{r})} ds' \tag{6.16}$$

Considering the kernel of the integral in numerator in 6.1,

$$
\begin{aligned}
Kernel &= (F^x_{hh}(\theta,\phi))^2 (F^x_{hh}(\theta,\phi))^* (F^x_{hv}(\theta,\phi))^* \\
&= |F^x_{hh}(\theta,\phi)|^2 \times \\
&\quad \left[\frac{-j\beta e^{(-j\beta R)}}{4\pi R}\eta \int_S (-J_x \sin\theta + J_y \cos\phi - J_z \sin\phi) e^{(j\beta(\vec{r'}+\vec{x}).\hat{r})} ds'\right] \times \\
&\quad \left[\frac{-j\beta e^{(-j\beta R)}}{4\pi R}\eta \int_S (J_x \cos\theta\cos\phi + J_y \cos\theta \sin\phi - J_z \sin\phi) e^{(j\beta(\vec{r'}+\vec{x}).\hat{r})} ds')\right]^* \\
&= |F^x_{hh}(\theta,\phi)|^2 \times e^{(j\beta\vec{x}.\hat{r})} e^{(-j\beta\vec{x}.\hat{r})} \times \\
&\quad \left[\frac{-j\beta e^{(-j\beta R)}}{4\pi R}\eta \int_S (-J_x \sin\theta + J_y \cos\phi - J_z \sin\phi) e^{(j\beta\vec{r'}.\hat{r})} ds'\right] \times \\
&\quad \left[\frac{-j\beta e^{(-j\beta R)}}{4\pi R}\eta \int_S (J_x \cos\theta\cos\phi + J_y \cos\theta \sin\phi - J_z \sin\phi) e^{(j\beta\vec{r'}.\hat{r})} ds')\right]^*
\end{aligned}
$$

Here, due to complex conjugate formulation of W_{hv}, the expression becomes independent of $\vec{x}$, and also $|F^x_{hh}| = |F_{hh}|$ since both differ only in phase. Therefore the integral kernel becomes,

$$
\begin{aligned}
Kernel &= |F_{hh}(\theta,\phi)|^2 F_{hh}(\theta,\phi)(F_{hv}(\theta,\phi))^* \\
&= (F_{hh}(\theta,\phi))^2 (F_{hh}(\theta,\phi))^* (F_{hv}(\theta,\phi))^*
\end{aligned}
\tag{6.17}
$$

which is the integral kernel, when antenna is at the origin (Equation 6.12). Above derivation proves that the parameter W_{hv} is independent of the position of the antenna with respect to the origin. It should be noted that in above derivation, the magnitude of the far-field radiation has been assumed to be constant when the position of the antenna is changed with respect to the origin. This assumption is valid only when the antenna is moved to a small distance and origin is not in the far-field of the antenna.

6.2.2 Validation by Simulation

In order to check the validity of the above derivation, far-field patterns for different relative positions of the antenna were calculated (using HFSS). W_{hv} was calculated for these different sets of far-field data. Figure 6.6 shows three different positions of the antenna with respect to

the origin, which were used in this analysis. In position A (Figure 6.6a), the antenna is kept in front of the origin (121,0,0). This position is considered, since in the measurement facility at UCLA, the AUT is placed 121 mm in front of the origin of the spherical near-field chamber. Position B has the origin at the corner of the patch antenna, whereas position C has origin at the center of the aperture of the antenna.

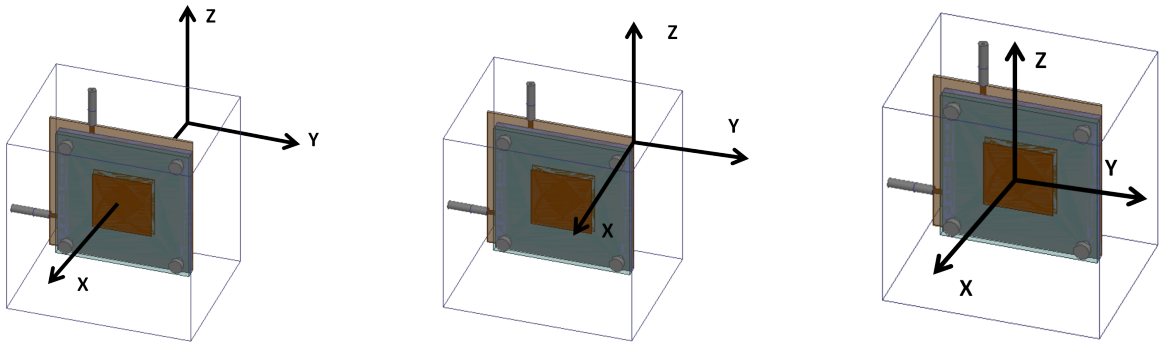

(a) Position A **(b)** Position B **(c)** Position C

Figure 6.6: Three cases of choice of antenna positions for testing its effect on W_{hv}.

Figure 6.7 shows the calculated far-field for three antenna positions. As expected, the magnitude of co and cross-polar fields are same for the three cases. The phase of fields is symmetrical in positions A and C, but is asymmetrical for position B, because of asymmetric position of the antenna with respect to the origin. Also, position A shows more variation in phase as the observation point moves away from broadside. Overall, significant changes in the far-field phase can be observed, as the antenna position is moved with respect to the origin.

Calculated W_{hv} parameter for three antenna positions is listed in Table 6.1. It is clear that, the parameter remains same for different positions of the antenna near the origin. This validates the mathematical proof provided in previous section.

6.3 Conclusion

The difference in the values of W-parameters from measurement as compared to from simulation arises due to small phase and/or magnitude variations. These relatively small errors can magnify

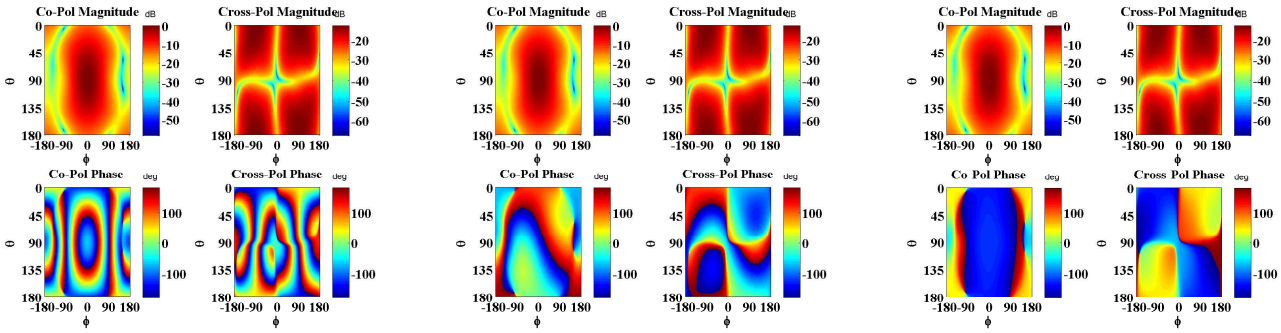

(a) Position A **(b)** Position B **(c)** Position C

Figure 6.7: Far-field distribution for different positions of the antenna.

Table 6.1: W_{hv} and W_4 for three antenna positions

	Position A	Position B	Position C
W_{hv}	-22.44 dB	-22.44 dB	-22.44 dB
W_4	-20.4 dB	-20.4 dB	-20.4 dB

because of the integration over the entire space and can create significant differences in measured results. It has been shown that a small phase error of ±5 deg can create a difference as large as 3 - 6 dB in the calculated W_{hv} value.

W-parameters are found to be independent of the position of the antenna with respect to the coordinate system origin (assuming origin is not in the far-field of the antenna). Analytical proof has been presented and the property is also validated by simulations conducted for various positions of the a antenna with respect to the origin.

CHAPTER 7

Conclusion

The complete body of work can be broadly divided into two main parts- analysis part and the design part. In the analysis part, certain basic aspects of a rectangular patch antenna have been studied, with a new strategy of near-field model. The objective of designing the required antenna element for the given application of the weather radar is the design part of the work. Concluding remarks on the work presented in this thesis have been presented as below.

7.1 Analysis

A high H-plane cross-pol has been a conventional problem for rectangular patch antennas. In contrast to previous studies conducted on cross-pol by various authors, in current work, the near-field of the patch antenna has been utilized to understand the cross-polar radiation from the coaxially fed, rectangular patch antennas. It has been shown that a high H-plane cross-pol in the far-field can indeed be modelled as asymmetries (or errors) in the near-field of the antenna. An asymmetry in the near-field electric field magnitude is expected due to probe offset in the antenna, but interestingly, this offset in probe also manifests itself as a deviation of phase from what is ideally expected. A close match between the trends in the near-field phase/magnitude errors and the far-field H-plane cross-pol has been found in various parametric studies conducted. Overall, this work provides an intuitive understanding of the cross-pol generation in rectangular patches with the help of graphical visualization.

Furthermore, this near-field model is applied to understand the mechanism of cross-pol reduction on two popular antenna configurations: (1) differentially fed patches and (2) array with rotating feeding. In the case of differentially fed patches, the near-field errors generated from two

(out of phase) excitations get cancelled out creating a low H-plane cross-pol. In the rotating feed configuration, due geometrical rotation of the neighbouring elements, asymmetric fields from a single element still creates a symmetric field distribution over the entire array aperture. This action restores the H-plane cross-pol of the antenna to a lower value.

Next in analysis part, a comprehensive study of slot loaded patch antennas has been undertaken. Slot loading is becoming a popular method for size reduction and/or bandwidth enhancement. In this work, it has been shown that subject to differing positions and orientations of the slot in a rectangular patch antenna, RF-mechanism and radiation mechanism of the antenna can show variations. Four popular slot-loaded antennas have been considered: C-shaped, double C-shaped, U-slotted and E-shaped patch antenna and relation between the performance parameters of these antennas and the slot position/orientation has been drawn. Once again, the near-field model developed before has been utilized to intuitively understand the radiation mechanism in these antennas. To conclude, it has been shown that C and double C-shaped patches are compact antenna designs with high cross-polar radiation and narrow bandwidth, where as E-shaped and U-slotted designs are relatively large with wide bandwidth.

7.2 Design

In the design part of the work, a high bandwidth, high isolation dual-polarized, low cross-pol rectangular stacked patch antenna to be used in S-band weather radar has been developed and demonstrated. The work has been conducted as an evolution from single-pol stacked patch design to dual-pol stacked patch design to differentially fed, dual-pol stacked patch design. This evolution of design clearly demonstrates a better cross-pol and port isolation performance when a differential feeding configuration is used. The final design meets the projected goals of 300 MHz bandwidth with -30 dB isolation and therefore can be utilized in S-band weather radar array.

It is believed by the author that for the first time, recently published parameters critical to the performance evaluation of antennas in weather radar scenarios, called W-parameters have been calculated from simulation and measurement data on a demonstrated hardware. Therefore,

the work provides complete characterization of the antenna element for the weather radar array application. Various simulation studies are conducted on these parameters, which demonstrate their dependence on phase and amplitude variations of the far-field in a practical patch element design. These studies suggest that W-parameters are sensitive to the small phase or amplitude variations in the far-field. Similarly, variations of W-parameters with changing position of the antenna with respect to the coordinate system have been mathematically analyzed and it is found that these parameters are independent of the choice of the antenna position. This result is further verified by numerical full-wave simulations. The development and then complete characterization of the stacked patch antenna element, along with the study of W-parameters, would prove helpful in designing weather radar systems.

References

[1] "Polarimetric doppler radar," http://www.nssl.noaa.gov/research/radar/dualpol.php, NOAA's National Severe Storm Facility, [Online; accessed 26-May-2012].

[2] Y. Wang and V. Chandrasekar, "Polarization isolation requirements for linear dual-polarization weather radar in simultaneous transmission mode of operation," *IEEE Transactions on Geoscience and Remote Sensing*, vol. 44, no. 8, pp. 2019–2027, Aug. 2006.

[3] C. Wolff, "Radartutoria," http://www.radartutorial.eu/15.weather/wx23.en.html, [Online; accessed 26-May-2012].

[4] K. V. Beard and C. Chuang, "A new model for the equilibrium shape of raindrops," *Journal of Atmospheric Science*, vol. 44, no. 11, pp. 1509–1524, 1987.

[5] "Differential reflectivity from raindrops and WSR-88D rainfall estimation," http://www.chill.colostate.edu/w/Differential_Reflectivity_from_Raindrops_and_WSR-88D_Rainfall_Estimation, Colorado State University- CHILL National Radar Faility, [Online; accessed 26-May-2012].

[6] G. Zhang, R. Doviak, D. Zrnic, and J. Crain, "Phased array radar polarimetry for weather sensing: Challenges and opportunities," *Geoscience and Remote Sensing Symposium*, pp. 449–452, 2008.

[7] W. Wasylkiwskyj and W. K. Kahn, "Theory of mutual coupling among minimum-scattering antenna," *IEEE Transactions on Antenna and Propagation*, vol. AP-18, no. 2, pp. 204–216, March 2008.

[8] D. Zrnic, R. Doviak, G. Zhang, and A. Ryzhkov, "Bias in differential reflectivity due to cross coupling through the radiation patterns of polarimetric weather radars," *Journal of Atmospheric and Oceanic Technology*, vol. 27, no. 10, pp. 1624–1637, Oct. 2010.

[9] V. Chandrasekar and R. J. Keeler, "Antenna pattern analysis and measurements for multiparameter radars," *Journal of Atmospheric and Oceanic Technology*, vol. 10, no. 5, pp. 674–683, Oct. 1993.

[10] D. N. Moisseev, C. M. N. Unal, H. W. J. Russchenberg, and L. P. Ligthart, "Improved polarimetric calibration for atmospheric radars," *Journal of Atmospheric and Oceanic Technology*, vol. 19, no. 12, pp. 1968–1977, Dec. 2002.

[11] A. V. Ryzhkov and D. S. Zrni, "Depolarization in ice crystals and its effect on polarization measurements," *Journal of Atmospheric and Oceanic Technology*, vol. 24, no. 7, pp. 1256–1267, 2007 July.

[12] J. C. Hubbert, S. M. Ellis, M. Dixon, and G. Meymaris, "Modeling, error analysis and evaluation of dual-polarization variables obtained from simultaneous horizontal and vertical polarization transmit radar. part i: Modelling and antenna errors." *Journal of Atmospheric and Oceanic Technology*, vol. 27, no. 10, pp. 1583–1598, Oct. 2010.

[13] Y. Wang and V. Chandrasekar, "Polarization isolation requirements for linear dual-polarization weather radar in simultaneous transmission mode of operation," *IEEE Transactions on Geoscience Remote Sensing*, no. 44, pp. 2019–2028, 2006.

[14] Y. Wang, V. Chandrasekar, and V. N. Bringi, "Characterization and evaluation of hybrid polarization observation of precipitation," *Journal of Atmospheric and Oceanic Technology*, vol. 23, no. 4, pp. 552–572, April 2006.

[15] S. Bhardwaj and Y. Rahmat-Samii, "Understanding the cross-pol. generation in patch antennas: A near-field approach," in *URSI*, Boulder, Colorado, Jan. 2012.

[16] P. Hammer, D. V. Bouchaute, D. Verschraeven, and A. V. de Capelle, "A model for calculating the radiation field of microstrip antennas," *IEEE Transactions on Antenna and Propagation*, vol. 27, no. 2, pp. 267–290, March 1979.

[17] G. Dubost, "Far-field radiated by rectangular patch microstrip antenna," *Electronics Letters*, vol. 18, no. 23, pp. 991–992, Nov. 1982.

[18] M. L. Oberhart and Y. T. Lo, "New simple feed network for an array module of four microstrip elements," *Electronics Letters*, vol. 23, no. 9, pp. 436–437, Apr. 1987.

[19] W. F. Richards and Y. T. Lo, "An improved theory for microstrip antennas and applications," *IEEE Transactions on Antenna and Propagation*, vol. 29, no. 1, pp. 38–46, Jan. 1981.

[20] R. Q. Lee, T. Huynh, and K. F. Lee, "Experimental study of the cross-polarization characteristics of rectangular patch antennas," *Antennas and Propagation Society International Symposium*, vol. 2, pp. 636–639, June 1989.

[21] T. Huynh, K. F. Lee, and R. Q. Lee, "Cross polarization characteristics of rectangular patch antennas," in *Antennas and Propagation Society International Symposium*, vol. 2, June 1988, pp. 708–711.

[22] C. A. Balanis, *Antenna Theory: Analysis and Design*, 3rd ed. John Wiley and Sons, Inc.

[23] A. C. Ludwig, "The definition of cross polarization," *IEEE Transactions of Antenna and Propagation*, vol. 21, no. 1, pp. 116–119, Jan. 1973.

[24] C. A. Balanis, *Advanced Engineering Electromagnetics*. John Wiley and Sons, Inc.

[25] Y. Hu, D. R. Jackson, J. T. Williams, S. A. Long, and V. R. Komanduri, "Characterization of the input impedance of the inset-fed rectangular microstrip antenna," *IEEE Transactions of Antennas and Propagation*, vol. 56, no. 10, pp. 3314–3318, Oct. 2008.

[26] S. Lung, S. Yang, K. F. Lee, A. K. Kishk, and K. M. Luk, "Cross polarization studies in rectangular patch antenna," *Microwave and Optical Technology Letters*, vol. 50, no. 8, pp. 2099–2013, Aug. 2008.

[27] A. Petosa, A. Ittipiboon, and N. Gagnon, "Suppression of unwanted probe radiation in wideband probe-fed microstrip patches," *Electronics Letters*, vol. 35, no. 5, pp. 355–357, March 1999.

[28] J. Huang, "Low cross-pol linearly polarized microstrip array," in *Antennas and Propagation Society International Symposium*, vol. 35, no. 5, Dallas, TX, USA, May 1990.

[29] G. Kossiavas and A. Papeirnik, "The C patch: A small microstrip element," *Electronics Letters*, vol. 25, no. 4, pp. 253–254, March 1989.

[30] M. Sanad, "Double C-patch antennas having different aperture shapes," in *IEEE APS International Symposium*, June 1995, pp. 2116–2119.

[31] R. Bhalla and L. Shafai, "Resonance behaviour of single U-slot and dual U-slot antenna," in *IEEE APS International Symposium*, vol. 2, June 2001, pp. 700–703.

[32] F. Yang and Y. Rahmat-Samii, "Wideband dual parallel slot patch antenna (DPSPA) for wireless communications," in *IEEE APS International Symposium, Salt Lake City, UT*, vol. 3, July 2000, pp. 1650–1653.

[33] M. Haque, D. Mitra, and B. Ghosh, "Miniaturized C-slot patch antenna for wireless communication," *IEEE Conference on Signal Processing and Communication (SPCOM)*, vol. 46, pp. 1–4, July 2010.

[34] R. Sujith, S. Mridula, P. Binu, D. Laila, R. Dinesh, and P. Mohanan, "Compact CPW-fed ground defected H-shaped slot antenna with harmonic suppression and stable radiation characteristics," *Electronics Letters*, vol. 46, pp. 812–814, June 2010.

[35] F. Yang, X. X. Zhang, X. Ye, and Y. Rahmat-Samii, "Wide-band e-shaped patch antennas for wireless communications," *IEEE Transactions on Antenna and Propagation*, vol. 49, no. 7, pp. 1094–1100, July 2001.

[36] Y. Ge, K. Esselle, and T. Bird, "E-shaped patch antennas for high-speed wireless networks," *IEEE Transactions on Antenna and Propagation*, vol. 51, no. 9, pp. 3213–3219, Sep. 2003.

[37] T. Huynh and K.-F. Lee, "Single-layer single-patch wideband microstrip antenna," *Electronics Letters*, vol. 5, no. 16, pp. 1310–1312, Aug. 1995.

[38] F. Yang, Y. Rahmat-Samii, and X.-X. Zhang, "Authors reply to comments on wide-band E-shaped patch antennas for wireless communications," *IEEE Transactions on Antenna and Propagation*, vol. 51, pp. 2541–2542, Dec. 2003.

[39] M. Sanad, "Very small double C-patch antenna contained in a PCMCIA standard PC card," in *Proceedings Inst. Elect. Eng. 9th Conference on Antennas and Propagation (ICAP95), Eindhoven, Netherlands*, Apr. 1995, pp. 117–120.

[40] ——, "Non-planar shorted double C-patch antennas for portable communication equipment," in *IEEE APS International Symposium, Baltimore, MD*, vol. 1, July 1996, pp. 738–741.

[41] L. Zald, G. Kossiavas, J. Dauvignac, and A. Papiernik, "Very compact double C-patch antenna," *Electronics Letters*, vol. 34, no. 10, pp. 933–934, May 1998.

[42] S. Bhardwaj and Y. Rahmat-Samii, "A comparative study of C-shaped, E-shaped and U-slotted patch antennas," *Microwave and Optical Technology Letters*, vol. 54, no. 7, pp. 1746–1757, July 2012.

[43] "Honeycomb data sheets," http://www.hexcel.com/Resources/honeycomb-data-sheets, Hexcel, [Online; accessed 26-May-2012].

[44] L. I. Basilio, M. A. Khayat, J. T. Williams, and S. A. Long, "The dependence of the input impedance on feed position of probe and microstrip line-fed patch antennas," *IEEE Transactions of Antennas and Propagation*, vol. 49, no. 1, pp. 45–47, Jan. 2001.

[45] M. Manteghi, "Analytical calculation of impedance matching for probe-fed microstrip patch antennas," *IEEE Transactions of Antennas and Propagation*, vol. 57, no. 12, pp. 3972–3975, Dec. 2009.

[46] A. Saban, "A new broadband stacked two-layer microstrip antenna," in *IEEE APS International Symposium Digest*, vol. 21, no. 4, 1983, pp. 307–308.

[47] J. Dahele and K. Lee, "Experimental study of the effect of substrate thickness on single and stacked circular-disc microstrip antenna," in *IEEE APS International Symposium*, vol. 20, May 1982, pp. 66–69.

[48] R. Lee, K. Lee, and J. Bobinchak, "Characterisitics of a two-layer electromagnetically coupled rectangular patch antenna," *Electronics Letters*, vol. 23, pp. 1070–1072, Sep. 1987.

[49] P. Bhatnagar, J. Daniel, K. Mahdjoubi, and C. Terret, "Displaced multilayer triangular elements widen antenna bandwidth," *Electronics Letters*, vol. 24, pp. 962–964, July 1988.

[50] P. Li, H. W. Lai, K. M. Luk, and K. L. Lau, "A wideband patch antenna with cross-polarization suppression," *IEEE Antennas and Wireless Propagation Letters*, vol. 3, no. 1, pp. 211–214, Dec. 2004.

[51] D. Guha, M. Biswas, and Y. M. M. Antar, "Microstrip patch antenna with defected ground structure for cross polarization suppression," *IEEE Transactions on Antenna and Propagation*, vol. 4, pp. 4555–458, March 2005.

[52] Z. N. Chen and M. Y. W. Chia, "Center-fed microstrip patch antenna," *IEEE Transactions on Antenna and Propagation*, vol. 51, no. 3, pp. 483–487, March 2003.

[53] Q. Xue, Senior, X. Y. Zhang, and C.-H. K. Chin, "A novel differential-fed patch antenna," *IEEE Antennas and Propagation Letters*, vol. 5, pp. 471–473, 2006.

[54] Z. Wang, S. Fang, and S. Fu, "Broadband stacked patch antenna with low VSWR and low cross-polarization," *ETRI Journal*, vol. 32, no. 4, pp. 618–621, Aug. 2010.

[55] K. M. Luk, C. Mak, Y. Chow, and K. Lee, "Broadband microstrip patch antenna," *Electronics Letters*, vol. 34, no. 15, pp. 1442–1443, July 1998.

[56] Y.-X. Guo, C.-L. Mak, K.-M. Luk, and K.-F. Lee, "Analysis and design of L-probe proximity fed-patch antennas," *IEEE Transactions on Antenna and Propagation*, vol. 49, no. 2, pp. 145–149, Jan. 2001.

[57] X.-Y. Zhang, Q. Xue, B.-J. Hu, and S.-L. Xie, "A wideband antenna with dual printed L-probes for cross-polarization suppression," *IEEE Antennas and Wireless Propagation Letters*, vol. 5, pp. 388–390, 2006.

[58] Y.-X. Guo, K.-W. Kho, and L. C. Ong, "Wideband dual-polarized patch antenna with broadband baluns," *IEEE Transactions on Antenna and Propagation*, vol. 55, no. 1, pp. 78–83, Jan. 2007.

[59] K. S. Ryu and A. A. Kishk, "Wideband dual-polarized microstrip patch excited by hook shaped probes," *IEEE Transactions on Antennas and Propagation*, vol. 5, no. 12, pp. 3645–3649, Dec. 2008.

[60] H. Wong, K.-L. Lau, and K.-M. Luk, "Design of dual-polarized L-probe patch antenna arrays with high isolation," *IEEE Transactions on Antenna and Propagation*, vol. 52, no. 1, pp. 45–52, Jan. 2004.

[61] Y. Rahmat-Samii, K. S. Kona, , M. Manteghi, S. Yueh, W. J. Wilson, J. S. Dinardo, and D. Hunter, "A novel lightweight dual-frequency dual-polarized sixteen-element stacked patch microstrip array antenna for soil-moisture and sea-surface-salinity missions," *IEEE Antennas and Propagation Magazine*, vol. 48, no. 6, pp. 33–46, Dec. 2006.

[62] K.-L. Wong and T.-W. Chiou, "Finite ground plane effects on broad-band dual polarized patch antenna properties," *IEEE Transactions on Antennas and Propagations*, vol. 51, no. 4, pp. 903–904, Apr. 2004.

[63] C. A. Balanis, *Advanced Engineering Electromagnetics*, 3rd ed. John Wiley and Sons, Inc.